UNITED AIRCRAFT CORPORATION

United Aircraft Research Laboratories

EAST HARTFORD, CONNECTICUT

United Aircraft Research Laboratories

UNITED AIRCRAFT CORPORATION

EAST HARTFORD, CONNECTICUT 06108

UARL - Report K-910900-7

Experimental Investigations to Simulate the Thermal Environment and Fuel Region in Nuclear Light Bulb Reactors using an R-F Radiant Energy Source

Contract No. SNPC-70

REPORTED BY Ward C. Roman
Ward C. Roman

Jerome F. Jaminet
Jerome F. Jaminet

APPROVED BY James W. Clark
James W. Clark, Chief
Fluid and Systems Dynamics

DATE September 1971

NO. OF PAGES 99

COPY NO. 27

FOREWORD

An exploratory experimental and theoretical investigation of gaseous nuclear rocket technology is being conducted by the United Aircraft Research Laboratories under Contract SNPC-70 with the joint AEC-NASA Space Nuclear Systems Office. The Technical Supervisor of the Contract for NASA was Captain C. E. Franklin (USAF) for the first portion of the contract performance period and was Dr. Karlheinz Thom for the last portion of the contract performance period. Results obtained during the period September 16, 1970 and September 15, 1971 are described in the following seven reports (including the present report) which comprise the required second Interim Summary Technical Report under the Contract:

1. Roman, W. C. and J. F. Jaminet: Experimental Investigations to Simulate the Thermal Environment and Fuel Region in Nuclear Light Bulb Reactors Using an R-F Radiant Energy Source. United Aircraft Research Laboratories Report K-910900-7, September 1971. (present report)

2. Klein, J. F.: Experiments to Simulate Heating of the Propellant in a Nuclear Light Bulb Engine Using Thermal Radiation from a D-C Arc Radiant Energy Source. United Aircraft Research Laboratories Report K-910900-8, September 1971.

3. Bauer, H. E.: Initial Experiments to Investigate Condensation of Flowing Metal-Vapor/Heated-Gas Mixtures in a Duct. United Aircraft Research Laboratories Report K-910900-9, September 1971.

4. Rodgers, R. J., T. S. Latham and H. E. Bauer: Analytical Studies of Nuclear Light Bulb Engine Radiant Heat Transfer and Performance Characteristics. United Aircraft Research Laboratories Report K-910900-10, September 1971.

5. Latham, T. S. and H. E. Bauer: Analytical Design Studies of In-Reactor Tests of a Nuclear Light Bulb Unit Cell. United Aircraft Research Laboratories Report K-910900-11, September 1971.

6. Krascella, N. L.: Spectral Absorption Coefficients of Helium and Neon Buffer Gases and Nitric Oxide-Oxygen Seed Gas Mixture. United Aircraft Research Laboratories Report K-910904-2, September 1971.

7. Palma, G. E. and R. M. Gagosz: Effect of 1.5 Mev Electron Irradiation on the Transmission of Optical Materials. United Aircraft Research Laboratories Report K-990929-2, September 1971.

Report K-910900-7

Experimental Investigations to Simulate the Thermal Environment and Fuel Region in Nuclear Light Bulb Reactors using an R-F Radiant Energy Source

TABLE OF CONTENTS

TABLE OF CONTENTS (Continued)

Report K-910900-7

Experimental Investigations to Simulate the Thermal Environment and Fuel Region in Nuclear Light Bulb Reactors using an R-F Radiant Energy Source

SUMMARY

Experiments were continued to develop test configurations and technology necessary to simulate the thermal environment and fuel region in nuclear light bulb reactors. The test program was conducted using the UARL 1.2-megw r-f induction heater which has 7.8-cm-ID work coils and operates at approximately 5.5 MHz. Several types of models were installed inside the coils to achieve different program objectives. All models were basically cylindrical vortex chambers with highly cooled fused silica peripheral walls and copper end walls. Argon was used to drive the vortexes. R-F power level, chamber pressure and argon flow rate were adjusted to provide the desired r-f plasma discharge test conditions.

One portion of the program involved r-f tests of models having configurations presently envisioned as suitable for tests in a driver reactor, particularly the Nuclear Furnace under construction at the Los Alamos Scientific Laboratory. The in-reactor tests will involve uranium plasmas with equivalent black-body radiating temperatures between 3333 and 3910 K; the chamber pressure will be 500 atm. In the r-f tests reported herein, a 2/3-scale version of a possible in-reactor unit cell configuration --- a 14-cm-long chamber with an inside diameter of 5.7 cm --- was tested with argon plasma discharges radiating at equivalent black-body temperatures up to 4670 K. In some tests, simulated fuels in the form of uranium hexafluoride, tungsten hexafluoride and tungsten particles were injected into the plasma discharge from probes located at the centers of the two end walls. The results are encouraging since very little of the injected simulated fuel was deposited on the transparent peripheral wall.

The maximum test chamber pressure attained in r-f tests with in-reactor-type model configurations was 40 atm. This pressure is twice the maximum level attained previously with smaller models having fused silica pressure vessels and was limited by existing cooling water pump capability. In these tests, a fiberglass filament-wound pressure vessel was used between the transparent peripheral wall of the chamber and the r-f coils. One of these filament-wound pressure vessels, which were developed at UARL as part of the NASA program, was hydrostatically tested to 550 atm --- greater than the 500 atm in-reactor requirement --- where the test was terminated due to leakage from the pressure vessel.

Another major portion of the program involved r-f tests of models having peripheral walls constructed from thin-walled fused silica tubes, as in the nuclear light bulb engine. The ultimate objective of this effort is to demonstrate the capability of such thin-wall, internally cooled structures to remain intact in the

thermal environment of the engine. In the tests reported herein, models constructed from 0.125-mm-thick tubes were tested at r-f plasma discharge powers up to 116 kw and pressures up to 21 atm --- greater than twice the power and pressure levels of previous tests. This increased performance was due to a greatly improved argon buffer gas injection configuration which is highly cooled yet maintains the injection turbulence level as low as possible. The highest radiant flux at the wall was 0.77 kw/cm^2, compared with an estimated 23.4 kw/cm^2 for the reference engine and 0.40 to 0.76 kw/cm^2 for early in-reactor test configurations. Higher levels of power, pressure and radiating flux should be attainable in future tests in which the newly developed filament-wound pressure vessels can be used.

It is recommended that development of the test configurations and technology necessary for r-f tests of in-reactor models at 500 atm should be pursued with immediate emphasis in these areas: (1) development of diagnostic techniques for measuring the average partial pressure of simulated fuel inside the test chamber at elevated pressures; (2) tests with simulated-fuel injection to achieve high average partial pressure ratios in a configuration with the fuel-cloud-radius-to-cavity-radius ratio of approximately 0.6; (3) modification of the r-f induction heater test tank, heat exchangers, pump system and other equipment to permit safe operation at 500 atm; and (4) design, fabrication, cold-flow testing and hydrostatic testing of an in-reactor model which can subsequently be tested at in-reactor radiant energy flux levels and pressures in the 1.2-megw r-f induction heater.

RESULTS AND CONCLUSIONS

1. R-F tests with a 2/3-scale version of a possible in-reactor unit cell configuration resulted in the following levels of performance:

(a) The maximum steady-state power deposited into the plasma discharge was 258 kw. The diameter of this discharge was 2.3 cm, compared with the 5.7-cm diameter of the fused silica transparent wall surrounding the discharge. The power density was 6.62 kw/cm^3 and the maximum power radiated through the transparent wall was 200 kw. The radiation flux, based on the surface area of the discharge, was 2.52 kw/cm^2, which is equal to the flux from a black-body radiating at 4670 K. The flux levels expected in early in-reactor tests correspond to radiating temperatures between 3333 K and 3910 K and power densities between 1.3 and 2.34 kw/cm^3. Thus, the expected radiating temperatures were exceeded by at least 18 percent and the power densities exceeded by at least 180 percent. The calculated fuel-cloud-radius-to-cavity-radius ratio of the in-reactor configuration is 0.6; the maximum plasma-discharge-radius-to-peripheral-wall-radius ratio obtained in the r-f plasma radiant energy source tests was 0.44.

(b) The maximum chamber pressure achieved with the outer fused silica tube serving as the pressure vessel was 22.5 atm. This was limited by the allowable hoop and thermal stresses. The fused silica tube was replaced with a fiberglass filament-wound pressure vessel having a wall thickness of 0.28 cm which allowed steady-state operation of the plasma at chamber pressures up to 40 atm. R-F tests were limited to this chamber pressure by the installed water cooling equipment and factors of safety placed on the existing pneumatic and hydraulic hardware. No difficulties were encountered which would prevent operation at pressures higher than 40 atm after modifications to this equipment. In preparation for such tests, one filament-wound tube was hydrostatically tested to 550 atm where the test was terminated due to leakage. The chamber pressure required for in-reactor tests is 500 atm.

(c) Radiation efficiencies, i.e., the percent of the total power deposited into the plasma that was radiated through the inner transparent wall, approached 80 percent at chamber pressures near 20 atm.

(d) Simulated-fuel injection tests using uranium hexafluoride and tungsten hexafluoride indicated that these gases could be injected into the discharge with little or no deposition on the inner transparent wall. Up to 8 percent concentration (by partial pressure) of tungsten hexafluoride in argon carrier gas was injected. The corresponding tungsten mass flow rate was about 0.6 gm/sec. This was the maximum concentration possible with the available gaseous fuel injection system at the time of the tests (a new system with increased capability was built but could not be tested due to time limitations). Initial tests

were also conducted with injection of micron-sized tungsten particles. The results were less satisfactory than with gaseous simulated fuels; due to the unsteady flow of seeds in the argon carrier gas, some deposition occurred on the transparent wall. However, necessary improvements should be made, and particle injection should be pursued in future tests.

2. R-F tests of models having peripheral walls constructed from thin-walled fused silica tubes resulted in the following levels of performance:

(a) The maximum power deposited into the r-f plasma discharge was about 116 kw and the corresponding power radiated through the wall was 55.6 kw. These levels are roughly twice the levels attained in previous tests. The maximum radiant heat flux incident on the peripheral wall was about 0.77 kw/cm^2*. The maximum total heat deposition in the transparent wall was about 0.13 kw/cm^2. This total heat deposition is considerably less than the maximum experienced in previous tests where undesirable high convection and conduction heat loads dominated the total wall heat flux. The model used in this particular test was cooled using compressed air. This test was conducted near the end of the program and time was not available to continue to higher power levels after premature axial coolant tube failure occurred at the 116 kw power level. After minor modifications to the model, significant increases in the total discharge power should be possible in future tests.

(b) The maximum chamber pressure achieved was 21 atm. Maximum pressure was limited by the allowable hoop and thermal stresses in the fused-silica pressure vessel surrounding the model. Higher pressures can be attained using a fiberglass filament-wound tube.

(c) The range of the plasma-discharge-radius-to-peripheral-wall-radius ratio in the gas-cooled model tests was approximately 0.40 to 0.64. For the water-cooled model tests the range of the radius ratio was estimated from the gas-cooled model test data and the known test conditions to be approximately 0.40 to 0.70. The radius ratio expected in the in-reactor unit cell is 0.6 and that of the reference engine is 0.85.

*For reference, the radiant heat flux incident on the peripheral wall expected in the full-scale engine is 23.4 kw/cm^2, and that expected in in-reactor tests is about 0.40 to 0.76 kw/cm^2.

INTRODUCTION

An experimental and theoretical investigation of different phases of gaseous nuclear rocket technology is being conducted by the United Aircraft Research Laboratories (UARL) under Contract SNPC-70 administered by the joint AEC-NASA Space Nuclear Systems Office. This investigation is currently directed toward evaluating the feasibility of the nuclear light bulb engine concept.

Details of this engine concept are discussed in Refs. 1 through 5. Figure 1(a) illustrates the principle of operation with a cross-sectional sketch of the top half of the nuclear light bulb reference engine unit cavity. The full-scale reference engine consists of a cluster of seven such cavities. In brief, the concept is based on the transfer of energy by thermal radiation from fissioning gaseous nuclear fuel (uranium) contained in a vortex, through an internally cooled transparent wall, to seeded hydrogen propellant flowing in an annulus surrounding the transparent wall. The hydrogen propellant is seeded with sub-micron tungsten particles to increase its opacity. A transparent buffer gas, such as neon, is injected near the inner surface of the transparent wall to form the vortex which contains and isolates the fuel from the wall. In addition, the neon buffer gas prevents diffusion of the nuclear fuel to the wall. High purity, internally gas-cooled, fused silica tubes (tube wall thicknesses in the range of 0.125 to 0.25 mm) appear suitable for the transparent wall. The neon and the entrained gaseous nuclear fuel and fission products exit through ports located on the centerline of the end wall of the cavity. Cold neon bypass gas is used to rapidly cool the hot exhaust gas mixture, thereby condensing the fuel. The condensed fuel is centrifugally separated from the neon and pumped back into the fuel containment region of the vortex. The neon is further cooled and pumped back into the cavity to drive the vortex.

Because of the high temperatures obtainable in the fuel region, engines of this type offer the ultimate potential of providing values of specific impulse greater than 3000 sec and engine thrust-to-weight ratios greater than unity. A summary of the performance characteristics is presented in Ref. 6. This closed-cycle fuel system concept is also unique because the physical interface between the nuclear fuel and the seeded hydrogen propellant (the internally cooled transparent wall) offers the possibility of providing perfect containment of the gaseous nuclear fuel and fission products.

The research program discussed in this report is concerned with simulating the thermal environment and fuel region in nuclear light bulb type reactors, including the testing of internally cooled transparent walls in a high-radiant-energy-flux environment. Major emphasis is placed on use of the UARL 1.2-megw r-f induction heater in tests designed to simulate many of the problems which are inherent in determining the feasibility of the nuclear light bulb reactor concept. Previous investigations (Refs. 7 and 8) were directed at developing a non-nuclear r-f plasma radiant energy source that could ultimately provide steady-state radiant energy fluxes similar to those expected in a full-scale reactor. Recently completed investigations related to other areas of nuclear light bulb engine technology are reported in Refs. 9 through 14.

Increased emphasis has been placed on research necessary in preparation for tests of small-scale models of a nuclear light bulb unit cell in a driver reactor with high thermal neutron flux levels, such as the Nuclear Furnace under construction at Los Alamos Scientific Laboratory. Analytical studies were conducted (Ref. 12) to define the characteristics of an in-reactor test configuration of a nuclear light bulb unit cavity. Figure 1(b) is a sketch illustrating an in-reactor unit cell test configuration of a nuclear light bulb cavity. The vortex region consists of an approximately 6.6-cm (2.6-in.)-ID by 17.8-cm (7-in.)-long cylindrical cavity. As in the reference engine unit cavity (Fig. 1(a)), the buffer gas is injected tangentially near the periphery of the cavity. The uranium fuel is injected at the centers of the symmetrical end walls.

Figure 1(c) shows the basic r-f plasma radiant energy source configuration used in the present investigation. The r-f plasma discharge has a length of 14.0 cm (5.5 in.) and a maximum diameter of approximately 2.5 cm (1.0 in.). The transparent peripheral walls of the test chamber are concentric, water-cooled, fused silica tubes. As in the reference engine unit cavity and in-reactor unit cell, a symmetric pair of end walls form the axial boundary of the test chamber. To establish the required radial-inflow vortex flow pattern, argon gas is injected through vortex injectors symmetrically located on each end wall. Each end wall contains a thru-flow port on the centerline to remove the exhaust gas from the vortex chamber. The r-f plasma discharge occurs in the region between the end walls with the major axis colinear with the thru-flow port axis.

The primary objectives of the research reported herein were (1) to develop test configurations and technology necessary to simulate the conditions which are expected to exist in the fuel region of the reference engine unit cavity and in an in-reactor unit cell (including injection of simulated fuel and high pressure test conditions) and (2) to demonstrate that transparent-wall models similar to those which might be employed in a nuclear light bulb engine, having wall thicknesses down to 0.125 mm (0.005 in.), can be fabricated and operated in the required environments. Another objective was to design, fabricate and conduct static tests of a 500-atm, fiberglass filament-wound pressure vessel of a type suitable for future high pressure tests involving r-f plasma and in-reactor simulation testing.

The experimental investigation was divided into four parts, each having specific objectives. Accordingly, this report is divided into sections which describe the research and results obtained in each part: the radiant energy source tests, initial simulated-fuel injection tests, transparent wall model tests, and 500 atm filament-wound pressure vessel tests. The principal equipment common to several of the programs is described in the following section of the report.

DESCRIPTION OF PRINCIPAL EQUIPMENT

UARL 1.2-Megw R-F Induction Heater

Background

The experiments described in this report were conducted using the UARL 1.2-megw r-f induction heater. This heater was constructed during 1966 and 1967 as part of the UARL Corporate-sponsored program on gaseous-core nuclear rocket technology. The heater was designed to ultimately be capable of depositing approximately 0.6 megw of r-f power into a relatively small plasma discharge. In its present configuration, the heater has deposited about 0.26 megw of r-f power into a 40 cm^3, steady-state plasma discharge. Corporate-sponsored tests employing a salt-water load (uniform electrical conductivity) have continued to further develop and verify operation of all r-f induction heater components. During these tests, up to 0.31 megw was deposited into the salt-water load at an overall system efficiency, defined as total r-f power deposited in the load divided by the total d-c power supplied to the heater, of about 45 percent.

Primary Heater Components and Test Tank

A detailed description of this equipment is given in Ref. 7. A block diagram showing the primary components of the heater is presented in Fig. 2. The approximate operating frequency of 5.5 MHz is selected by means of an L-C type variable frequency oscillator whose 0.5-w output is amplified to approximately 2 kw using a neotron amplifier. The 2-kw output is used to provide r-f excitation for the basic r-f induction heater stages which receive d-c power from a common saturable-reactor-controlled power supply. The 2-kw excitation drives a 40-kw output amplifier which in turn drives a 80-kw buffer amplifier which is the actual driving stage for the final power amplifiers. All these stages contain controls for tuning the matching circuit at the final power amplifier input. This allows individual adjustment to be made to the various amplifier systems, thus aiding in increasing the overall system efficiency. The r-f output power of up to 880 kw is supplied by two power amplifier tubes which drive a resonant tank circuit (resonator section) of unique design. The output of the two power amplifiers is resonated by a push-pull resonator. All stages are operated class "C" to provide for maximum efficiency. The power and voltage levels noted in Fig. 2 correspond to the maximum rated r-f output and d-c voltage for the various amplifier stages. The saturable-reactor-controlled power supply for the 40-kw, 80-kw, and final power amplifier stages is continuously variable in d-c voltage from 2 kv to approximately 24 kv. This provides flexibility in selecting the power levels for the various experimental test requirements. The maximum total d-c input power to the power amplifiers employed in plasma discharge tests during this program was 685 kw. The r-f induction heater has been operated with a salt-water load at input d-c power levels exceeding 750 kw.

The resonator section (part of which is visible in Fig. 3) consists of two arrays of ten vacuum capacitors and two work coils for coupling of the r-f power to the load (i.e., the plasma discharge). The resonator section vacuum capacitors

are water-cooled and r-f chokes are installed in the cooling water lines. Each resonator section is connected to a single-turn work coil (see Fig. 3). The two single-turn work coils each consist of five water-cooled 0.475-cm-OD copper tubes which are silver-soldered together to form a single structure. The coils are 7.8-cm in diameter and are silver plated to reduce resistive heating due to the high coil current.

The resonator section is located within a 1.7-m-dia cylindrical aluminum test tank. The front aluminum dome of the test tank contains five 10-cm-dia fused silica windows which allow observation of the test chamber from different angles. Several modifications were made to the basic test tank described in Ref. 7. These aided in providing greater accessibility and flexibility for the various tests employing the r-f radiant energy source. An overhead trolley and winch system was fabricated and installed. This facilitates removal of the front dome from the test tank and allows rapid access to the test section for inspection after completion of a test series. New copper test tank end flanges were also fabricated to permit direct routing of gas and coolant lines into the aluminum test tank. A Micalex support fixture was attached to the base of the aluminum test tank and forward section of the resonator to hold the various test configurations concentrically within the r-f work coils. A pair of water-cooled tie rods were installed within the test tank to minimize tank deflection under high axial pressure loads (see Fig. 3).

All components of the r-f induction heater are water-cooled, requiring a total of approximately 50 gpm of cooling water. Voltage, current, and power meters together with strip-chart recorders are used during the tests for continuously monitoring the r-f induction heater power characteristics. Measurements are made of all the cooling water and gas flow rates, associated temperature rises, and all electrical quantities necessary for performing a component and overall-system energy balance on the r-f equipment. A detailed description of the control consoles used in the 1.2-megw r-f induction heater tests is given in Ref. 8. A set of single- and dual-channel strip-chart recorders (approximately 0.5-sec response time) and an automatic stepping-type temperature recorder were used to permit simultaneous monitoring of the various critical measurements during the tests.

The r-f input power to the plasma discharge is determined by the r-f voltage supplied to the resonator section of the heater (Fig. 2) and the impedance of the plasma and resonator which, in turn, determines the current level. The impedance of the plasma is determined by its size and electrical conductivity. The r-f voltage applied to the resonator section was measured with a capacitive type voltage probe.

Gas and Cooling Water Systems

Figure 4 is a schematic of the argon gas and high-pressure cooling water flow systems. Argon gas was supplied to the test chamber from an eleven-bottle argon supply having a total capacity of 2500 scf. This permitted long run time capability. Flowmeters were used to measure the argon weight flow rate during most of the tests. For tests at chamber pressures above about 20 atm, a sonic orifice flow-metering system was used (see Fig. 4). The exhaust gas was removed from both ends of the

test chamber and routed to a single flow control valve which permitted varying the chamber pressure. The exhaust gases were then ducted to the exhaust system and trap located on the laboratory roof.

To provide the necessary water cooling, two closed-loop cooling systems, each having a total storage capacity of approximately 75 gal, are used. A low-pressure system employing tandem centrifugal pumps can supply up to 100 gpm of cooling water at 11 atm. A high-pressure system using a positive displacement pump supplies up to 20 gpm of cooling water at 35 atm. A surge accumulator is used to damp out the pressure pulsations to less than one percent. Each coolant loop had a 70-gal capacity, open top, stainless steel tank as a storage reservoir. Figure 4 shows additional details, including the locations of heat exchangers and flow-metering equipment.

Plasma Starting System

The basic starting system consists of a high-frequency, high-voltage spark starter and an auxiliary d-c arc starter. Figure 5 is a schematic of the plasma starting system and test chamber. As in previously reported tests, a pair of retractable tungsten tipped electrodes, located along the centerline of the test chamber, was used. A centrally located control panel permitted selection of the type of starting sequence which would provide the ionization level necessary for sustained coupling with the r-f power. In some tests, only the high-frequency starter mode was employed. In others, only the auxiliary d-c arc or combination high-frequency/direct-current arc was used. Additional details of the d-c starter assembly and control console are described in Ref. 7.

Test Chamber

Figure 6 is a sketch of the basic test chamber, r-f work coils, and plasma discharge for the r-f radiant energy source tests. A pair of concentric water-cooled fused silica tubes located concentrically within the r-f work coils form the outer boundary of the test chamber. The nominal dimensions of the outer and inner fused silica tubes are 6.5-cm (2.54-in.)-ID by 7.3-cm (2.88-in.)-OD and 5.7-cm (2.24-in.)-ID by 6.1-cm (2.40-in.)-OD, respectively. The annulus between the tubes was used for water coolant. A symmetrical pair of end walls are used to form the axial boundary of the test chamber. In the majority of tests employing the r-f plasma radiant energy source, the distance between end walls was 14 cm (5.5 in.). The various end-wall configurations installed in the test chamber will be described subsequently. To reduce the intense radiation from the source incident on the surrounding components, known concentrations of an organic, water soluble dye (nigrosine CI-50420) were added to the test-chamber cooling water.

Diagnostic Equipment and Data Analysis Methods

Total Radiation Measurements

The power radiated from the plasma was measured using the specially constructed radiometer and chopper wheel assembly described in Ref. 7. The transmission characteristics of the radiometer optical system and the various calibrated filters used in the tests reported herein are shown in Fig. 7(a). A Reeder RLB-500 thermopile detector with a Barium Fluoride (BaF_2) window was used as the radiometer sensing element. The output was connected to an operational amplifier and displayed on a strip-chart recorder. Internal r-f shielding and chokes were used to electrically isolate the radiometer system. For purposes of measuring the amount of radiation within different wavelength bands, the cutoff wavelengths were determined by the 50-percent transmission levels of the individual filters, BaF_2 window, or annular cooling water layer located between the two fused silica tubes within the test chamber (Fig. 6). The transmission level of the 2-mm water layer shown in Fig. 7(a) was calculated from the absorption coefficients for pure water given in Ref. 15. The total power radiated from the plasma was calculated assuming isotropic radiation, including allowance for blockage due to the r-f work coils.

As mentioned previously, nigrosine dye was used to reduce the intense radiation from the r-f plasma radiant energy source by adding known concentrations to the test chamber cooling water. Nigrosine was selected after tests were conducted to determine the type of dye or pigment with the most desirable characteristics (see Ref. 7). These tests included verification that the absorption characteristics of the coolant with dye added were not influenced by radiation from the plasma source or by the bulk temperature of the coolant for the range of test conditions employed. Results of other tests showed the water-dye coolant used absorbed negligible amounts of r-f energy. Figure 7(b) shows experimental results of the radiation attenuation obtained using a range of concentrations of nigrosine dye up to 7500 ppm (on a weight basis). The solubility of nigrosine dye in water is approximately 1.0 gm/gm at 353 K (Ref. 16). The ability to attenuate almost all of the total incident radiation is important for future tests at higher powers and pressures. In these tests, filament-wound pressure vessels will be used as the outer peripheral wall, and these must be protected from the intense radiation.

Plasma Diameter Measurements

The optical scanning system used to obtain the plasma diameter is described in detail in Ref. 7. The basic system includes a photomultiplier, collimating tube and fiber optic tube attached to a traversing mechanism. The output from the phototube enters a signal conditioner and is then fed to a strip-chart recorder. The fiber optic tube and traversing mechanism were located on the central view port of the dome of the test tank. This permitted scans of the discharge diameter at the axial midplane location. See Ref. 7 for additional details on the intensity cutoff criterion used, and for comparison with diameters determined from photographs using various neutral density filters.

Photographic Equipment and Viewing System for Recording and Observing Plasma Behavior

Photographs and movies taken from several of the view ports permitted an estimation to be made of the discharge size and shape for selected tests. Continuous observation of the discharge was accomplished using a projection screen system. A 45.7-cm focal length convex lens and neutral density filter system was used to project an image of the plasma discharge onto an overhead viewing screen. Horizontal and vertical grid lines placed on the screen also permitted estimates to be made of the changes in the discharge size and shape as the test parameters were changed.

Spectral Emission Measurements

A schematic of the optical system used to obtain spectral measurements is shown in Fig. 8. Details of the system, calibration and data processing procedures are discussed in Ref. 7. A Jarrel-Ash 0.25-meter Ebert monochromator mounted on a traversing table was used to obtain chordwise scans of the plasma discharge at several stations along the axial extent of the discharge. A calibrated 34.2-cm focal length lens was positioned 67.3 cm from the major axis of the plasma discharge (see Fig. 8). Scans were made of the continuum at 4320 Å by traversing the monochromator diametrically through the image as shown in Fig. 8. The scanning rate was 12.7 cm/min. In addition, wavelength scans between 3500 Å and 8300 Å were made at a scanning rate of 1000 Å/min. A 5600 Å cutoff filter was placed in front of the monochromator entrance slit (see Fig. 8) when spectral scans at wavelengths greater than 5600 Å were made to minimize second-order effects from lines at shorter wavelengths. As reported previously (Ref. 7), the 4320 Å continuum represents the best documented continuum region of an argon plasma. Various calibrated neutral density filters were located in front of the monochromator entrance slit to reduce the intensity of the incident light corresponding to different test conditions. The photomultiplier output went into a signal processor and was then displayed on a strip-chart recorder modified to operate at paper feed rates up to 76.2 cm/min.

Determination of Energy Balance

Figure 6 is a sketch of the radiant energy source configuration showing the power breakdown. The total power deposited into the plasma discharge, Q_T, was obtained from an overall energy balance. It was obtained by adding together the power lost by radiation, Q_R; the power deposited into the annular coolant by combined conduction, convection and radiation, Q_W; the power deposited into the end-wall assemblies by combined conduction, convection and radiation, Q_E; and the power convected out the exhaust ducts, Q_L.

The power radiated from the source which passed through the internally cooled transparent peripheral wall and water-dye coolant was measured with the radiometer system described previously. By monitoring the flow rate and associated temperature rise of the coolant flowing in the annulus between the inner and outer fused silica tubes, the total power deposited in the peripheral wall was calculated. When dye was used in the annular coolant loop it was necessary to replace the standard flowmeters with calibrated magnetic-type flowmeters. The associated inlet and exit coolant temperatures were monitored with copper-constantan thermocouples located

as close to the test region as possible. Similarly, by monitoring the flow rate and associated temperature rise of the coolant flowing in each end wall, the total power deposited in the end walls was determined. Depending on the test configuration, various types of water-cooled exhaust gas heat exchangers located in each of the two separate exhaust lines permitted determination of the power convected out the thru-flow port exhausts.

Determination of Source Radiation Characteristics

To calculate the radiant energy flux at the surface of the plasma discharge, it is necessary to determine the plasma discharge size and shape and the total radiated heat transferred through the inner fused silica tube of the test chamber. The optical scanning device, described previously, permitted a determination of the discharge diameter. Photographic techniques using different filter densities, camera shutter speeds, and film exposure time, allowed an estimate to be made of the overall shape of the plasma discharge. Diameter and shape changes due to the influence of varying test parameters could be systematically compared.

For the data reported herein, the total radiated heat transferred through the inner fused silica tube, $Q_{R,T}$, is defined as $Q_{R,T} = Q_R + Q_W - Q_{C'}$ where Q_R is the radiated power as measured by the radiometer system, Q_W is the power deposited in the peripheral-wall coolant, and $Q_{C'}$ is the power conducted through the inner fused silica tube. Since $Q_{C'}$ was not measured directly, estimates of $Q_{C'}$ were made by calculating the maximum heat flux which could be conducted through the inner fused silica tube. This estimate was based on experimental test experience (Ref. 8) and careful examination, under polarized light, of the inner fused silica tubes before and after the hot-flow tests. For the tests reported here, no significant traces of residual thermal stress were found in the tubes after exposure to the high radiant energy flux conditions. Refer to Ref. 8 for additional details on the assumptions used and the calculation procedure.

RADIANT ENERGY SOURCE PROGRAM

Introduction

Earlier tests using the 1.2-megw r-f induction heater concentrated on investigating vortex fluid dynamic techniques for confining plasma discharges and on determining the effects of parameters, such as pressure, power, and flow rate, on their radiating characteristics (Refs. 7 and 8). These experiments were aimed at developing an intense radiant energy source capable of producing radiant energy fluxes approaching those expected in a full-scale nuclear light bulb engine. These previous tests demonstrated that it is possible to deposit large amounts of steady-state r-f power into a very small plasma discharge. Tests were conducted at chamber pressures up to about 19 atm. The maximum steady-state radiant energy flux achieved in an ellipsoidal plasma discharge (major axis 5.1 cm) was 7.6 kw/cm^2, which corresponds to an equivalent black-body radiating temperature of 6040 K. For reference, the nuclear light bulb engine operates at 8333 K. The test results also indicated that the total discharge power, the chamber pressure, the argon vortex weight flow rate, and the operating frequency were interrelated in determining the stable operating conditions for a given chamber geometry. As a result, an operating envelope was established which permitted successful operation of the confined plasma discharge at thermal conditions approaching those required for full-scale engine simulation.

The research program reported herein has emphasized tests of small-scale models similar to configurations which could be tested in a driver reactor, such as the Nuclear Furnace. One specific goal was to develop an approximately 2/3-scale version of an early in-reactor test unit cell and to test this model at radiant energy flux levels equal to those expected in an actual in-reactor simulation test. Another goal was to develop a fiberglass filament-wound pressure vessel and to use it in tests with an r-f plasma radiant energy source at chamber pressures up to 40 atm.

Description of Test Equipment and Procedures

Fused Silica Pressure Vessel Configuration

The basic radiant energy source test chamber geometry used in these tests was described previously (see Fig. 6). To arrive at a design for safe operation at high power and pressure levels, calculations and static tests were performed to estimate the stress limits (both hoop and thermal) in the various transparent fused silica tubes used in the test chamber. The results indicated that by using the test chamber shown in Fig. 9, i.e., a concentric set of fused silica tubes having the dimensions shown, significantly high power ($\approx$ 250 kw) and pressure levels ($\approx$ 20 atm) could be achieved. Reference 8 includes test data on the strength of fused silica tubes of the type used. The end walls shown in Fig. 9 were the same as those used in the radiant energy source tests reported in Ref. 8 where they are described in detail. The spacing between the end walls was increased from 5 cm to 14 cm to permit simulation of the 2/3-scale in-reactor configuration. Each end wall contained

a 0.47-cm-dia thru-flow port on the centerline which was used to remove the argon test gas from the vortex chamber.

To provide end-wall simulation similar to that of the nuclear light bulb unit cell, a 0.95-cm-thick water-cooled copper disc (Fig. 9) was mounted on each 2.03-cm-dia end wall such that the surface of the disc toward the plasma discharge source was flush with the end-wall surface (Fig. 9). The surfaces of both end walls and discs were highly polished to increase their reflectivity. The results of separate tests conducted using the actual polished end walls indicated approximately 75 percent of the total radiation incident on the polished end-wall surface in the wavelength band from 0.25 to 1.3 microns was reflected.

To establish the desired radial-inflow vortex flow pattern, eight stainless steel vortex injectors were located equally spaced around the outer periphery of each copper disc (Fig. 9). These injectors were flush with the disc surface. The injectors were silver soldered in position such that the argon entered the test chamber in a circumferential direction only, i.e., the injection velocity had zero axial component. The majority of tests employed vortex injectors with an inside diameter of 0.234 cm; the corresponding buffer-gas injection area, A_j, was 0.686 cm^2. Injector inside diameters of 0.107 cm and 0.17 cm were used in some tests to provide information on the effect of injection velocity on the characteristics of the plasma discharge. Previous cold-flow results (Ref. 17) indicated that stable vortex flow patterns occurred at injection Reynolds numbers, $Re_{t,j}$, comparable with those of the tests reported herein (approximately 10^5). The argon injection velocities ranged between about 5 and 200 m/sec. During preliminary tests, temperature sensitive paint was applied to various end-wall components to verify the water-cooling effectiveness and to assure that r-f heating of the vortex injector assemblies was small.

Filament-Wound Pressure Vessel Configuration

Figures 10 and 11 show the filament-wound pressure vessel configuration used in the high pressure tests. The same basic test chamber orientation and scaling as shown in Fig. 9 was employed. A filament-wound fiberglass tube and inner silicone rubber liner replaced the outermost fused silica tube of the prior geometry. This provided the necessary strength requirements to permit safe operation at 40 atm with the configuration shown in Fig. 10 while still using the 7.8-cm-dia r-f work coils. A detailed discussion of the design, development and fabrication of the filament-wound tubes is included in a later section of the report.

The configuration shown in Fig. 10 comprises an integral assembly, i.e., no additional or external compression bolts or fixtures are required. Both the axial and radial loads are carried by the pressure vessel. The axial pressure load is transmitted to the filament-wound tube from the end walls by shear forces in the retainer flanges. The stainless steel retainer flanges each consist of four pieces (to allow assembly) and are held in place with cap screws.

Figure 11 is a photograph showing the primary components of this configuration. The silicone rubber sealing liner prevents seepage of the annular coolant through

the wall of the filament-wound tube. The liner contains 5 percent titanium dioxide (TiO_2) which was added to increase its opacity and provide additional thermal protection for the filament-wound tube. A ridge is integrally molded into each end of the liner. This ridge fits into a groove in the sealing ring (see Fig. 10) to prevent leakage at the ends of the tube assembly. The water-dye coolant is used to protect the liner and filament-wound tube from the thermal radiation. The small amount of radiation which passes through the water-dye mixture is absorbed by the liner which is convectively cooled by the water-dye mixture. It is estimated that the liner and filament-wound tube will operate at a maximum temperature of about 400 K. The operating limit of the tube and liner, based on the manufacturers' recommended service temperature for the epoxy binder and silicone rubber, is approximately 425 K.

As in the previous configuration, the end walls were located concentrically within the fused silica tube and filament-wound pressure vessel assembly. The axial distance between the end-wall faces was 14.0 cm (5.5 in.). Both copper end-wall surfaces were polished to increase their reflectivity. A thru-flow port diameter of 0.79 cm (0.312 in.) was used, which was larger than the port diameter in the previous model. This diameter was increased to compensate for blockage in tests (discussed later) which employed simulated-fuel injection probes. In addition, the results reported in Ref. 8 indicated the possibility that one or both end-wall thru-flow ports were approaching choked conditions during high-power tests. The end-wall cooling system was designed to conservatively provide adequate cooling for heat deposition rates of approximately 1.5 kw/cm^2. For comparison, this heat deposition rate is about two times the highest measured in r-f plasma tests to date. The heat flux capability was calculated by assuming zero reflectivity from the copper surface, incipient boiling of the water coolant, and that the bulk temperature at the exit of the coolant passage is in the range of 283 to 373 K.

Eight 1.07-mm (0.042-in.)-ID stainless steel vortex injectors were equally spaced around the periphery of each end wall. The injector tips were flush with the end-wall surface and were positioned such that the argon entered the test chamber in the circumferential direction. The total injection area, A_j, was 0.144 cm^2 (0.022 $in.^2$). A static pressure tap (see Fig. 11) was located near the periphery of the end wall for measurement of the chamber pressure.

Figure 12 is a photograph of the entire filament-wound pressure vessel configuration installed in the r-f induction heater. One section of the Micalex support bracket is visible in the photograph. Also illustrated is the location of the temperature sensitive paint used to monitor the surface temperature of the filament-wound tube and the water-cooled r-f shield surrounding the stainless-steel retainer flanges. The quick-disconnect gas and cooling water connections shown permit rapid removal of the entire test configuration from the test tank. The relatively short end-wall assemblies permitted installation of the simulated-fuel injection probes concentrically within the thru-flow duct. However, because of the short end-wall assemblies, a greater fraction of the total power contained in the exhaust gas must be removed by other water-cooled components located downstream of the end-wall assemblies. New exhaust gas heat exchangers, shown in Fig. 12, were installed to handle this heat load.

Test Procedures

The operating procedures used during typical tests employing the 1.2-megw r-f induction heater are discussed in detail in Ref. 7. The auxiliary starting system shown in Fig. 5 permitted moderately high-power-level r-f plasma discharges to be reliably started at pressures exceeding one atm. Prior to starting the r-f plasma discharge, the r-f drive system (see Fig. 2) was pretuned for the proper resonant frequency. Following initiation of the discharge, the r-f drive system was then retuned to compensate for the resonant frequency change due to the presence of the discharge within the r-f work coils. All required measurements and data acquisition were then taken at a particular test condition with an average run time of about 1 hr. It should be emphasized that to maintain a stable discharge, the combination of r-f operating frequency, total discharge power, chamber pressure, and argon weight flow rate are interrelated for each given configuration tested. Simultaneous changes in at least two of these parameters were usually necessary to maintain a stable plasma. Where possible, several of the independent variables (see Fig. 6) were held as constant as possible to permit systematic comparisons to be made and important trends to be noted.

Discussion of Test Results

Tests with Fused Silica Pressure Vessel Configuration

Energy Balance for Highest Power Operating Condition

Figure 13 is a sketch of the radiant energy source configuration with details of the energy balance for the highest power operating condition, which also was the test condition for maximum radiation through the inner transparent wall. See Fig. 9 for details of the test configuration.

This test condition resulted in a total discharge power of 258 kw with 200 kw of radiated power being transferred through the inner peripheral wall. The corresponding key test conditions were: pressure, 15 atm; total d-c input power, Q_I = 685 kw; r-f operating frequency, f = 5.5083 MHz; and argon weight flow rate, W_A = 9.1 gm/sec. The power breakdown is as follows: 26.8 kw was radiated through the peripheral-wall water-dye coolant; 182.2 kw was deposited into the peripheral-wall water-dye coolant; the total power deposited in both end walls was 44 kw; and 5.1 kw was convected out both thru-flow exhaust ducts. The relatively low amount of power in the argon exhaust thru-flow is attributed to the large transfer of exhaust power to the cooling water of the relatively long (75-cm) surrounding end-wall assemblies prior to the exhaust flow reaching the end-wall exit location.

The discharge diameter at the axial midplane in this test was 2.27 cm. The discharge shape is shown by the shaded area in Fig. 13. The discharge was cylindrical over the central portion with approximately conical end regions. The discharge volume in this test was 39.7 cm^3 and the corresponding surface area was 79.6 cm^2. The plasma-discharge-radius-to-peripheral-wall-radius ratio, r_6/r_1, was 0.4 compared to the calculated fuel-cloud-radius-to-cavity radius ratio of 0.6 for the in-reactor configuration.

The fraction of the discharge power radiated through the inner peripheral wall, $Q_{R,T}/Q_T$, was 0.79. Thus, the plasma was operating in a radiation-dominated mode. The radiant energy flux achieved at the surface of the discharge for this test condition was 2.52 kw/cm^2, corresponding to an equivalent black-body radiating temperature, T^*, of 4670 K (based on total heat flux and equivalent surface area). For reference, the range of total radiated heat flux expected at the edge of fuel in a possible in-reactor unit cell is about 0.67 to 1.27 kw/cm^2; the corresponding range of T^* is 3333 to 3910 K. The calculated power densities required for the in-reactor unit cell range between 1.3 and 2.34 kw/cm^3. The power density achieved in this test was 6.62 kw/cm^3.

The r-f system coupling efficiency (defined by the ratio of r-f power deposited in the load to the total d-c input power) for this case was 37.8 percent. It was not possible to attain total discharge powers higher than 258 kw due to present limits on the capability of the r-f induction heater d-c power supply. If required in future tests, higher power levels can be reached if the electrical impedance of the discharge and resonator as seen by the r-f transmitter is increased. This will result in a decrease in the plate current required to maintain a given r-f coil voltage. To some extent this can also be achieved by adjustments in the r-f heater output circuit.

Plasma Geometric Characteristics and Stability

The effects of varying the total discharge power on the diameter of the discharge, measured at the axial midplane, are illustrated in Fig. 14. Data are shown over a range of chamber pressure, argon weight flow, and r-f operating frequency. For reference, the upper two horizontal dashed lines show the inside diameter of the r-f work coils and the inside diameter of the inner fused silica tube of the test chamber. The plasma discharge could be maintained in a stable geometry with diameters ranging between 1.5 and 2.5 cm. The larger diameters could be obtained by decreasing the argon weight flow rate until indications of turbulence or plasma asymmetry occurred. This was verified by color movies taken of the discharge through several of the test tank view ports. Frame-by-frame study of the movies yielded information concerning the relative stability. Distinct periodic radial pulsations, amounting to about 5 percent of the discharge diameter, were observed at 360 Hz (the ripple frequency of the three-phase power supply).

Separate tests employing different sized vortex injectors permitted the injection velocity to be varied while maintaining the argon weight flow rate approximately constant. In general, the total discharge power, resonator voltage and total power radiated from the discharge increased, and the discharge diameter decreased, with increasing injection velocity. These results were used in selecting the size of the vortex injectors used in the high pressure filament-wound pressure vessel tests.

The r-f operating frequency is also an independent parameter which affects both the discharge geometry and electrical characteristics. Tests were conducted in which the r-f operating frequency was varied above and below the unloaded resonant frequency (i.e., the resonant frequency without the discharge present). Typically, for a frequency shift of approximately 85 kHz, up to a 40-percent change in discharge diameter resulted. The technique of shifting the frequency during operation was

used in some tests to vary the discharge diameter and, hence, cause changes in the radiant energy flux. This frequency shift technique together with varying the vortex injection velocity, changing the diameter of the r-f work coils, and changing the diameter of the inner transparent wall may be used in future tests to permit simulating the calculated fuel-cloud-radius-to-cavity-radius ratio of the in-reactor configuration.

Factors which Influence Source Radiation Characteristics and Power Loss Mechanisms

Calculations of the radiant energy flux at the surface of the discharge were made for the data shown in Fig. 14. Recall that the radiant energy flux is defined as the total radiated heat transferred through the inner peripheral wall of the test chamber divided by the discharge surface area. The total radiated heat was subject to the conduction correction discussed previously. The flux defined in this way is approximately equal to the true radiant energy flux.

Figure 15 shows the variation of radiant energy flux with total discharge power. The highest flux level achieved was 2.52 kw/cm^2 which occurred at a total discharge power of 258 kw and a chamber pressure of 15 atm (i.e., at the maximum power condition discussed previously). This flux corresponds to an equivalent black-body radiating temperature T^* of 4670 K.

In Fig. 16, the variations of radiation efficiency, total discharge power, and argon weight flow rate with chamber pressure are shown for the test conditions of Figs. 14 and 15. As expected, modest increases in chamber pressure result in significant increases in the fraction of total discharge power that is radiated through the inner fused silica tube. As the chamber pressure was increased to approximately 15 atm and above, this fraction approached 0.8. Note that, in general, as the chamber pressure was increased, the total discharge power and argon weight flow rate were also increased. Increasing the chamber pressure allows operation of the r-f plasma in a highly radiation-dominated mode, assuming accompanying increases also occur in total discharge power and argon weight flow rate. These accompanying increases are necessary to maintain a satisfactory, stable discharge. The effect of increasing the total discharge power on the radiation efficiency at nearly constant pressure is discussed in Ref. 7. In general, the radiation efficiency decreases somewhat as both the total discharge power and argon weight flow rate are reduced at constant pressure.

Typical test results are shown in Fig. 17 for the power radiated through the peripheral-wall coolant in various wavelength bands. A sketch of the configuration including a photograph taken of the plasma discharge as viewed through a central view port is shown at the top. The test conditions are shown in the lefthand column of the table. Three cases are included: the first is with no dye added to the annular coolant, the second case is with 800 ppm of nigrosine dye added to the annular coolant, and the third case is with a total of 1600 ppm of dye added (resulting in the fraction of total incident radiation transmitted through the water-dye layer being reduced to about 0.1). The approximate distributions of the power radiated through the annular coolant, in kw, in four wavelength bands are shown in the table. Note that, for the first case (no dye), approximately 76 percent of the

total power radiated through the annular coolant is in the wavelength band from 0.72 to 1.3 microns. For reference, approximately 64 percent of the radiation from a black-body at 3910 K (maximum level expected in in-reactor unit cell) is between 0.25 and 1.3 microns.

The second and third cases shown in Fig. 17 illustrate the effect of adding relatively strong concentrations of dye to the annular coolant. For both cases, the percent of total power radiated through the annular coolant that is in the 0.72- to 1.3-micron wavelength band was approximately 88 percent. For the third case, the dye concentration was sufficient to reduce the total radiation transmitted by an order of magnitude (as expected based on the data in Fig. 7(b)).

Results of Spectral Emission Measurements

Spectral emission measurements were made using the optical system shown in Fig. 8 to obtain an estimate of the temperature distribution in the r-f plasma discharge. Measurements were made at the axial midplane and midway between the axial midplane and the end wall. The monochromator system was aligned so that it scanned across chords of the discharge at the desired axial location. The absolute value of the plasma continuum radiation was measured at a wavelength of 4320 Å. By assuming thermodynamic equilibrium, the radial temperature distribution through the plasma was determined from the continuum radiation measurements using the method described in Ref. 18 for relating the continuum intensity to the temperature. A machine program employing the Abel inversion method was used to convert the measured chordal intensities to radial intensities. A complete description of the data reduction techniques is presented in an appendix of Ref. 19.

A sketch of the configuration and chordal scan locations is shown at the top of Fig. 18. The test conditions were the same as those shown in Fig. 17. Two typical radial distributions of temperature are shown in Fig. 18, one at the axial midplane and one midway to the end wall. The plasma radius determined using the fiber optic scanning system is also shown. Both temperature profiles exhibit the distinct off-axis peak noted in previous tests (e.g., Ref. 7). The peak temperature for the axial midplane location was approximately 11,500 K and occurred off the axis at about the midradius. The peak temperature for the other profile was about 11,000 K, also occuring at approximately the midradius. Comparison of radiated power per unit volume with temperature for an argon plasma using the test conditions corresponding to those in Fig. 17 and the theoretical results presented in Ref. 7 over the wavelength range from 0.3 to 1.0 microns indicate an average temperature difference of approximately 600 K exists between the calculated and the measured temperatures (based on integrated average intensity). This difference is considered to be within the accuracy of the measurement technique, data reduction procedure, and assumptions used. Reference 7 contains additional information on the r-f argon plasma radiant energy source ultraviolet portion of the spectrum between about 0.15 and 0.43 microns.

Summary of Key Results and Comparison with In-Reactor Test Unit Cell Conditions

Figure 19 summarizes the results of all tests conducted with the 2/3-scale in-reactor radiant energy source configuration without simulated fuel injection. The variation in radiant energy flux with total power deposited in the r-f plasma discharge is presented. The equivalent black-body radiating temperature, T^*, is given on the right-hand ordinate. The horizontal dashed lines indicate the range of flux levels expected in an early in-reactor test (i.e., $3333 \leq T^* \leq 3910$ K). The shaded area indicates the envelope of all data. The range of steady-state equivalent black-body radiating temperatures achieved in the tests reported herein bounded, by a considerable margin, the range of flux levels expected in early in-reactor tests. The maximum T^* achieved, 4670 K, exceeds the maximum T^* expected in early in-reactor tests by approximately 18 percent. The calculated fuel-cloud-radius-to-cavity-radius ratio of the in-reactor configuration is 0.6. The maximum ratio of the plasma-discharge-radius-to-peripheral-wall-radius obtained in the r-f plasma radiant energy source tests was 0.44.

The early in-reactor tests require chamber pressures of about 500 atm. The highest chamber pressures in these tests with fused silica tubes was 22.5 atm. At chamber pressures above 22.5 atm, the inner fused silica tube fractured due to excessive hoop and thermal stresses. To permit increases in chamber pressure, initial tests of filament-wound pressure vessels for use in future high pressure r-f plasma radiant energy source tests were conducted. These are described in the following section.

Tests with Filament-Wound Pressure Vessel Configuration

Preparatory Hydrostatic and R-F Tests without Plasma Discharge

Prior to using the configuration shown in Figs. 10, 11, and 12 in r-f radiant energy source tests, cyclic hydrostatic tests were conducted to verify that the assembled configuration was suitable for safe use at pressures up to 40 atm. The filament-wound pressure vessel used in these tests was wound using resin L-266 (details of the resins used in the filament-wound pressure vessel development program are discussed later). In these tests, the internal pressure on the liner and filament-wound pressure case was increased to 50 atm (to provide 10 atm factor of safety), maintained for 5 min, and then reduced to 1 atm. This procedure was repeated 10 times. A vernier caliper, sensitive to approximately 0.25 mm, was attached to measure the radial expansion. No detectable change in the diameter of the pressure vessel was noted over the range of pressures from 1 to 50 atm. Some pinching of the rubber liner was noted during post-test inspection. Minute traces of rubber were found between several of the axial plies on the inside surface of the pressure vessel. This is attributed to movement of some of the inner axial plies of the filament-wound tube under pressure. The small circumferential displacement of these axially oriented fibers near the inner surface of the tube did not affect the water-tight sealing of the rubber liner. It is anticipated, however, that as chamber pressures in future r-f plasma tests reach levels significantly above 50 atm, additional circumferential plies may be required to limit expansion of the pressure vessel. It may also be desirable to increase the thickness of the rubber liner.

United Aircraft Research Laboratories UNITED AIRCRAFT CORPORATION

October 15, 1971

National Aeronautics and Space Administration
Washington, D. C. 20546

Attention: Office of Technical Information
and Educational Programs, Code ETL

Subject: Transmittal of reports comprising the second Interim Summary Technical Report under Contract SNPC-70, "Investigation of Gaseous Nuclear Rocket Technology"

Enclosures:
(A) Report K-910900-7
(B) Report K-910900-8
(C) Report K-910900-9
(D) Report K-910900-10
(E) Report K-910900-11
(F) Report K-910904-2
(G) Report K-990929-2

Gentlemen:

Copies of seven reports, Enclosures (A) through (G), which comprise the second Interim Summary Technical Report under Contract SNPC-70 between the joint AEC-NASA Space Nuclear Systems Office and the Research Laboratories of United Aircraft Corporation, are being sent to you as part of the general distribution of reports under this Contract.

Very truly yours,

UNITED AIRCRAFT RESEARCH LABORATORIES

George H. McLafferty
Senior Program Manager

GHM/svd

Following the hydrostatic tests, tests were conducted using the 1.2-megw r-f induction heater, but with no plasma discharge present. These tests were conducted to verify that none of the individual components which made up the test configuration heated excessively due to r-f fields. They also served to verify that the clearances between the retainer flanges and main r-f transmission lines were adequate to prevent a possible arc-over. Temperature sensitive paints (covering the range from 360 to 425 K) were applied to many of the components, including the filament-wound pressure vessel (see Fig. 12). The resonator voltage of the r-f system was increased to approximately 4 kv and maintained for several minutes. The results indicated that the large stainless-steel retainer flanges were r-f heating; after several minutes, they reached a temperature of approximately 380 K. Several coils of water-cooled copper tubing were then attached to each flange assembly. In addition, a 0.8-mm thick copper band, acting as an r-f shield, was installed around the cooling coils (see Fig. 12). These modifications provided satisfactory r-f field protection to the flanges.

Exploratory R-F Plasma Discharge Tests

In the first test series, the discharge power and pressure were maintained at low levels (less than about 20 kw and 10 atm, respectively) to develop operating procedures and gain experience with the filament-wound pressure vessel configuration. Because the pressure vessel is opaque, visual observations of the discharge size and shape were not possible. The r-f discharge was started easily using the auxiliary starting system shown in Fig. 5. Only the high-frequency, 15 kHz, high-voltage, 18 kv, starter system was required in these tests. Post-test inspection revealed all components of the test configuration were in satisfactory condition. The 57-mm-ID fused silica tube was clean, as were the end walls. No signs of deterioration were noted on either the liner or filament-wound pressure vessel. Analysis of the data indicated all water-cooling provisions were adequate.

Another test series was conducted at chamber pressures up to 22.5 atm. These tests were terminated due to the appearance of smoke in the vicinity of the filament-wound pressure vessel. Inspection of the pressure vessel revealed the source of the smoke to be localized r-f heating of the resin in the filament-wound tube. The surface of the tube was charred over a confined area (≈ 4 cm^2) beneath one of the r-f work coils.

The amount of power per unit volume (w/cm^3) dissipated in the tube material is given by

$$P_{r-f} = 0.556 \times 10^{-12} f \epsilon E_o^2 \tan \delta$$

where f = r-f operating frequency in Hz, ϵ = dielectric constant of the resin, E_o = electric field strength in volts/cm, and $\tan \delta$ = dissipation factor for the resin.

Calculations indicate that approximately 25 to 50 watts of r-f power could be dissipated in that local area due to r-f heating of the resin. To determine if the r-f heating to the resin had weakened the filament-wound tube, a post-test hydrostatic pressure check was conducted. The tests indicated that no damage to the structural strength of the vessel had occurred. It was concluded that a resin having a dissipation factor substantially lower than that of L-266 was required.

A new pressure vessel was fabricated using resin type 63. Cyclic hydrostatic tests to 50 atm were then conducted, with satisfactory results, and r-f plasma tests were resumed.

Summary of Key Results of R-F Plasma Discharge Tests

To determine the effect of chamber pressure on the other discharge characteristics, the argon weight flow rate was maintained approximately constant during the tests ($P_D > 6$ atm). In addition, the saturable reactor power control was not varied at pressures above 20 atm; thus, the total power deposited into the plasma was determined by the other parameters. A breakdown of the power losses for the highest pressure operating point, 40 atm, is shown in Fig. 20. For this test, a total of 35 kw was deposited into the plasma discharge. Other test conditions are shown at the top of Fig. 20.

As shown in Fig. 20, sixty-six percent of the total power deposited into the discharge, or 23.1 kw, was absorbed by the water-dye coolant at this 40-atm test condition. Both end-wall assemblies absorbed a total of 5.6 kw, or 16 percent of the total power deposited into the discharge. The remaining power, 6.3 kw or 18 percent, was deposited into the exhaust gas heat exchangers. The opaque nature of the pressure vessel and liner combined with the heavy concentration of the dye in the annular cooling resulted in no measurable amount of radiation being emitted.

It is estimated that the discharge diameter was about 2.5 cm, based on previous tests with the fused silica pressure vessel at similar test conditions, except for lower pressure.

Figure 21 summarizes the results of the test series conducted with the filament-wound pressure vessel at pressures from 1 to 40 atm. As mentioned previously, no attempt was made to maximize the plasma discharge power as the pressure was increased above 20 atm --- the saturable reactor power control and the argon weight flow rate were held approximately constant. Figure 21(a) shows the variation of total discharge power with chamber pressure for these tests. Note that the total discharge power decreased at pressures above about 20 atm. Figure 21(b) shows the effect of chamber pressure on the fraction of total discharge power deposited into the annular coolant. Results from a similar test at lower pressure, conducted using a fused silica pressure vessel, are shown by the square symbols in Figs. 21(a) and (b). It is evident in both tests that a decrease in total discharge power accompanying an increase in chamber pressure results in a decrease in the fraction of total power deposited into the annular coolant. This is also shown in the results of Ref. 7.

The maximum chamber pressure was limited to 40 atm by the pressure capability of the existing cooling water flow system --- primarily by the glands and pressure case of the positive displacement pump. Operation at 40 atm for several minutes also resulted in overheating of the high-pressure pump motor.

Inspection of the test configuration revealed no internal damage or indications of local r-f heating. The 57-mm-ID fused silica tube was clean, as were the polished end walls. Inspection under polarized light indicated that the fused silica tube had no induced residual thermal stresses.

Future modifications to the pressure capability of the supporting hardware (in particular, the cooling water systems) will permit operation at significantly higher pressures. No r-f system limitations were evident to indicate it would not be possible to operate an argon r-f plasma at 500 atm, the chamber pressure corresponding to reference engine and early in-reactor unit cell test conditions.

SIMULATED-FUEL INJECTION PROGRAM

Introduction

Operation of the nuclear light bulb engine and in-reactor test unit cell requires that gaseous or particulate fuel be continuously and uniformly injected into the fuel region of the vortex. Successful operation of the engine also depends on employing a transparent buffer gas, injected near the inner surface of the transparent wall to form the vortex which contains and isolates the fuel from the wall. Further, it is necessary to achieve ratios of fuel partial pressure to chamber total pressure of about 0.3, and to minimize diffusion of the fuel to the transparent wall. Additional related conditions expected for the reference engine and in-reactor test unit cell are shown in Table I.

The overall objective of the simulated-fuel injection program was to initiate development of small-scale models and the associated technology necessary to simulate the conditions which are expected to exist in the fuel region of nuclear light bulb reactors. Specific goals included developing and testing, using the 1.2-megw r-f induction heater, an approximately 2/3-scale version of an early in-reactor test unit cell with simulated-fuel injection. The aim of these initial tests was to inject seed materials into the discharge region in reasonably heavy concentrations with minimum deposition of the seed material on the transparent peripheral wall.

Description of Equipment and Procedures

Test Chamber Configuration and Simulated-Fuel Injection Probes

Figure 22 shows a cross section of the test configuration. The test configuration was similar to that shown in Fig. 10 except that a fused silica pressure vessel was used. This configuration was selected since it permitted rapid installation and removal of the test chamber from the test tank.

Eight 0.234-cm (0.092-in.)-ID stainless steel vortex injectors were located equally spaced around the periphery of each end wall. The injector tips were flush with the end-wall surface and were positioned such that the argon entered the test chamber in the circumferential direction only. The total injection area, A_j, was 0.685 cm^2 (0.106 $in.^2$). This injector size and arrangement was selected to minimize the radial accelerations present in the fuel region; it was desirable to achieve g levels comparable to those expected in an early in-reactor test configuration, i.e., 20 to 50 g. A thru-flow port diameter of 0.792 cm (0.312 in.) was used to compensate for the blockage due to the presence of the simulated-fuel injection probes and to provide a slightly larger exhaust area than used in tests without simulated-fuel injection. A static pressure tap was located near the periphery of the end wall for measurement of the chamber pressure.

Figure 22 shows one of the symmetric pair of simulated-fuel injection probes used in the tests. The probes were located concentrically within the thru-flow ducts and protruded 1.90 cm (0.75 in.) into the test chamber from the faces of the

end walls. Figure 23 shows a sketch and photographs of the simulated-fuel injection probe. These 17.8-cm-long water-cooled probes were fabricated from three concentric tubes as illustrated by the cross-sectional sketch in the upper left of Fig. 23. A polished copper end cap formed the tip. The probes were assembled using silver solder and were pressure checked to 50 atm. The coolant flow directions are shown in Fig. 23.

Figure 24(a) is a photograph of the configuration installed in the 1.2-megw r-f induction heater test tank as viewed through the central view port of the tank. The Micalex vertical support brackets under each copper end-wall assembly locate the test chamber concentrically within the r-f work coils. The off-axis location of the exhaust gas heat exchanger is also visible. Figure 24(b) is the same view except the r-f plasma discharge is present. The probes protruding into the plasma discharge region are evident in this photograph.

Based on the results of exploratory tests with the configuration shown in Fig. 22, the r-f plasma could be initiated in the test chamber without the use of the auxiliary starting system. The resonator voltage required for breakdown to occur within the test chamber was significantly lower than that which was required using the other configurations of this test program. The argon flow rate and chamber pressure had to be maintained at relatively low levels, however, for this starting procedure to be employed. This procedure permitted the simulated-fuel injection probes to be permanently located within the test chamber, thus eliminating the need for high pressure seals and a probe actuation system. It also provided an uncontaminated argon r-f plasma during the start-up.

Gaseous Simulated-Fuel Handling System

Figure 25 is a schematic of the flow system used in tests employing tungsten hexafluoride (WF_6) and uranium hexafluoride (UF_6) as simulated fuels. The schematic also shows the pressurized argon system used for the vortex buffer-gas injection. A glass-lined pressure canister (rated working pressure of 10 atm) was used to store the premixed simulated fuel. The following batching procedure was used: (1) the canister was evacuated; (2) the desired amount of simulated fuel vapor was introduced by placing the simulated-fuel storage vessel in a cold bath at the temperature corresponding to the desired vapor pressure and allowing the pressures to equalize; and (3) the canister was charged with argon carrier gas to the desired pressure (normally 10 atm). Figure 25 shows the location of the various flow metering and monitoring equipment used. A neutralizing gas trap was fabricated and located on the roof of the laboratory. A valve arrangement permitted by-passing the exhaust trap for tests not employing simulated fuels. Electrical resistance heater tape was used to maintain the copper lines transporting the simulated fuel and argon carrier at an elevated temperature.

Particulate Simulated-Fuel Dispersal System

Injection of simulated fuel in particulate form offers advantages over gaseous fuel injection, particularly from the standpoint of preventing condensation of simulated fuel in the fuel injection duct at high pressures. Figure 26 is a schematic

of the particle feeder system used. Argon served as the carrier gas and micron-sized tungsten particles (1-10 microns nominal diameter) were used as simulated fuel. The feeder system consisted of a powder canister mounted on an electromagnetic vibrator, a variable-speed worm screw to meter powder out of the canister, and a carburetor and deagglomeration chamber to disperse the powder within the argon carrier gas. The pressurizing connection between the canister and the main carrier gas stream (see Fig. 26) serves to equalize the pressure at both ends of the metering screw. The electromagnetic vibrator aids in preventing agglomeration of the particles and stratification of particles of different bulk densities. The vibration amplitude is adjusted by means of a potentiometer. The powder flow rate is determined primarily by the rotation speed of the feed-screw. The powder canister was limited to a working pressure of 3 atm.

Discussion of Test Results

Tests with Gaseous Simulated-Fuel Injection

Several exploratory tests were conducted to investigate the effects of the argon buffer-gas weight flow rate, chamber pressure, argon carrier-gas weight flow rate and injection velocity on the behavior of the discharge. The effects of varying the buffer-gas flow rate and chamber pressure on the discharge behavior in this configuration agreed with the trends noted previously for configurations without simulated-fuel injection. Various discharge diameters and shapes could be obtained, ranging from a relatively small-diameter (≈ 1.5 cm) cylindrical plasma with conical end regions to a relatively large-diameter plasma (≈ 2.8 cm) with almost cylindrical end regions (i.e., approximately square corners near the end walls). This latter case was obtained at moderate pressures (< 10 atm) and at low argon weight flow rates (< 1.35 gm/sec). In this mode of operation the discharge was very sensitive to changes in any of the primary variables. Part of this may be attributed to the relatively low power levels used in the initial tests. An interesting observation was made when investigating the effect of varying the argon carrier-gas flow rate on the behavior of the discharge. A darkening of the discharge core in the vicinity of the probe was noted at low injection flow rates; as the argon carrier-gas flow rate was increased, the core became darker and extended along the entire axis of the discharge. The effect of this cold carrier gas injected into the plasma discharge was also noted in the measurement of the total radiation emitted from the test chamber. The radiation decreased, possibly indicating that the increased axial convection had reduced the plasma temperature. The results of these tests indicated that simulated-fuel injection flow rates approaching those used in driving the vortex could be used; at higher flow rates, some distortion of the plasma discharge was noted.

A summary of the test results employing gaseous simulated-fuel injection, including the primary vortex flow, simulated-fuel flow, and operating conditions is presented in Table II. The data in the first column correspond to the case of argon carrier gas only (no simulated fuel) being injected into the discharge. The next four cases shown are for increasing concentrations of WF_6, ranging from a low of 1 percent concentration (by partial pressure) relative to the carrier gas

to a high of 8 percent concentration. The argon carrier-gas weight flow rate for the 1, 2, and 4 percent concentration cases were maintained approximately constant at 1 gm/sec. For the 8 percent concentration case, the argon carrier-gas weight flow rate was reduced 25 percent. Note that increasing simulated-fuel flow rates were used in each case.

Figure 27(b) shows the discharge with WF_6 being injected (4 percent concentration case). All tests involved operating the discharge steady-state with the simulated fuel injected for fixed time intervals of 2 or 4 min.

The presence of tungsten in the argon discharge was evident from measurements of the total radiation, from color photographs and high-speed movies of the discharge, and from spectral emission data taken from 0.35 μ (3500 Å) to 0.83 μ (8300 Å). In particular, the argon I 4158.59 Å line, the tungsten 4102.70 Å line, and the continuum at 4320 Å were used. As an example, Figure 28 compares representative emission spectra between 4044 Å and 4334 Å obtained from the argon plasma alone and then with the addition of the WF_6 as the simulated fuel. The data were taken on the centerline of the discharge at the axial midplane for the 4-percent-concentration case. Catalogued Argon I and Tungsten I lines are indicated in Fig. 28 over a wavelength interval where the tungsten lines present were free from the influence of overlapping argon lines. Analysis of all the spectral emission data indicates that several of the argon lines at wavelengths greater than 0.6 μ (6000 Å) occur in regions not affected by the presence of the tungsten background spectrum. In future tests involving stronger concentrations of simulated fuel, it is possible that these lines may be used to calculate the radial temperature distributions within the discharge.

After each test period for a fixed time interval, the front dome was removed and the fused silica tube that formed the inner peripheral wall was carefully inspected. No significant deposition of tungsten was noted on the peripheral wall in any of these tests. These results are most encouraging since tungsten weight flow rates corresponding to the 8-percent-concentration case approach 0.6 gm/sec (1.3×10^{-3} lb/sec). Eight percent concentration was the maximum achievable with the existing pressure canister and batching procedures. There were no indications that higher concentrations could not be employed in future simulated-fuel injection tests.

The sixth case in Table II corresponds to the test conditions using 0.5 percent concentration by partial pressure of UF_6. This concentration was the maximum that could easily be batched using the existing equipment at the time of the tests. A new system with increased capability was built but could not be tested due to time limitations. Figure 29 shows the vapor pressure curves for tungsten hexafluoride and uranium hexafluoride. This comparison serves to illustrate the difficulty in batching and handling UF_6 as compared to WF_6. For example, to inject pure UF_6 into a test chamber at 5 atm without condensation occurring in the inlet lines requires wall temperatures in excess of the boiling point of water. Comparison of the triple points of WF_6 and UF_6 indicates that higher temperatures are required for higher concentrations of UF_6 as the simulated fuel. The addition of the heater tapes (see Fig. 25) to the fuel handling system help to maintain the line temperatures high enough to eliminate any fuel condensation. The argon carrier-gas weight flow rate for this test with UF_6 was set at about 0.5 gm/sec. The test

involved operating the discharge steady-state with the simulated fuel injected for 4 min. As with the tests employing WF_6 as the simulated fuel, the presence of uranium in the argon discharge was evident from the diagnostic measurements of radiation and the spectral emission data. Post-test inspection of the fused silica tube revealed no significant deposition of uranium or uranium compounds.

Tests with Particulate Simulated-Fuel Injection

Several tests were conducted using 1 to 10 micron nominal diameter tungsten particles and the particle feeder system shown in Fig. 26. Typical results are shown in the last column of Table II. As noted, the tests were conducted at test conditions similar to those used in the gaseous simulated-fuel injection tests. The chamber pressure was only 2 atm due to the pressure limitation of the powder canister. Due to the low chamber pressure, the argon vortex weight flow rate was reduced slightly to permit maintaining relatively low radial accelerations. The tungsten seeds were fed into only one of the simulated-fuel injection probes; otherwise the configuration was the same as that shown in Fig. 22. The estimated average tungsten concentration was 89 percent. The test duration was for two minutes. Some pulsations were noted in the seed feed system in cold-flow tests; these were also evident during the r-f tests. Pulsations occurred in the electrical parameters of the discharge and in the diagnostic read-outs. In addition, some larger diameter particles were noted rotating in the test section (at approximately the axial midplane) during the tests. Post-test inspection of the inner fused silica tube indicated some wall coating. However, the deposit was easily washed from the tube indicating that it consisted of small particles and not plating such as would occur if tungsten vapor had been condensed on the tube. In addition, about 2 gm of tungsten particles ($\approx 100\ \mu$ dia) was found inside the test chamber.

These results are encouraging but indicate further research on developing a feeder system to operate at high pressures is required. Successful operation of the nuclear light bulb engine and in-reactor test unit cell requires that gaseous or particulate fuel be continuously and uniformly injected into the fuel region of the vortex at high pressures (500 atm). Further, it is necessary to achieve ratios of fuel partial pressure to chamber total pressure of about 0.3 and to minimize diffusion of the fuel to the transparent wall. From the standpoint of partial pressure ratios, if a uniform distribution of seed material in the test volume and complete thermal and chemical equilibrium is assumed, then for the test case using tungsten particles, the volume-averaged fuel partial pressure ratio would be about 0.39. Unfortunately, due to the strong temperature gradients present within the test chamber, uncertainty in the uniformity and mass flow rate of the particle seed material used, and in particular its distribution within the fuel region, it was impossible to estimate the actual volume averaged fuel partial pressure ratio. Future complementary research should be directed toward development of diagnostic techniques for measuring the average partial pressure of simulated fuel in an opaque test chamber at in-reactor test conditions.

TRANSPARENT-WALL MODEL PROGRAM

Introduction

The nuclear light bulb engine requires a transparent wall to separate the propellant region from the fuel region and to contain the fuel region vortex flow. This transparent wall must have structural integrity, provision for internal cooling, and provision for tangential injection of a buffer gas. Absorption of thermal radiation from the fuel region by the wall must be minimized.

The transparent wall structure for each unit cavity of the reference engine (Fig. 1(a)) is 48.9 cm in diameter by 182.9 cm long. The size of the structure, combined with the above constraints, make conventional transparent-wall designs unsuitable. The bursting stress due to coolant pressure drop in a 182.9-cm length precludes use of two large-diameter concentric tubes or a continuous coiled structure. The most suitable structure would consist of a large number of short, small diameter, thin-walled tubes formed in a circumferential arrangement with provision for neon buffer-gas injection, such as the arrangement shown in Fig. 1 of Ref. 20. Some pertinent dimensions, heat loads and coolant flow rates for the reference engine wall are listed in the first column of Table III.

Internal cooling of the transparent wall is required to remove heat deposited by radiation, conduction and convection. Hydrogen will be employed as the wall coolant due to its high heat capacity and high radiation transmission at low temperatures. The walls must be thin (approximately 0.125 mm) to conduct the heat to the coolant with a suitable wall temperature drop. The inner wall temperature must be high enough (about 800 C) to allow thermal annealing to reduce coloration opacity due to irradiation from the fuel, yet low enough to maintain high wall strength and minimize devitrification (which normally occurs in fused silica at temperatures of about 1100 C). Therefore, the temperature of the wall must be maintained between relatively narrow limits. Favorable results of recent experiments described in Ref. 21 indicate that the net effects of ionizing radiation and optical bleaching of the fused silica may enable a greater temperature difference across the wall to be used (ΔT of approximately 500 C). In the engine calculations (Ref. 22), the allowable temperature difference across the wall was assumed to be 111 C. The total heat deposited in the wall is about equally divided between heating from the propellant region side and heating from the fuel region side.

As presently conceived, the engine transparent wall will be made from high purity fused silica. High purity (consequently, high transmission) is necessary to minimize thermal radiation deposition in the walls. The opacity of the wall material in the ultraviolet portion of the spectrum is the primary factor governing radiant heat deposition in the transparent wall. Substitution of single-crystal beryllium oxide for fused silica as the transparent-wall material would result in a significant reduction in the ultraviolet cutoff wavelength and a corresponding increase in permissible fuel radiating temperature (Ref. 22). Also, synthetic quartz crystals have been successfully grown with ultraviolet cutoffs as low as 0.147 microns (Ref. 23). However, the difficulty of growing single-crystal beryllium oxide or quartz, as well as the necessary handling and forming

operations, preclude their use in tests at the present time. The method most likely to be successful in reducing the wall heat deposition is to seed the fuel and buffer gas with a material which absorbs in the ultraviolet portion of the spectrum where the wall has high absorption characteristics. Further discussion of this approach is available in Ref. 11.

The region outside of the transparent wall in the reference engine will contain hydrogen propellant seeded with tungsten particles to increase its opacity. An unseeded buffer layer of hydrogen will be maintained along the transparent wall to keep the seeds off the wall.

The ultimate purpose of the transparent-wall model program is to simulate, as much as possible, the thermal environment of the actual transparent wall using the 1.2-megw r-f induction heater. One objective in the present program was to continuously increase the discharge power and radiant energy flux at the model wall to higher levels. Another objective was to increase the operating pressure up to 20 atm and to utilize axial coolant tubes with wall thicknesses down to 0.125 mm.

Previous work in this program (see Refs. 7 and 20) resulted in improved techniques and a great amount of experience in model fabrication. However, operation of these models to higher powers was limited by inadequate cooling of the peripheral-wall injectors. Accordingly, in the present program, highly cooled peripheral-wall injectors and end walls were designed. The model assembly was designed to take advantage of the increased ease of access in the 1.2-megw heater test tank provided by the modifications described previously in this report.

Description of Equipment and Procedures

Transparent-Wall Model Configurations

Several model configurations utilizing both 0.125- and 0.25-mm wall thickness axial coolant tubes with compressed air and water cooling, respectively, were tested. Sketches of the basic model configuration are shown in Figs. 30 and 31. The model consists of fused silica peripheral walls, two internally cooled copper end walls, and two diametrically opposed peripheral-wall argon injectors which span the vortex chamber. The end walls for this model are similar to those used in the simulated-fuel injection tests discussed previously (see Fig. 22) with the exception that the end-wall argon vortex injectors were eliminated and slots for the axial coolant tubes and peripheral-wall injectors were added. The end walls were designed to successfully withstand a heat flux of at least 1.5 kw/cm^2 when operated with high pressure (20-atm inlet pressure) cooling. This calculated heat flux is based on zero reflectivity at the surface. For comparison, the highest heat flux at the end walls in all tests to date in the 1.2-megw r-f heater is approximately 0.8 kw/cm^2. Two concentric fused silica tubes are located between the end walls to form the pressure vessel for the model. Cooling water (usually with nigrosine dye added to attenuate radiation) flows in the annulus between the two tubes.

The hot argon gas exits from the vortex chamber into the thru-flow ducts where it is cooled approximately to ambient temperature by the end-wall cooling and the thru-flow heat exchangers. The thru-flow disconnects and heat exchangers (see Fig. 30)

are removable, which allows rapid disassembly of the model for replacement of the axial coolant tubes.

The axial coolant tubes and the peripheral-wall injectors are shown in detail in Fig. 31. The axial coolant tubes are installed at a diameter of 3.25 cm in two segments separated by the two diametrically opposed peripheral-wall injectors. The tubes are sealed in the slots in the end walls using a silicone rubber potting compound (RTV).

A new method was devised in the present program to reduce the turn-around time required to fabricate the model. In this method, the tubes are first potted as a flat wall segment in a jig using a liquid version of the normal silicone rubber potting compound (RTV). This assures that the RTV will flow into the narrow gaps between the tubes where most leaks occurred in past models. Two of these wall segments can then be easily potted into the slots in the model end walls.

The peripheral wall injectors shown in Fig. 30 are designed with the water cooling passage located between the high temperature plasma and the argon plenum for maximum cooling efficiency. These injectors are theoretically capable of withstanding a heat flux of at least 1.8 kw/cm^2 with the cooling water at 20 atm inlet pressure and assuming zero reflectivity of the inner surface. The argon is transmitted from the plenum through the water passage and injected into the vortex chamber using a total of 144 copper hypo tubes having a total injection area of 0.292 cm^2. The hypo tubes are 0.5-mm-ID by 0.9-mm-OD with a length to diameter ratio of approximately five.

Although the peripheral wall injectors are primarily designed for greatly improved cooling characteristics, maintaining good injection flow characteristics is also important to obtain a low level of turbulence in the vortex flow. A low turbulence level results in a low convective heat load to the transparent wall and to the peripheral-wall injectors. To obtain a qualitative indication of their flow characteristics, the peripheral-wall injectors were installed in a lucite-walled model and flow visualization tests were conducted using water. The model had the same basic dimensions (3.25-cm ID by 10.16-cm long) as the transparent-wall model tested in the 1.2-megw r-f heater.

Two flow visualization models were tested, one having smooth peripheral walls, the other having a rough wall formed by bonding 1.53-mm-OD tubes over part of the model peripheral wall. The rough-wall model configuration is shown in Fig. 32. Four 0.190-cm-ID tubes on each end wall were used to remove bypass flow. As in the transparent-wall model, the thru-flow ports were 0.793-cm in diameter. Three dye injection locations were used: (1) in the peripheral wall, 3.4 cm (one-third the chamber length) from the end wall, (2) in the peripheral wall at the axial midplane, and (3) on one end wall at the midradius. The vortex injectors and all dye injectors were mounted flush with the wall surface.

The models were tested at several bypass ratios and configurations. A complete list of all test conditions is given in Table IV. Observations of the dye streamers indicated that the injectors produced flow patterns as good as, or better than,

those obtained with any past peripheral-wall injectors. However, there was a noticeable amount of turbulence in the buffer region due to jet mixing. The degree of turbulence was such that virtually no difference in the flow patterns produced near the periphery of the model was noted for the rough-walled model compared to the smooth-walled model. As noted in past tests (see Ref. 24), a stagnation surface and recirculation zones were formed under proper flow conditions. As in past water tests, bypass flow was required to increase β_t to a sufficiently high value ($\beta_t > 30$) to obtain these flow conditions. In r-f heated tests, bypass flow is not required to obtain a confined plasma discharge. The flow patterns were approximately symmetric about the axial midplane of the model. When dye was injected from either (1) the peripheral wall between the end wall and axial midplane or (2) the end wall, it was noted that most of the dye remained on the side of the axial midplane from which it was injected.

The complete installation of the transparent-wall model in the 1.2-megw r-f induction heater test tank is shown in Fig. 33. The axial coolant tubes and injectors are located concentrically within the r-f work coils. Four 0.97-cm-dia steel compression rods (see Fig. 30) arranged symmetrically at each end of the model transmit the axial load due to the pressure in the model to flanges on the test tank. Axial movement of the flanges is restrained by two 1.27-cm-dia steel tie-rods connecting the flanges. These tie-rods, surrounded by water-cooled copper jackets, are visible in the photograph in Fig. 33. Prior to any heated tests, the total axial strain of the model under pressure was determined experimentally with dial indicators to be less than 0.0127 mm at a pressure of 9 atm. Because of the flexibility of the axial-coolant-tube installation, an axial strain less than 0.25 mm should cause no damage to the fused silica tubes. Thus, it was considered certain that this model installation could easily contain pressures up to 20 atm. Also visible in Fig. 33 are the disconnect points (unions) which allow the model to be easily installed and removed as a unit from under the r-f heater work coils.

Test Procedures

In general, the operating procedures employed with the transparent wall model in the 1.2-megw r-f induction heater are the same as those employed with the other models described previously in this report. One major difference in operating technique is the requirement to maintain the model coolant pressure within plus-or-minus 1 to 3 atm of the chamber pressure to prevent rupture of the axial coolant tubes or their sealant. This was true at least for the water-cooled model tests. In the compressed-air cooled model tests, the coolant pressure could only be maintained within 1 to 7 atm less than the chamber pressure due to leakage of some of the air into the vortex chamber. However, no deleterious effects of this leakage were noted.

Diagnostic equipment and data analysis methods were also the same as those described previously in this report. Complete calorimetric measurements were made of the heat input to all cooling water and gas flows, and of the radiant energy escaping the model. Also, during the tests utilizing compressed-air cooling of the model tubes, photographs of the plasma discharge were taken at selected operating conditions. The diameter of the plasma discharge was determined approximately by

scaling to known dimensions in the photographs. A representative diameter determination for the water-cooled case was not possible due to the multiple reflections occurring within the model test section; this gave a large, diffuse appearance to the discharge, with no defined boundaries. An approximate radiant energy flux was then calculated by assuming an ellipsoidal shape for the discharge.

The starting system employed during transparent-wall model testing is shown in Fig. 5. This starting system is the same one employed in the high pressure tests with the filament-wound pressure vessel except that the 12 kw d-c power supply was also used. To operate the starting system, the starter rods are inserted in the model through the thru-flow ducts. The ends of the rods are positioned near the right end wall such that there is a small gap between them. Upon actuation of the starting system, the 6 kv r-f power supply initiates a small arc between the rod ends. The d-c current to the starter rods is then activated while the left starter rod is simultaneously withdrawn across the vortex chamber. This creates a d-c arc of approximately 3 kw and of sufficient duration to sustain coupling of the r-f to the plasma discharge.

The addition of the d-c power supply to the r-f starting system was found necessary when problems were encountered in the first tests. In these preliminary tests, various methods for initiating a plasma in the central region of the model were attempted. However, all methods resulted in arcing to the peripheral-wall injectors, and argon breakdown outside of the model axial coolant tubes. Initiating a plasma by direct r-f breakdown of argon at 1 atm chamber pressure was attempted first, since this method had proven successful in previous tests with the simulated-fuel injection model. This resulted in damage to the model axial coolant tubes. A start under vacuum (absolute pressure of approximately 5 mm Hg) was attempted, and also proved unsuccessful. Further testing was attempted using the arc starting technique used successfully in the filament-wound pressure vessel tests described in a previous section. However, after withdrawal of the starting rods, breakdown occurred spontaneously outside of the model coolant tubes in the same manner as in the previous attempts described above.

Since these efforts did not solve the starting problems, some basic measurements on the effect of the r-f field on the model geometry were performed to determine the electrical phenomenon causing the arcing and breakdown. To avoid further damage to the model, a mock-up of the end walls and injectors was fabricated. These mocked-up parts simulated the dimensions, location, and material in the actual model, except for the transparent walls themselves.

Tests were conducted in which the amount of r-f heating of the mock-up injectors was measured with the injectors electrically isolated and also non-isolated from the end walls. Also, the azimuthal position of the injectors was varied to determine the effect on breakdown of injector position relative to the transmission line taps and r-f work coil connectors. The results of these tests were inconclusive in that they indicated little difference in the amount of r-f heating with the injectors non-isolated versus isolated. Also, the azimuthal position of the injectors had no noticeable effect on the amount of r-f heating or on any tendency for arcing to the injectors to occur. For all the tests, the steady-state r-f heating of both injectors

was approximately 0.25 kw at 5 kv resonator voltage. However, successful and reliable plasma initiation was obtained with the higher power starting system by employing it at an r-f resonator voltage below that which caused arcing in the model. Once r-f plasma initiation occurred, an increase in the chamber pressure shifted the threshold condition for arcing significantly above the operating voltage and precluded any chance for arc-over or breakdown to occur.

Discussion of Test Results

Tests at High Power and Pressure Operating Conditions

Figure 34 is a summary plot showing the total discharge powers and chamber pressures at which tests were conducted. Table III presents detailed information for the highest power and highest pressure test conditions; it also lists the corresponding values for the reference engine and for an early in-reactor test unit cell.

The highest total discharge power was 116 kw and the highest model chamber pressure attained was 21 atm. Each of these test conditions is at least a factor of two greater than previous tests with a transparent-wall model. The allowable hoop and thermal stresses in the fused silica concentric tubes used as the pressure vessels in the model limited the maximum pressure to approximately 21 atm.

An attempt to increase the total discharge power above 116 kw resulted in destruction of the compressed-air-cooled axial tubes, probably due to a combination of several factors. One factor might have been the leakage of cooling air from the model tubes. If the cooling air through the tubes were drastically reduced, the tubes could have failed due to overheating. More likely, the cause of tube failure was the dynamic pressure due to the high velocity (33 meters/sec at failure) of the injected argon impinging on the tubes. This seems the most plausible since tube failure occurred only at the locations directly in line with the injected argon. This force, combined with any devitrification of the fused silica tubes that might have occurred during the several days of testing, could have caused failure of the tubes.

Several methods could be used in future tests to prevent premature tube breakage. The simplest method would be operation at a higher chamber pressure (10.2 atm at failure) to reduce the injection velocity. Another more difficult method would be the use of a solid array of tubes to increase the wall strength.

Gas-cooled models were used extensively in the present program with very good results. Based on heat transfer analysis, it was estimated that the wall temperatures were approximately 30 percent higher for the compressed-air-cooled, 0.125-mm-thick tubes (425 C) than for the water-cooled, 0.25-mm-thick tubes (325 C), at similar test conditions. However, even these higher temperatures were well below the allowable limit (1500 C) for fused silica. In spite of the higher wall temperatures, the use of compressed air cooling results in several advantages, such as increased visibility of the boundary of the plasma discharge.

Figure 35 shows the energy balance for the highest power operating condition. The largest fraction of the discharge power was radiated through the transparent wall and absorbed in the annular water-dye coolant. The total d-c input power was approximately 470 kw and the total discharge power was 116 kw.

Breakdown of Power Radiated and Power Deposited in Model Components

Figures 36 through 39 provide additional information on the power radiated and deposited in various model components over the complete range of test conditions. In all the plots, a dashed line indicates a constant fraction of the total discharge power which was radiated or deposited. The cross-hatched regions are envelopes of data from Refs. 7 and 20.

In Fig. 36, the variation of power radiated through the transparent wall with total discharge power is shown. For the water-cooled model tests, these data are conservative since the data are not corrected for the radiated power absorbed by the cooling water in the model tubes. Both the power radiated and the fraction of power radiated were significantly greater in the present tests than in the previous tests reported in Refs. 7 and 20. This was due to the higher total discharge power and the increased operating pressures in the present program.

For the water-cooled model tests, the amount of power deposited in the model coolant tubes, shown by the circle symbols in Fig. 37, was about the same as that in some of the previous tests --- approximately 20 percent --- or slightly greater. Some of the previous tests resulted in greater amounts of power deposited in the model coolant tubes (greater than 50 percent). However, in these tests the plasma was not confined, and virtually all the power deposited in the model coolant tubes was from convection rather than radiation.

The amount of radiated energy absorbed directly by the water in the coolant tubes is indicated approximately in Fig. 37 by differences in the values of the ordinates between the data points for water cooling and those for air cooling. For the water-cooled models, roughly half of the total energy deposited in the tubes and coolant by conduction, convection and absorption of radiation was deposited directly into the water by radiation. This assumes that the amount of radiant energy absorbed directly by the air coolant is negligible.

It is interesting to note that very little of the power radiated from an argon plasma is at wavelengths below 0.3 microns (see Refs. 8 and 25). The uv cutoff wavelengths (50 percent transmittance) for water and the fused silica model tubes are approximately the same (about 0.18 --- see Refs. 7 and 20). Thus, very little of the radiant energy absorbed directly by the water is in the uv portion of the spectrum. In fact, most of the radiant energy deposited directly in the water coolant must be in the ir portion of the spectrum since the ir cutoff wavelength (50 percent transmittance) for water is approximately 1.3 microns while that for fused silica is approximately 2.6 microns (Ref. 7). This is corroborated by the data in Ref. 25 which indicates that approximately 29 percent of the total power radiated from an argon plasma is in the wavelength band from 1.0 to 2.5 microns.

Figure 38 shows the power deposited in the injectors. In the present tests, the power deposited was consistently about 10 percent of the total discharge power. This is greater than the levels in some previous tests since the new injectors have a different cooling configuration and different surface areas exposed to the plasma discharge as a result of the designed increase in cooling capability. The new injectors occupy 12.4 percent of the total peripheral-wall cylindrical surface area. If the peripheral-wall injectors absorbed all of the incident radiation (zero reflectivity), for the cases given in Table III, they would absorb approximately 9 percent of the total discharge power. Combining this with the power absorbed due to convection gives a total power absorbed of 10.6 percent of the discharge power. The fact that this calculated value is greater than the amount of power actually absorbed and that some of the power absorbed was due to direct r-f heating indicates that some of the incident radiation was reflected. From the data of Table III, it is estimated that the peripheral-wall injectors reflected 15 to 25 percent of the incident radiation.

Figure 39 shows the variation of power deposited in the end walls and thru-flow exhausts with total discharge power. It is difficult to make a direct comparison with the data from previous tests due to the differences in model designs and operating conditions. The most significant result from the present tests is that this fraction remained nearly constant with increasing discharge power. It is desirable to reduce this fraction to as low a value as possible. In future tests at higher pressure levels, the fraction radiated should increase, and the fraction deposited in the end walls and thru-flow exhausts should therefore decrease.

Figure 40 shows the variation with chamber pressure of the fraction of total discharge power radiated through the transparent wall. As mentioned previously, the data for the water-cooled model tests are conservative since the data are not corrected for the radiant energy absorbed by the model cooling water. The fraction of the power radiated reached a maximum of about 50 percent for the water-cooled model tests and 60 percent for the air-cooled model tests. All of these radiant energy fractions are less than those attained in other tests with models that did not have a transparent wall (see Ref. 8) or that required in the reference engine (85 percent radiated at 500 atm pressure). However, this may be at least partially explained by variations in other test variables, such as plasma diameter and power level. The shape of a curve through the data in Fig. 40 would be similar to the shape of the curve in Ref. 8, although the magnitude of the fraction of power radiated is less.

The plasma discharge diameter was determined in some of the gas-cooled tests by photographic techniques. The range of the radius ratio, r_6/r_1 (edge of plasma discharge to peripheral wall) for the gas-cooled model tests was approximately 0.40 to 0.64. For the water-cooled model tests the range of the radius ratio, r_6/r_1, was estimated from the gas-cooled test data and the known test conditions to be approximately 0.40 to 0.70. These radius ratios are about 30 to 40 percent greater than those normally obtained in a confined r-f heated plasma discharge with end-wall injection. This appears to be the result of the first use of peripheral-wall argon injection at high power and pressure.

Summary of Key Results and Comparison with Reference Engine and In-Reactor Unit Cell Conditions

The primary objectives in the present program were to test transparent wall models to the highest possible discharge power at pressures up to 20 atm using axial coolant tubes with wall thicknesses down to approximately 0.125 mm. In obtaining high discharge powers it is important to maximize the radiant energy flux from the fuel region and to minimize the total heat deposited in the transparent wall. The direct-on spectral measurements of an argon plasma discussed in Ref. 8 have shown that there is very little radiation in the uv portion of the spectrum below the lower cutoff of fused silica. Thus, with a completely clean transparent wall, virtually all of the heat deposited in the wall is due to conduction and convection.

Several key parameters pertinent to the transparent wall are listed in Table III for the reference engine, the in-reactor test configuration, the present program, and for previous tests. In the present program, the highest total discharge power obtained was 116 kw and the maximum chamber pressure was 21 atm. For the highest power test, the radiant heat flux incident on the transparent wall was about 0.77 kw/cm^2. This compares with 23.4 kw/cm^2 for the reference engine. It is presently estimated that the in-reactor unit cell will have a radiant heat flux of 0.40 to 0.76 kw/cm^2 at the reflective aluminum wall. The radiant heat flux in these tests is difficult to determine since the radiant energy absorbed by the transparent wall can not be precisely separated from the convected energy. For the present tests, the radiant energy absorbed in the wall was estimated from the data obtained in the gas-cooled model tests.

The maximum chamber pressure in these tests was limited by the allowable hoop and thermal stresses in the fused-silica tubes used as the model pressure vessel. To increase the model operating pressure would require the use of a stronger pressure vessel which would require extensive modifications to the model. These modifications might include the use of a filament-wound pressure vessel in future tests. The maximum total discharge power was limited by the available time for repair and testing of the model after premature axial coolant tube failure occurred at the 116 kw power level. With appropriate modifications to the model, the experience gained in the present program should lead to significant increases in the total discharge power in future tests.

FILAMENT-WOUND PRESSURE VESSEL PROGRAM

Introduction

This section describes the development and initial tests of filament-wound pressure vessels for use in high-pressure r-f radiant energy source tests. In the future, tests in the 1.2-megw r-f induction heater and in-reactor tests will require that pressures up to 500 atm be employed. At these pressures, standard fused silica tubing, as used in most of the tests described previously, is not practical as a pressure vessel. However, fiberglass filament-wound tubes could be utilized at these pressures, provided they are compatible with the r-f and radiant energy source environment. Previous work in this area (see Appendix A of Ref. 8) resulted in successful pressurization of a small filament-wound tube to 530 atm. However, there was no axial loading of the tube in this test. Also, a filament-wound tube was tested as the pressure shell surrounding an r-f plasma at low power and pressure (Ref. 8).

The objective of the present program was to develop a filament-wound fiberglass pressure vessel capable of operating reliably at a pressure of 500 atm. The pressure vessel was required to carry both the axial and radial loads, and be suitable for use in the 1.2-megw r-f induction heater. This required the use, in fabricating the pressure vessel, of an epoxy resin that does not appreciably r-f heat.

Description of Equipment and Procedures

Two similar configurations of filament-wound pressure vessel test assemblies were designed. One configuration, for heated tests in the 1.2-megw r-f induction heater, has already been described in a previous section and is shown in Figs. 10, 11, and 12. The other configuration, designed for hydrostatic tests up to 500 atm, is illustrated in Fig. 41. In all tests in the present program, both the axial and radial loads are imparted to the pressure shell (rather than to an external fixture). The axial pressure load is transmitted to the filament-wound tube from the end walls by shear forces in the retainer flanges. The retainer flanges each consist of four pieces (to allow installation) and are held in place with cap screws. The silicone rubber sealing liner prevents seepage of water through the wall of the filament-wound tube. A ridge is integrally molded at each end of the liner. This ridge fits into a groove in the sealing ring to prevent leakage at the ends of the tube assembly.

The installation of the spacers shown in Fig. 41 was the result of a detailed review and analysis of the stresses produced when this configuration was pressurized. This was necessary after initial hydrostatic tests resulted in failure of the filament-wound tubes at approximately 300 atm pressure. Details of the results of these tests (and subsequent tests) will be discussed later.

The results of this analysis can best be understood by considering the force diagram shown in Fig. 42(a). The axial load, U, is transmitted from the end wall to the ends of the filament-wound tube (force F) by the retainer flanges. Since

the loading is approximately uniform over the surface, this force is assumed to act at the center of the inclined surface at the ends of the tube. The reaction F' to force F, acting at the center of the tube wall, and force F itself form a clockwise couple, Fa. Since the force on the tube ends can only act normal to the inclined surface (resultant force, R), a radial force, G, is established. This radial force and its reaction force G' form a counterclockwise couple, Gb. Because of the fixed geometry, couple Gb is always greater than Fa by a factor of approximately 2 and results in an unrestrained counterclockwise moment on the ends of the tubes. This moment caused buckling of the end of the tube and subsequent shearing of the glass fibers resulting in failure.

Modification of the tube support was made by installing the two spacers at each end of the tube, displacing the end walls and sealing rings inward (see Fig. 42(b)). This displaces the reacting force, G', inward such that the new couple, Gc, (if it exists at all) is clockwise and of small magnitude. The total resulting moment, Gc + Fa, is constrained by the retainer flanges on the tube outer diameter and the sealing ring on the tube inner diameter.

The problem discussed in the preceeding paragraphs was due to the complicated geometry resulting from the constraint that the pressure vessel be designed for installation and tests in the 1.2-megw r-f heater. The resulting geometric limitations, such as the geometry of the end flanges, to permit installation under the heater work coils, are more restrictive than encountered in most applications of filament-wound pressure vessels.

Filament-wound tubes used in this program were made by the Materials Laboratory at United Aircraft Research Laboratories. The method for fabricating the tube to the precise size and shape required by the geometry shown in Fig. 41 is shown in Fig. 43. Not shown in Fig. 43 is the preliminary step of winding several layers of fiberglass and uncured liquid resin on a large cylinder. These layers are partially cured to facilitate handling and then cut into long narrow strips. The strips are placed longitudinally on the mandril assembly in as many layers as desired as illustrated in Fig. 43(a). After installation of the winding rings on the holding pins, the axial strips are doubled over the winding rings with the ends of the fiber strips overlapped. At this point, the circumferential layers of fiberglass are wound as shown in Fig. 43(b). For this part of the winding procedure the holding pins are retracted and the end caps installed. After all hoop layers have been wound, the molding flanges are installed and the tube is cured at the temperature and for the time required by the epoxy resin.

The resin materials used in fabricating the filament-wound tubes were chosen on the basis of their availability, high strength, and low r-f dissipation factor (the latter is a measure of a material's susceptibility to r-f heating). A low dissipation factor was required for the filament-wound tube employed in the high pressure r-f heated tests described in a previous section. The properties of each of the three resin materials used in fabricating all filament-wound tubes are detailed in Table V.

Discussion of Test Results

A summary of the configurations and materials employed in all filament-wound tubes fabricated during the present program is given in Table VI. Also included are the results of the hydrostatic tests. Note that tubes 5 and 6, which had spacers, were longer (25.7 cm, versus 22.9 cm for the others). Longer tubes were required to maintain the same distance between end walls (same liner length) as with the shorter tubes. Spacers were not required in the r-f plasma tests discussed previously since the maximum pressure employed (40 atm) was comparatively low.

The axial and circumferential strain in tube 5 was measured with three sets of dual strain gages located on the wall of the tube at each end and at the axial midpoint. The axial strain (only) in all other tubes was measured approximately using a scale. The modulus of elasticity, E, shown in Table VI was calculated from the average of these strain measurements. There was no defined yield point noted from the strain data and the modulus of elasticity in both the axial and the hoop direction was reasonably constant up to failure of the tube.

Two filament-wound tubes were initially fabricated for hydrostatic testing and one (tube 2 in Table VI) for r-f testing. Tube 1 consisted of four axial layers and eight circumferential layers of fiberglass embedded in the epoxy resin binder. Tube 3 consisted of eight axial layers and ten circumferential layers of fiberglass.

During hydrostatic testing, tubes 1 and 3 failed at a pressure of approximately 300 atm when a retainer flange assembly broke loose. Inspection of the damaged tubes indicated that the axial fibers had broken both on the inside and on the outside of the tubes, near the winding rings. A photograph of tube 1 is shown in Fig. 44(a). The winding ring had separated from tube 1 and the rings on both tubes were distorted due to uneven loading. The fact that tube 3 failed at approximately the same stress loading as tube 1 indicated that the problem existed in the pressure vessel geometry rather than in the strength of the filament-wound tube. This conclusion led to the addition of the spacers as described previously.

The addition of the spacers resulted in successful hydrostatic testing of tube 5 and 6. Tube 6 was maintained at a pressure of 551 atm for more than a minute. However, a small amount of leakage, probably past the ridge at the end of the sealing liner, was noted during this period. During a subsequent test, this tube failed at 484 atm pressure when approximately 4.5 cm (axial distance) of hoop layers unraveled. As shown in the photograph of the tube in Fig. 44(b), the sealing liner then extruded through the separated axial fiber layers. It is believed that failure was caused by shearing of the fiber layers at the edge of the retainer flange. This problem should be easily correctable by redesigning the retainer flanges for a smoother transition at the edge and increasing the number of hoop layers to reduce the circumferential strain at the interface of the flanges with the tube. Prior to failure, tube 6 had been pressurized to 475 atm or greater five times. Tube 5 was pressurized to a maximum of 443 atm but did not fail. At 443 atm the leakage past the ridge at the end of the sealing liner became greater than the flow capacity of the high pressure pump.

As discussed in a previous section, problems were encountered in the r-f heated tests due to r-f heating of the initial filament-wound tube fabricated with epoxy resin L-266 (tube 2 in Table VI). This epoxy was originally selected because it had reasonable strength properties and a lower r-f dissipation factor than the epoxy ERL-2256 successfully tested in Ref. 8. As a result of this problem, filament-wound tube 4 was fabricated using a third epoxy resin (resin 63) with a very low r-f dissipation factor. This tube was employed successfully in the r-f heated plasma discharge tests at pressures up to 40 atm.

The dissipation factors of the epoxy resins alone (without fiberglass) are given in Table V. However, the dissipation factor of a sample composite using the No. 63 epoxy was measured and found to be 0.002 --- an order of magnitude greater than for the epoxy alone. This higher value is due to the fiberglass in the composite. All of the filament-wound tubes tested in this program have been fabricated using standard commercial S-glass which is not a pure fused silica. S-glass has the following composition: SiO_2, 65 percent; Al_2O_3, 25 percent; and MgO, 10 percent. Its dissipation factor is approximately 0.002.[3] Thus, this value is probably the lowest dissipation factor achievable in a fiberglass composite which must withstand high pressures.

The results of these initial hydrostatic (and r-f heated) tests indicate that filament-wound pressure vessels for use in r-f environments at high pressures can be routinely fabricated. However, additional development is required to optimize the electrical, thermal, and mechanical characteristics of the pressure vessel configuration.

REFERENCES

1. McLafferty, G. H. and H. E. Bauer: Studies of Specific Nuclear Light Bulb and Open-Cycle Vortex-Stabilized Gaseous Nuclear Rocket Engines. United Aircraft Research Laboratories Report F-910093-37, prepared under Contract NASw-847, September 1967. Also issued as NASA CR-1030.

2. Clark, J. W., B. V. Johnson, J. S. Kendall, A. E. Mensing and A. Travers: Summary of Gaseous Nuclear Rocket Fluid Mechanics Research Conducted Under Contract NASw-847. United Aircraft Research Laboratories Report F-910091-13, May 1967. Also Journal of Spacecraft and Rockets, Vol. 5, No. 8, August 1968.

3. McLafferty, G. H.: Investigation of Gaseous Nuclear Rocket Technology -- Summary Technical Report. United Aircraft Research Laboratories Report H-910093-46, prepared under Contract NASw-847, November 1969.

4. McLafferty, G. H.: Survey of Advanced Concepts in Nuclear Propulsion. Journal of Spacecraft and Rockets, Vol. 5, No. 10, October 1968.

5. Bauer, H. E., R. J. Rodgers and T. S. Latham: Analytical Studies of Start-Up and Dynamic Response Characteristics of the Nuclear Light Bulb Engine. United Aircraft Research Laboratories Report J-910900-5, prepared under Contract SNPC-70, September 1970. Also issued as NASA CR-111097.

6. Latham, T. S.: Summary of the Performance Characteristics of the Nuclear Light Bulb Engine. AIAA Paper No. 71-642, presented at the AIAA Seventh Propulsion Joint Specialist Conference, Salt Lake City, Utah, June 14-18, 1971.

7. Roman, W. C., J. F. Klein and P. G. Vogt: Experimental Investigations to Simulate the Thermal Environment, Transparent Walls, and Propellant Heating in a Nuclear Light Bulb Engine. United Aircraft Research Laboratories Report H-910091-19, prepared under Contract NASw-847, September 1969.

8. Roman, W. C.: Experimental Investigation of a High-Intensity R-F Radiant Energy Source to Simulate the Thermal Environment in a Nuclear Light Bulb Engine. United Aircraft Research Laboratories Report J-910900-4, prepared under Contract SNPC-70, September 1970. Also issued as NASA CR-110909.

9. Bauer, H. E.: Initial Experiments to Investigate the Condensation of Flowing Metal Vapor/Heated-Gas Mixtures in a Duct. United Aircraft Research Laboratories Report K-910900-9, prepared under Contract SNPC-70, September 1971.

10. Klein, J. F.: Experiments to Simulate Heating of Propellant by Thermal Radiation in a Nuclear Light Bulb Engine. United Aircraft Research Laboratories Report K-910900-8, prepared under Contract SNPC-70, September 1971.

REFERENCES (Continued)

11. Rodgers, R. J., T. S. Latham and H. E. Bauer: Analytical Studies of Nuclear Light Bulb Engine Radiant Heat Transfer and Performance Characteristics. United Aircraft Research Laboratories Report K-910900-10, prepared under Contract SNPC-70, September 1971.

12. Latham, T. S. and H. E. Bauer: Analtyical Design Studies of In-Reactor Tests of a Nuclear Light Bulb Unit Cell. United Aircraft Research Laboratories Report K-910900-11, prepared under Contract SNPC-70, September 1971.

13. Palma, G. E. and R. M. Gagosz: Effect of 1.5 Mev Electron Irradiation on the Transmission of Optical Materials. United Aircraft Research Laboratories Report K-990929-2, prepared under Contract SNPC-70, September 1971.

14. Krascella, N. L.: Spectral Absorption Coefficients of Helium and Neon Buffer Gases and Nitric Oxide-Oxygen Seed Gas Mixture. United Aircraft Research Laboratories Report K-910904-2, prepared under Contract SNPC-70, September 1971.

15. Anon.: International Critical Tables, Vol. V, McGraw-Hill Book Co., Inc., New York, 1930.

16. Lukens, R.: Private Communication. Fisher Scientific Corporation, Springfield, New Jersey, September 1970.

17. Mensing, A. E. and J. S. Kendall: Experimental Investigation of Containment of a Heavy Gas in a Jet-Driven Light-Gas Vortex. United Aircraft Research Laboratories Report D-910091-4, prepared under Contract NASw-847, March 1965.

18. Mensing, A. E. and J. F. Jaminet: Experimental Investigation of Heavy-Gas Containment in R-F Heated and Unheated Two-Component Vortexes. United Aircraft Research Laboratories Report H-910091-20, prepared under Contract NASw-847, September 1969.

19. Jaminet, J. F. and A. E. Mensing: Experimental Investigations of Simulated Fuel Containment in R-F Heated and Unheated Two-Component Vortexes. United Aircraft Research Laboratories Report J-910900-2, prepared under Contract SNPC-70, September 1970. Also issued as NASA CR-111101.

20. Vogt, P. G.: Development and Tests of Small Fused Silica Models of Transparent Walls for the Nuclear Light Bulb Engine. United Aircraft Research Laboratories Report J-910900-3, prepared under Contract SNPC-70, September 1970. Also issued as NASA CR-111100.

21. Palma, G. E.: Optical Absorption in Transparent Materials During 1.5 Mev Electron Irradiation. United Aircraft Research Laboratories Report J-990929-1, prepared under Contract SNPC-70, September 1970.

REFERENCES (Continued)

22. McLafferty, G. H.: Studies of Coolant Requirements for the Transparent Walls of a Nuclear Light Bulb Engine. United Aircraft Research Laboratories Report F-110224-6, March 1967.

23. Ballman, A. A., et al.: Synthetic Quartz with High Ultraviolet Transmission. Applied Optics, Vol. 7, No. 7, July 1968.

24. Travers, A.: Experimental Investigation of Radial-Inflow Vortexes in Jet-Injection and Rotating-Peripheral-Wall Water Vortex Tubes. United Aircraft Research Laboratories Report F-910091-14, prepared under Contract NASw-847, September 1967. Also issued as NASA CR-1028.

25. Marteney, P. J., A. E. Mensing, and N. L. Krascella: Experimental Investigation of the Spectral Emission Characteristics of Argon-Tungsten and Argon-Uranium Induction Heated Plasmas. United Aircraft Research Laboratories Report G-910092-11, prepared under Contract NASw-847, September 1968. Also issued as NASA CR-1314.

LIST OF SYMBOLS

A_S	Discharge surface area, cm^2
A_j	Buffer-gas injection area, cm^2
$A_{j,F}$	Simulated-fuel injection area, cm^2
a	Linear dimension, cm
b	Linear dimension, cm
C	Capacitor
c	Linear dimension, cm
d	Discharge diameter, cm
d_l	Tube diameter, cm
$d_l L/A_j$	Ratio of the product of tube diameter and tube length to injection area, dimensionless
E	Modulus of elasticity, N/m^2
E_o	Electric field strength, v/cm
F	Force, newtons
F'	Force, newtons
f	Frequency, MHz or Hz
G	Force, newtons
G'	Force, newtons
I_λ	Monochromatic intensity, kw/cm^2-ster
$I_{o,\lambda}$	Incident monochromatic intensity, kw/cm^2-ster
$I_\lambda/I_{o,\lambda}$	Internal transmittance, dimensionless
$(I/I_o)_{\Delta\lambda}$	Fraction of total radiation transmitted in wavelength band $\Delta\lambda$, dimensionless
L	Length of unit cavity, test section or transparent wall model, cm or m

LIST OF SYMBOLS (Continued)

L_o	Inductor
P	Total pressure, atm
P_D	Chamber pressure, atm
P_{r-f}	Power per unit volume dissipated in filament-wound tube material due to r-f fields, w/cm^3
Q_C	Power deposited into model tubes and coolant, kw
$Q_{C'}$	Power conducted through inner peripheral wall, kw
$Q_{C,C}$	Total power conducted-convected away from discharge, kw
Q_E	Power deposited in end-wall cooling water, kw
Q_{EX}	Power deposited in thru-flow heat exchangers, kw
Q_I	Total d-c input power to r-f induction heater, kw
Q_J	Power deposited in model peripheral-wall vortex injectors, kw
Q_L	Power convected out the exhaust ducts, kw
Q_R	Radiated power escaping test chamber as measured by radiometer, kw
Q_T	Total discharge power, kw
Q_W	Power deposited in annular coolant by combined conduction, convection and radiation, kw
$Q_{R,T}$	Total radiated power transmitted through the inner peripheral wall, $Q_R + Q_W - Q_{C'}$, kw
R	Force, newtons
Re_r	Radial Reynolds number, dimensionless
$Re_{t,j}$	Injection Reynolds number based on average inlet jet velocity, dimensionless
r	Local radius from center of chamber or discharge radius, cm

LIST OF SYMBOLS (Continued)

r_1	Radius of peripheral wall (cavity wall), cm
r_6	Radius of edge of plasma discharge or fuel cloud, cm
S	Solenoid
T	Temperature, deg K
T(r)	Radial temperature distribution
T_o	Transformer
T^*	Equivalent black-body radiating temperature, deg K
tan δ	Dissipation factor of the resin used in filament-wound tubes, dimensionle
t	Time, sec
U	Force, newtons
V	Discharge volume, cm^3 or velocity, m/sec
V_1	Buffer-gas velocity at the peripheral wall, m/sec
V_j	Average buffer-gas injection velocity, m/sec
V_R	Resonator voltage (zero-to-peak), kv
V_F	Simulated-fuel injection velocity, m/sec
W_A	Argon weight flow rate, gm/sec
W_F	Simulated-fuel injection flow rate through probes, gm/sec
W_C	Coolant weight flow rate, gm/sec
Z_P	Reflected plasma impedance, ohms
β_t	Secondary flow parameter, dimensionless
ϵ	Dielectric constant of the resin material, dimensionless
η	R-F system coupling efficiency, Q_T/Q_I, dimensionless
λ	Wavelength, microns or Angstroms

TABLE I

COMPARISON OF FLOW AND POWER CONDITIONS TO DATE IN FUEL REGIONS OF REFERENCE ENGINE, IN-REACTOR UNIT CELL AND R-F PLASMA RADIANT ENERGY SOURCE

	Reference Engine Configuration (Unit Cavity)	Nuclear Furnace In-Reactor Test Unit-Cell Configuration	R-F Plasma Radiant Energy Source Configuration
Flow Conditions			
Buffer Gas	Neon	Argon	Argon
Fuel	U-233	U-235	WF_6, UF_6
Cavity Pressure, atm	500	500	40
Average Fuel Partial Pressure, atm	175	195-190	---
Fuel Loading, gm (lb)	14.0×10^3 (30.9)	6.2-5.3 (0.014-0.012)	---
Average-Fuel-Density-in-Cavity-to-Buffer-Gas Density at "Edge of Fuel"	0.3	0.25	---
Buffer-Gas Flow Rate, gm/sec	1340	29	2.27-13.6
Buffer-Gas Injection Velocity, m/sec	8.3	2.9	1.52-45.7
Tangential Reynolds Number	9.6×10^5	9.6×10^5	10^4-10^5
Power Conditions			
Power Level, megw	657	0.19-0.342	0.19-0.258
Equivalent Black-Body Radiating Temperature, deg K (deg R)	8333 (15,000)	3333-3910 (6000-7000)	1670-4670 (3000-8400)
Total Power Radiated Through Peripheral Wall, megw	559	0.17-0.32*	0.2
Geometric Characteristics			
Unit Cavity or Unit Cell Shape	Cylindrical	Cylindrical	Cylindrical
Fuel Cloud Shape	Cylindrical	Cylindrical with Constricted Ends	Cylindrical with Constricted Ends
Peripheral Wall Material	Fused Silica	Reflective Aluminum Liner	Fused Silica

*Conducted through reflective aluminum liner.

TABLE I (Continued)

Geometric Characteristics (Cont'd.)	Reference Engine Configuration (Unit Cavity)	Nuclear Furnace In-Reactor Test Unit-Cell Configuration	R-F Plasma Radiant Energy Source Configuration
Inside Radius of Transparent Wall, cm	24.4	8.0	2.85
Fuel Cloud Radius-to-Inside Radius of Transparent Wall	0.85	0.6	0.44
Length of Transparent Wall, meters	1.83	0.213	0.14
Cavity Length-to-Diameter Ratio	3.75	2.7	2.5
Fuel-Cloud-Diameter-to-Cavity Diameter Ratio	0.85	0.6	0.44
Surface Reflectivity of Cavity Liner	0.9	0.9	N/A
$d_1 L/A_j$ - Dimensionless	200	183	116-556

NOTE: Values in last column indicate highest levels achieved in any given configuration to date.

TABLE II

TYPICAL RESULTS AND OPERATING CONDITIONS FOR INITIAL TESTS WITH SIMULATED-FUEL INJECTION

See Fig. 22 for Details of Test Configuration

Configuration Data: $d_1 L/A_j = 116$ $L/d_1 = 2.46$ $A_j = 0.685\ cm^2$ $(0.106\ in.^2)$ $A_{j,F} = 0.045\ cm^2$ $(0.007\ in.^2)$

VORTEX FLOW CONDITIONS	Case 1	Case 2	Case 3	Case 4	Case 5	Case 6	Case 7
Argon Weight Flow Rate, W_A - gm/sec (lb/sec)	2.26 (0.005)	2.26 (0.005)	2.26 (0.005)	2.26 (0.005)	2.26 (0.005)	2.26 (0.005)	1.13 (0.0025)
Vortex Injection Velocity, V_j - m/sec (ft/sec)	4.12 (13.5)	5.34 (17.5)	5.34 (17.5)	4.12 (13.5)	3.2 (10.5)	4.12 (13.5)	5.9 (19.3)
Injection Reynolds Number, $Re_{t,j}$	46.3×10^3	48.0×10^3	48.0×10^3	46.3×10^3	46.8×10^3	46.3×10^3	26.8×10^3
Chamber Pressure, P_D - atm	5	4	4	5	6.5	5	2
SIMULATED-FUEL FLOW CONDITIONS							
Simulated Fuel Used	Argon Carrier Only	WF_6 + Argon Carrier 1% Conc.	WF_6 + Argon Carrier 2% Conc.	WF_6 + Argon Carrier 4% Conc.	WF_6 + Argon Carrier 8% Conc.	UF_6 + Argon Carrier 0.5% Conc.	W Seeds + Argon Carrier Est. Avg. Conc. 8%
Simulated-Fuel Injection Flow Rate, W_F - gm/sec (lb/sec)	0.91 (0.002)	1.04 (0.0023)	1.13 (0.0025)	1.27 (0.0028)	1.59 (0.0035)	1.0 (0.0022)	2.04 (0.0045)
Simulated-Fuel Injection Velocity, V_F - m/sec (ft/sec)	22.6 (74)	32.9 (108)	33.2 (109)	27.2 (89)	21.6 (71)	24.5 (80)	28.2 (92)
Simulated Fuel-to-Vortex Gas Weight Flow Ratio, W_F/W_A	0.4	0.46	0.50	0.56	0.70	0.45	1.8
Simulated Fuel-to-Vortex Gas Injection Velocity Ratio, V_F/V_j	5.5	6.2	6.2	6.6	6.7	5.48	4.77
OPERATING CONDITIONS							
Operating Frequency, f-MHz	5.5242	5.5232	5.5234	5.5242	5.5242	5.5225	5.5796
Power Deposited In Plasma, Q_T - kw	27	32	34	38	39	55	35.5
Reflected Plasma Impedance, Z_p - ohms	203	240	268	274	287	275	206
Total Power Radiated To Radiometer, Q_R - kw (Radiometer Located at Left View Port)	5.5	5	8	10	13	18.2	3.6*

* Includes partial blockage due to wall coating and seed blockage - see text.

TABLE III

COMPARISON OF OPERATING CONDITIONS IN FULL-SCALE ENGINE AND IN-REACTOR GEOMETRY WITH MODEL TESTS AT HIGHEST POWER AND PRESSURE LEVELS

	UNIT CAVITY FULL-SCALE ENGINE REFERENCE ENGINE[a]	IN-REACTOR TEST CONFIGURATION	AXIAL COOLANT-TUBE MODELS					
			TESTED DURING PRESENT PROGRAM				FROM PREVIOUS PROGRAM	
			WATER-COOLED		GAS-COOLED		WATER-COOLED	
			HIGHEST POWER CASE	HIGHEST PRESSURE CASE	HIGHEST POWER CASE	HIGHEST PRESSURE CASE	HIGHEST POWER CASES FROM REF. 7	FROM REF. 20
Transparent-Wall Configuration	Circum-ferential	Axial	Axial	Axial	Axial	Axial	Axial	Axial
Inside Diameter, cm	48.9	6.60	3.25	3.25	3.25	3.25	3.93	3.23
Length Between Containing End Walls, cm	182.9	17.78	10.16	10.16	10.16	10.16	5.09	5.09
Length/Diameter Ratio	3.75	2.7	3.12	3.12	3.12	3.12	1.29	1.59
Number of Coolant Tubes	3000	1[f]	60	60	60	60	69	54
Tube Inside Diameter, cm	0.127	6.60	0.102	0.102	0.127	0.127	0.102	0.102
Tube Outside Diameter, cm	0.152	6.85	0.152	0.152	0.152	0.152	0.152	0.127
Tube Wall Thickness, cm	0.013	0.125	0.025	0.025	0.013	0.013	0.025[b]	0.013
Total Tube Surface Area, cm^2	88500	368.0	291.0	291.0	291.0	291.0	252.0[b]	164.5[b]
Cylindrical Surface Area, cm^2	28100	368.0[f]	90.8	90.8	90.8	40.8	94.0[b]	76.3[b]
Coolant Fluid	Hydrogen	Argon	Water	Water	Air	Air	Water	Water
Buffer Fluid	Neon	Argon	Argon	Argon	Argon	Argon	Argon	Argon
Buffer Injection Velocity, m/sec	7.6[c]	9.8	10.4	4.6	33.0	15.3	69	64
Buffer Weight Flow, gm/sec	1340	25.3	7.7	5.0	16.4	7.7	8.6	5.5
Chamber Pressure, atm abs	500	500	14.9	21.0	10.2	13.6	6.3	5.8
Equiv. Black-Body Radiating Temp., deg K_2	8333	3333-3910	3850	2890	4250	3920	--	--
Radiant Heat Flux at Edge of Fuel, kw/cm^2	27.6	0.67-1.27	1.2[g]	.0.38[g]	1.75	1.28	--	--
Heat Flux Incident on Transparent Wall, kw/cm^2								
Total	23.4	--	0.70	0.24	0.87	0.75	--	--
Due to Radiation	23.4	0.40-0.76[f]	0.56	0.21	0.77	0.64	--	--
Due to Conduction-Convection	--	--	0.14	0.03	0.10	0.11	--	--
Heat From Fuel Region Deposited in Transparent Wall (Per Unit Area), kw/cm^2 [e]								
Total	0.528	--	0.13	0.080	0.076	0.069	0.051	0.307
Due to Radiation	0.234	0.40-0.76[f]	0.09	0.058	0.042	0.044	0.003[d]	0.013[d]
Due to Conduction-Convection	--	--	0.04	0.022	0.034	0.025	0.048	0.294
Total Power In Fuel Region, kw	4.6×10^6	190.-342.	80.0	28.5	116.0	93.4	36.0	51.3

a Data obtained from Refs. 1 and 22

b Based on 7.6-cm length

c Assumed value of $V_1/V_j = 0.4$

d Assumed 5 percent of total radiation was deposited in transparent wall and coolant fluid

e Includes heat deposited directly in coolant fluid

f Reflective aluminum liner; no transparent wall

g Plasma diameter estimated using gas-cooled model data

TABLE IV

SUMMARY OF TEST CONDITIONS FOR TRANSPARENT-WALL MODEL FLOW VISUALIZATION TESTS

See Fig. 32 for Details of Test Configuration

$\beta_{t'} = d_1/L\,(Re_{t,j})^{0.8}/Re_r$

See Ref. 18 for Definitions of Parameters

Vortex Tube Diameter, cm	3.25
Vortex Tube Length, cm	10.2
Injected Water Flow Rate, gpm	0.42, 0.64*, 0.85
Water Injection Velocity, m/sec	0.92, 1.4*, 1.86
Jet Injection Reynolds Number, $Re_{t,j}$	1.25×10^4, 1.9×10^4*, 2.5×10^4
Radial Reynolds Number, Re_r	108.2, 64.5, 40.6, 17.0
Axial Bypass, percent	0, 40.5, 62.5, 84.3
Secondary Flow Parameter, β_t	8.4, 14, 22, 53
Average Flow Residence Time, sec	2.1, 3.5, 5.6, 13.3
Wall Conditions	(1) Smooth (2) Bumpy
Dye Injection Locations	(1) Axial Midplane (2) One-Third Axial Length (3) Right End Wall

*Qualitatively determined best injection condition for which other parameters listed were calculated.

TABLE V

PROPERTIES OF RESIN MATERIALS USED
FOR FILAMENT-WOUND TUBES

See Figs. 10 and 41 for Test Configurations Employing
These Resins in the Filament-Wound Tube

PROPERTY	RESIN MATERIAL L-266	RESIN MATERIAL 63	RESIN MATERIAL ERL 2256
Composition	Epoxy Novalac	Crosslinked Cyclo-aliphatic Epoxy	Modified Diglycidyl Ether of Bisphenol A
Preparation	45 Parts Catalyst to 100 Parts Resin by wt.	1% Catalyst by wt.	27 Parts Catalyst to 100 Parts Resin by wt.
Color	Green	Clear	Amber
Service Temp., deg C	≈175	150	150
Specific Gravity	1.25	0.95	1.15-1.17
Thermal Expansion, 10^{-6}/deg C	56	80	80
Viscosity, cps (Room Temperature)	15,000	Variable From 10-20,000	500-900
Thermal Conductivity, 10^{-5} cal/sec/cm^2/deg C/cm	5.0	40.0	82.6
Tensile Strength, 10^7 N/m^2	4.14	4.82	10.0

TABLE V (Continued)

PROPERTY	RESIN MATERIAL L-266	RESIN MATERIAL 63	RESIN MATERIAL ERL 2256
Flexural Strength, 10^7 N/m^2	8.27	8.27	15.5
Moisture Absorption-in 10 days @ 95% Rel Hum. Percent by Weight (Room Temperature)	0.5	0.42	0.5
Machineability	Good	Good	Good
Dielectric Strength, 10^7 volts/meter	1.93	1.97	1.62
Volume Resistivity, ohm-cm	6.0×10^{15}	10^{16}	$\approx 10^{16}$
Dielectric Constant	4.5 (for f = 100 to 10^{10} Hz)	2.4 (for f = 60 to 10^{10} Hz)	4.35 (for f = 60 to 10^{10} Hz)
Dissipation Factor (Loss Tangent)	0.015 (for f = 100 to 10^{10} Hz)	0.0005 (for f = 60 to 10^{10} Hz)	0.03-0.1 (for f = 60 to 10^{10} Hz)
Cure Cycle	16 hr at 200 deg C	16 hr at 120 deg C	2 hr at 80 deg C 2 hr at 160 deg C

TABLE VI

SUMMARY OF FILAMENT-WOUND TUBE CONFIGURATIONS AND TEST RESULTS

See Table V for Properties of Resin Materials

Tube	No. of Layers		Length (cm)	Epoxy Resin	R-F Or Hydro-Static Test	Spacer Used In High Pressure Test	Result; Tube Tested To (atm)	Calculated Modulus of Elasticity, E (N/m^2, (psi))
	Axial	Hoop						
1	4	8	22.9	L-266	Hydro-Static	No	Failed (293)	Axial Only: 1.63×10^9 (2.36×10^5)
2	4	8	22.9	L-266	Both	No	Burned Slightly In R-F Tests; Failed (256)	Data Not Taken
3	8	10	22.9	L-266	Hydro-Static	No	Failed (314)	Axial Only: 1.9×10^9 (2.75×10^5)
4	10	10	22.9	63 63HV	R-F	No	Successful Hydrostatic and R-F Tests To 40 atm; Not Tested To Failure	Data Not Taken
5	10	10	25.7	63 63HV	Hydro-Static	Yes	Tested To 443 atm; Did Not Fail, Excessive Leakage	(Average Of 3 Strain Gages) Axial: 6.0×10^9 (8.7×10^5) Hoop: 2.7×10^9 (3.9×10^5)
6	10	10	25.7	ERL 2256	Hydro-Static	Yes	Tested To 551 atm; Failed At 484 atm After 6 Cycles, Slight Leakage	Axial Only: 4.62×10^9 (6.7×10^5)

SKETCHES OF REFERENCE ENGINE UNIT CAVITY, IN-REACTOR UNIT CELL, AND R-F PLASMA RADIANT ENERGY SOURCE

(a) REFERENCE NUCLEAR LIGHT BULB ENGINE UNIT CAVITY

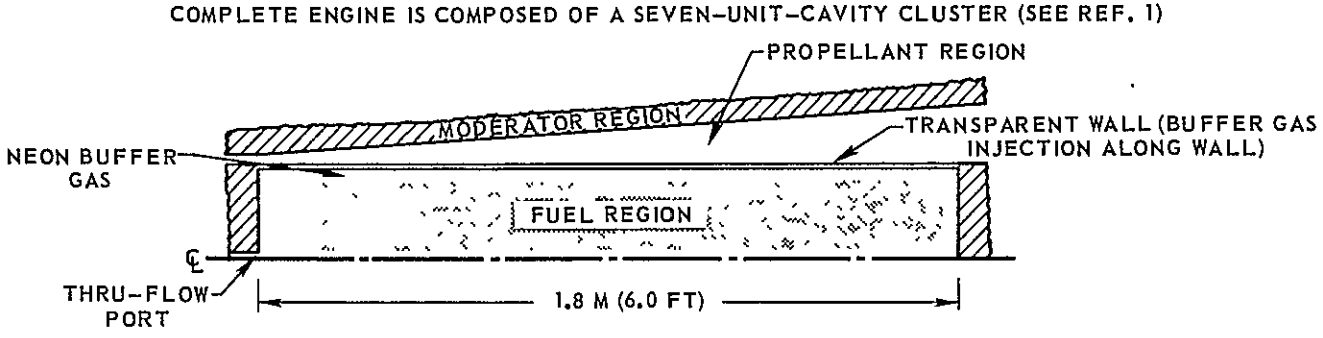

(b) IN-REACTOR UNIT CELL

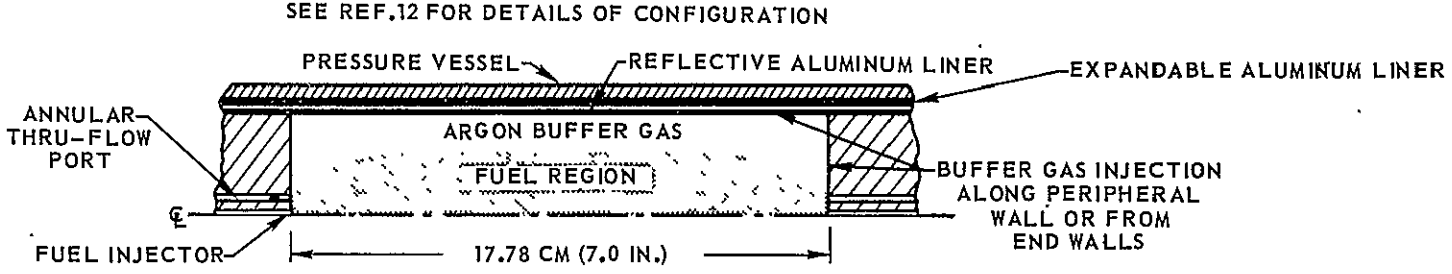

(c) R-F PLASMA RADIANT ENERGY SOURCE

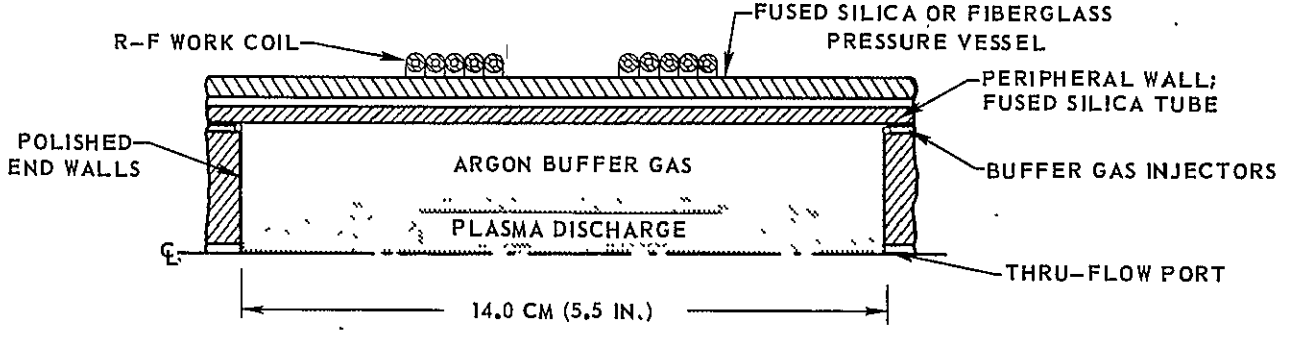

BLOCK DIAGRAM OF UARL 1.2-MEGW R-F INDUCTION HEATER

OPERATING FREQUENCY ≈ 5.5 MHz
POWER LEVELS SHOWN ARE MAXIMUM DESIGN VALUES
MAXIMUM TOTAL D-C INPUT POWER DURING THIS PROGRAM FOR POWER AMPLIFIERS 1 AND 2 WAS APPROXIMATELY 685 KW

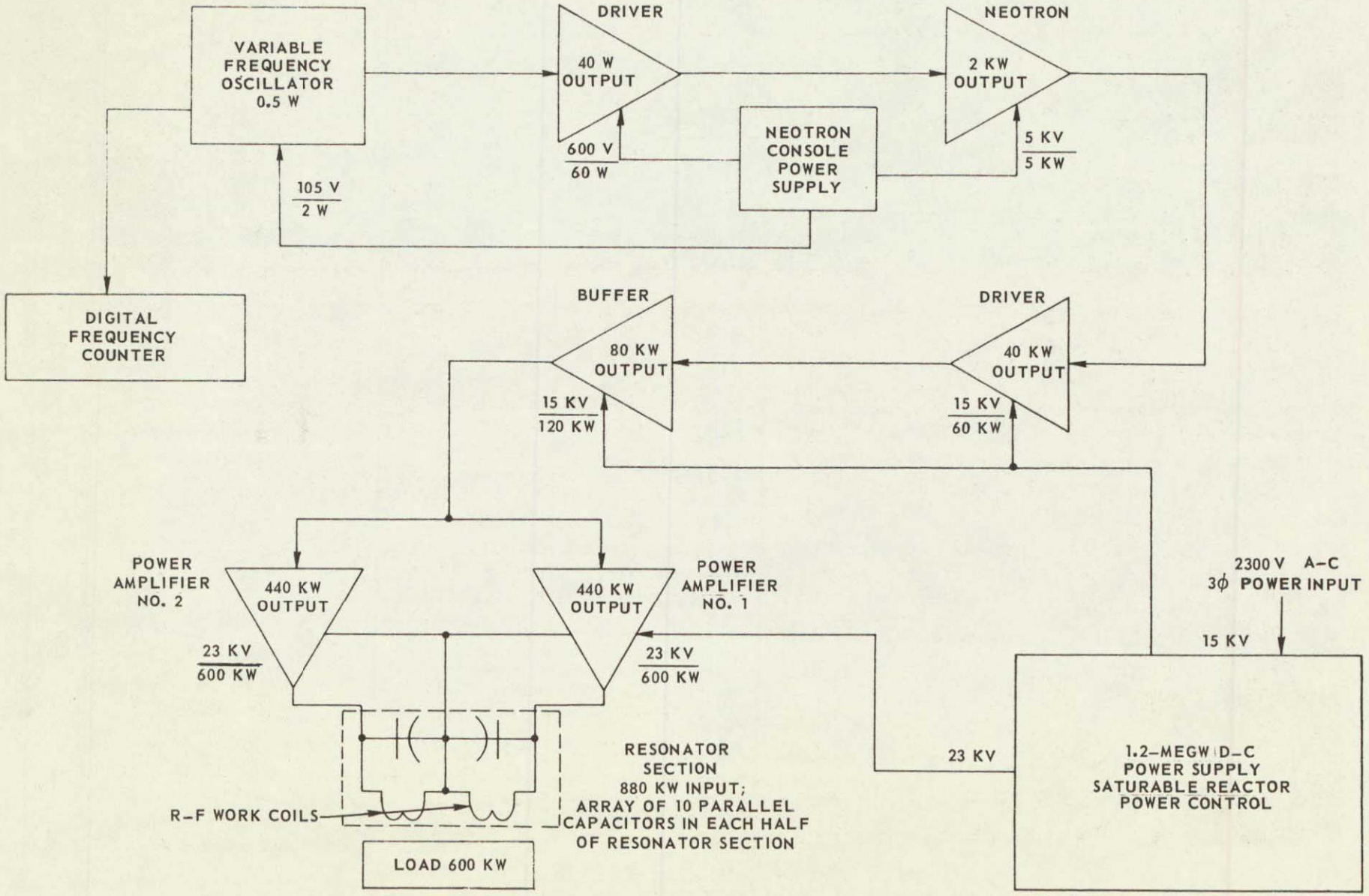

FIG. 2

K-910900-7

PHOTOGRAPH OF 1.2-MEGW R-F INDUCTION HEATER RESONATOR SECTION

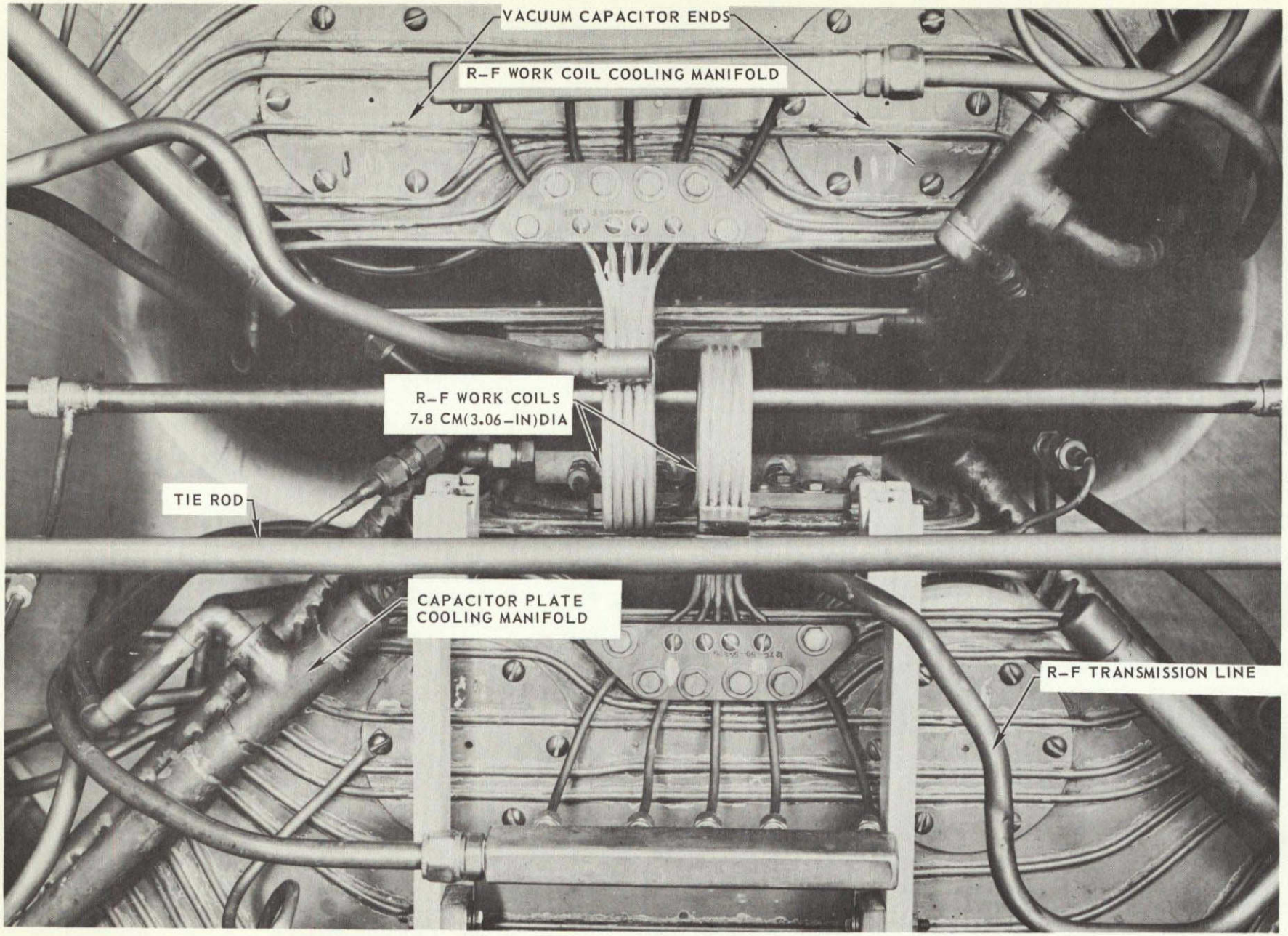

K-910900-7

FIG. 3

SCHEMATIC OF 1.2-MEGW R-F INDUCTION HEATER GAS AND COOLING WATER FLOW SYSTEMS

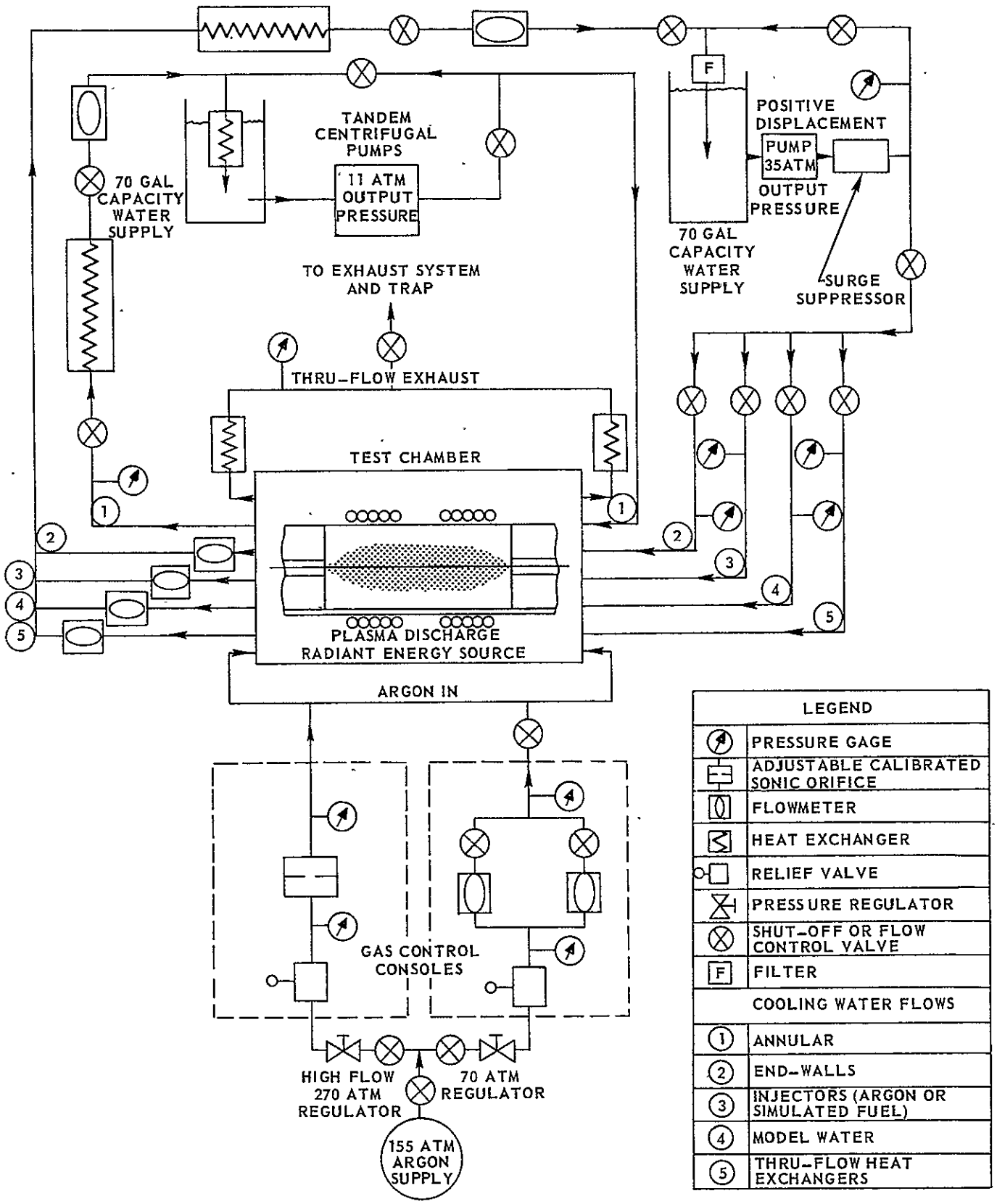

SCHEMATIC OF R-F PLASMA STARTING SYSTEM

SEE FIG. 6 FOR DETAILS OF TEST CHAMBER

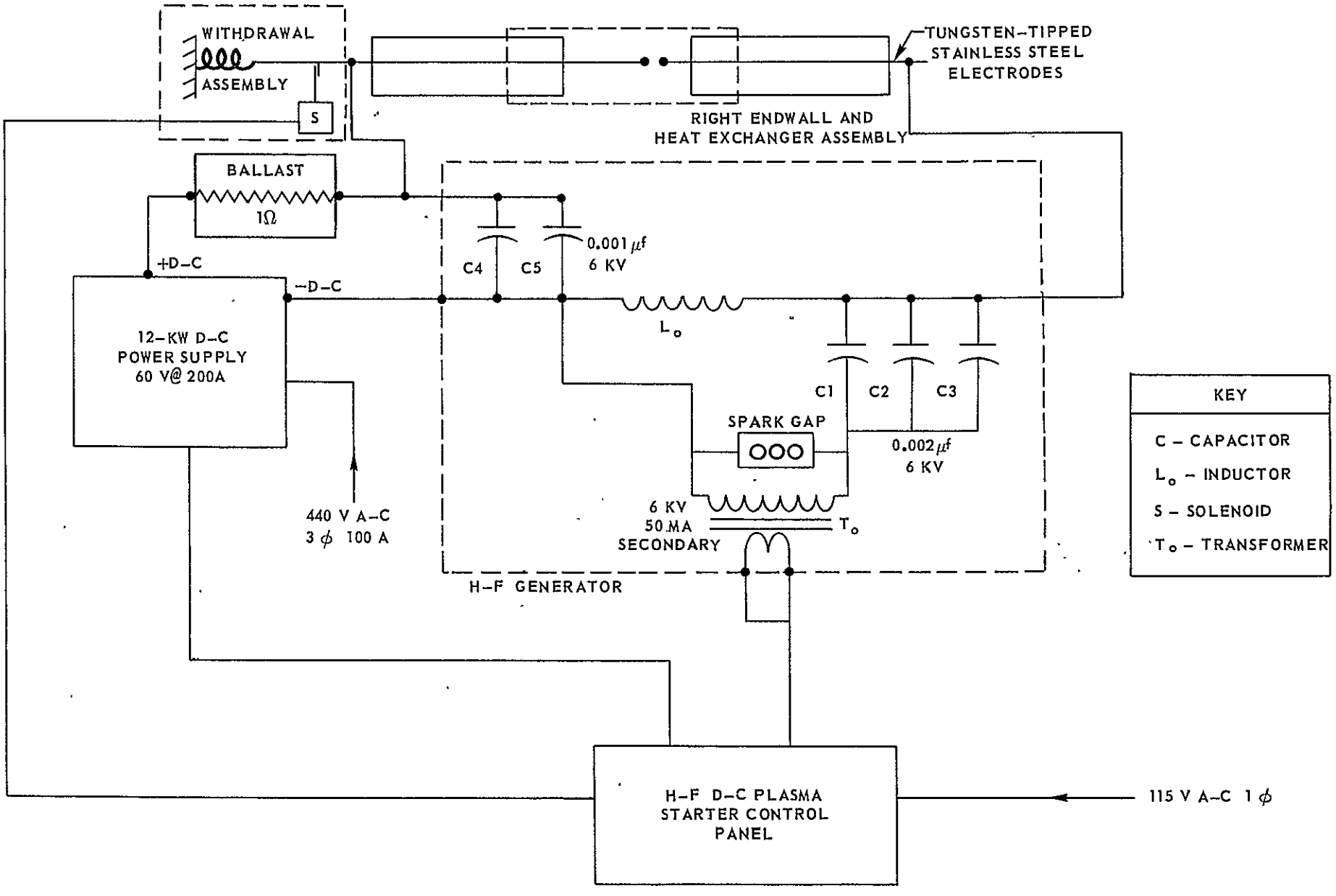

FIG. 5

SKETCH OF R-F RADIANT ENERGY SOURCE CONFIGURATION SHOWING POWER BREAKDOWN AND PRIMARY VARIABLES

INDEPENDENT VARIABLES	DEPENDENT VARIABLES
GEOMETRY	DISCHARGE DIAMETER, d
OPERATING FREQUENCY, f	TOTAL DISCHARGE POWER, Q_T
CHAMBER PRESSURE, P_D	RADIATED POWER, $Q_{R,T}$
ARGON WEIGHT FLOW RATE, W_A	CONDUCTED-CONVECTED POWER, $Q_{C,C}$
TOTAL D-C INPUT POWER, Q_I	RADIAL TEMPERATURE DISTRIBUTION, $T(r)$

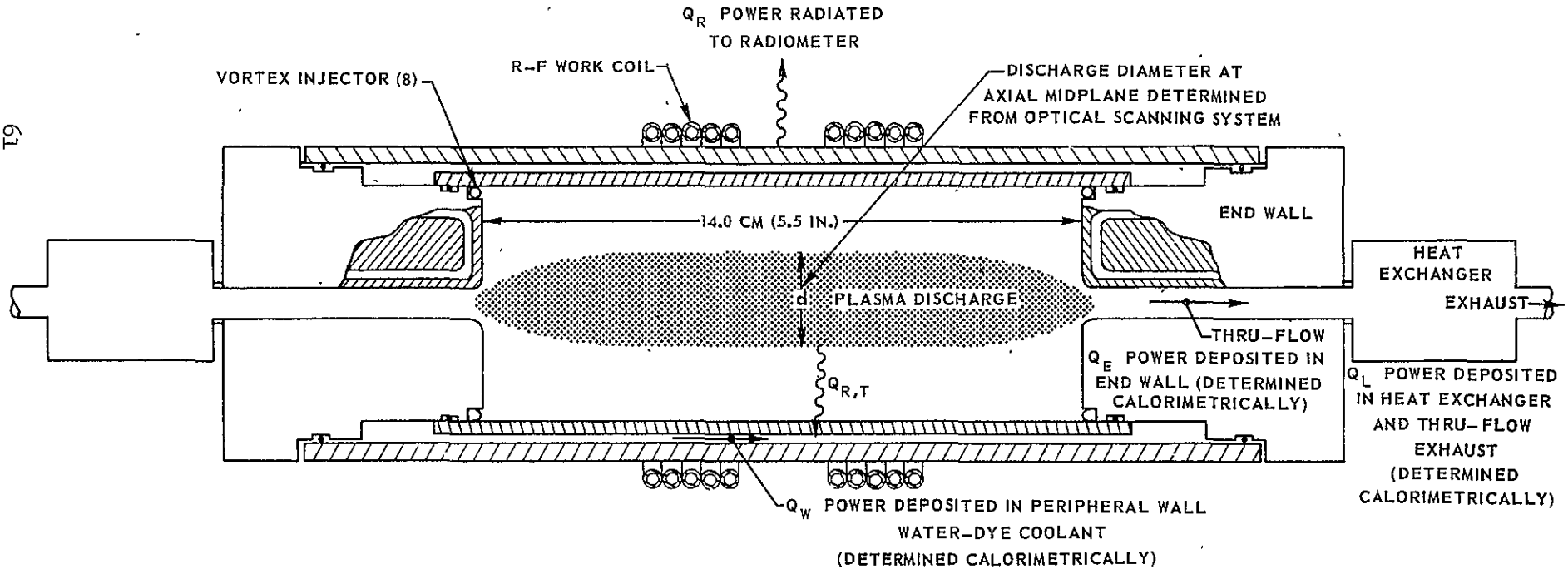

TOTAL POWER DEPOSITED IN R-F PLASMA DISCHARGE, $Q_T = Q_R + Q_W + Q_E + Q_L$

FIG. 6

TRANSMISSION CHARACTERISTICS OF RADIOMETER SYSTEM AND EFFECT OF DYE ON RADIATION ATTENUATION

(a) TRANSMISSION CHARACTERISTICS OF RADIOMETER OPTICAL SYSTEM

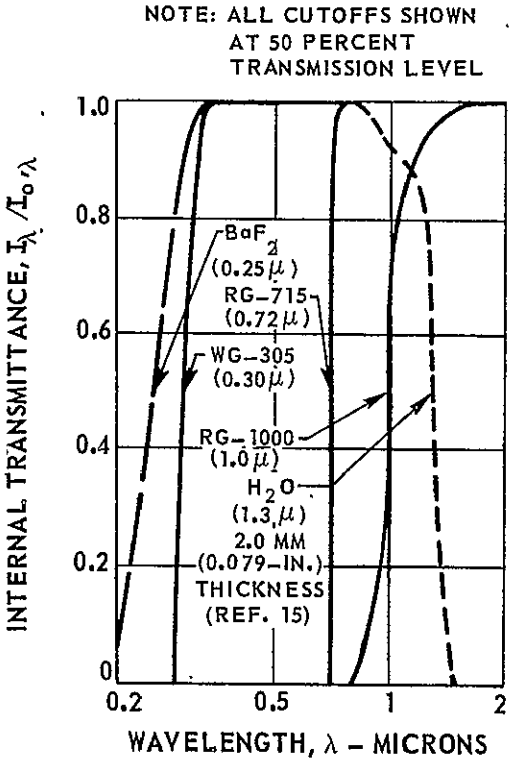

(b) EFFECT OF DYE CONCENTRATION ON RADIATION ATTENUATION IN PERIPHERAL-WALL COOLANT FLUID

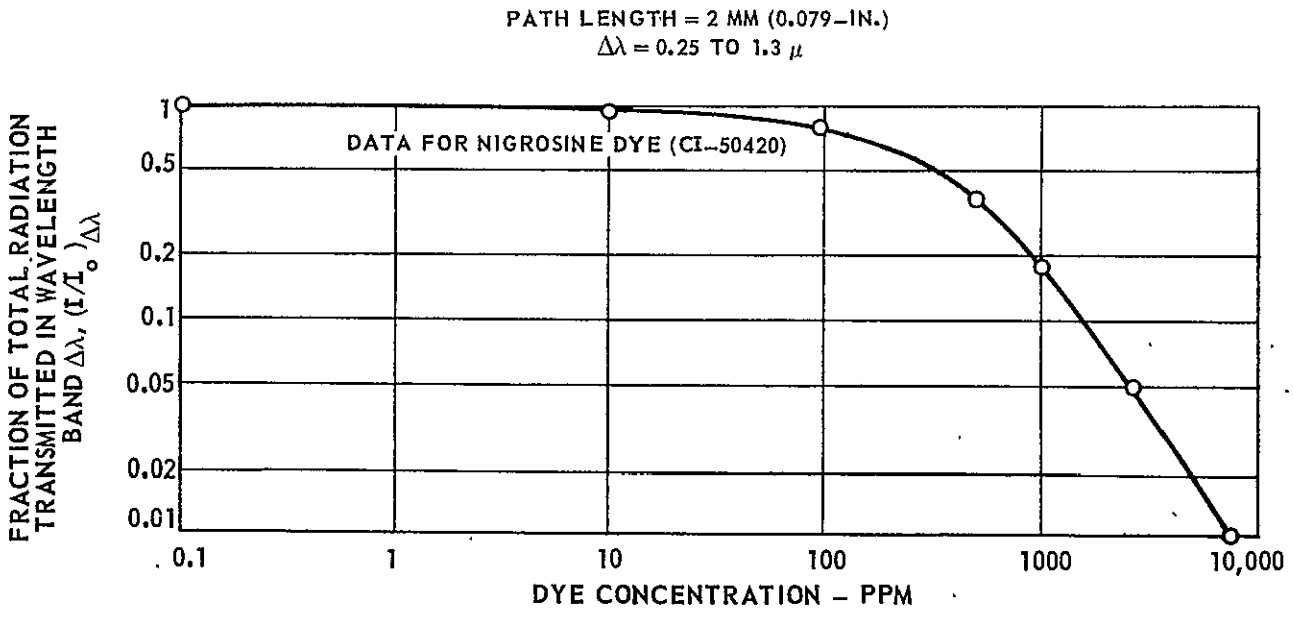

FIG. 7

SCHEMATIC OF OPTICAL SYSTEM FOR SPECTRAL MEASUREMENTS

(NOT TO SCALE)

EQUIPMENT WITHIN DASHED OUTLINE MOUNTED ON TABLE WITH SLIDE MECHANISM AND TRAVERSED ACROSS IMAGE OF R-F PLASMA DISCHARGE

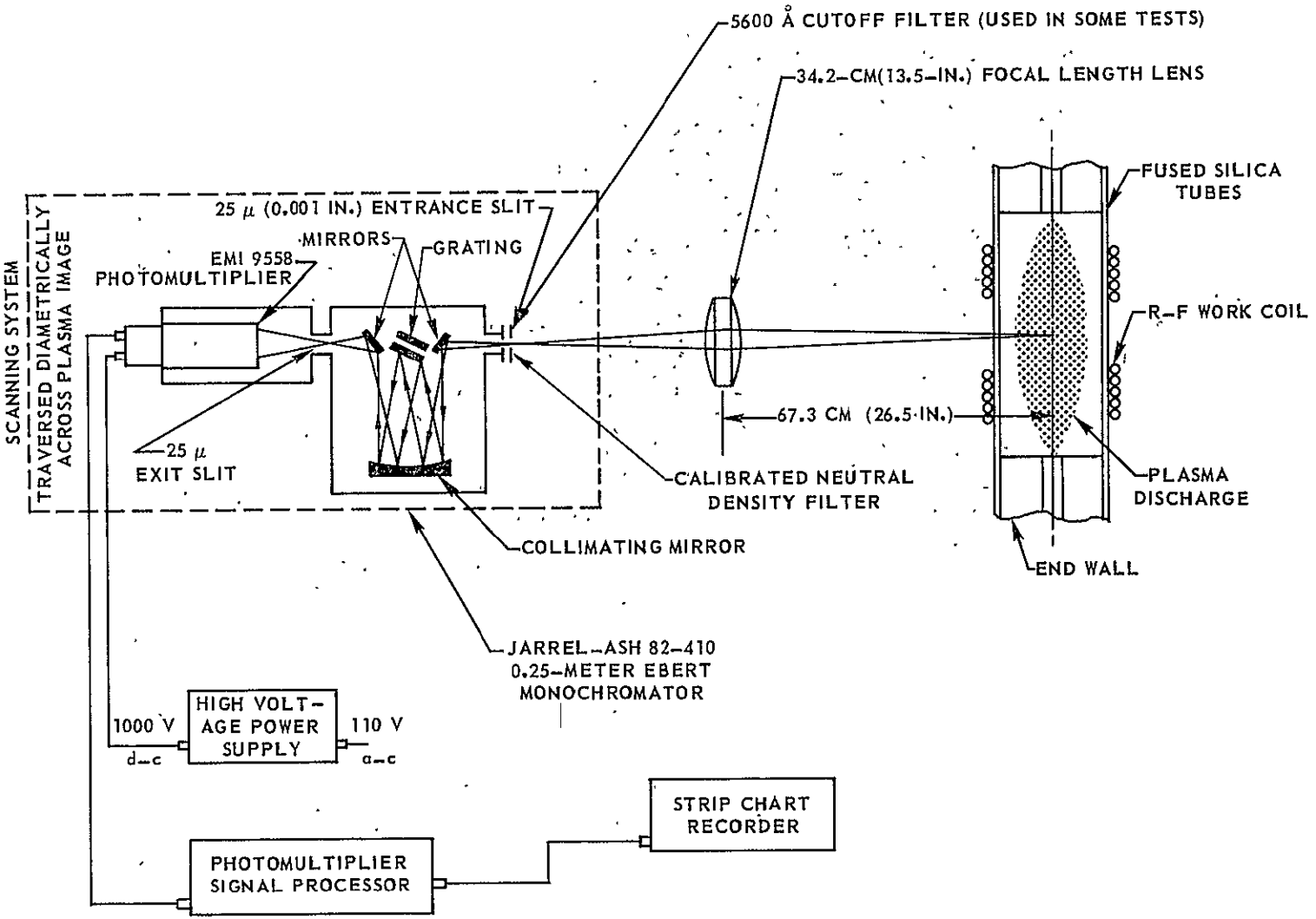

FIG. 8

SKETCH OF FUSED SILICA PRESSURE VESSEL CONFIGURATION USED IN RADIANT ENERGY SOURCE TESTS

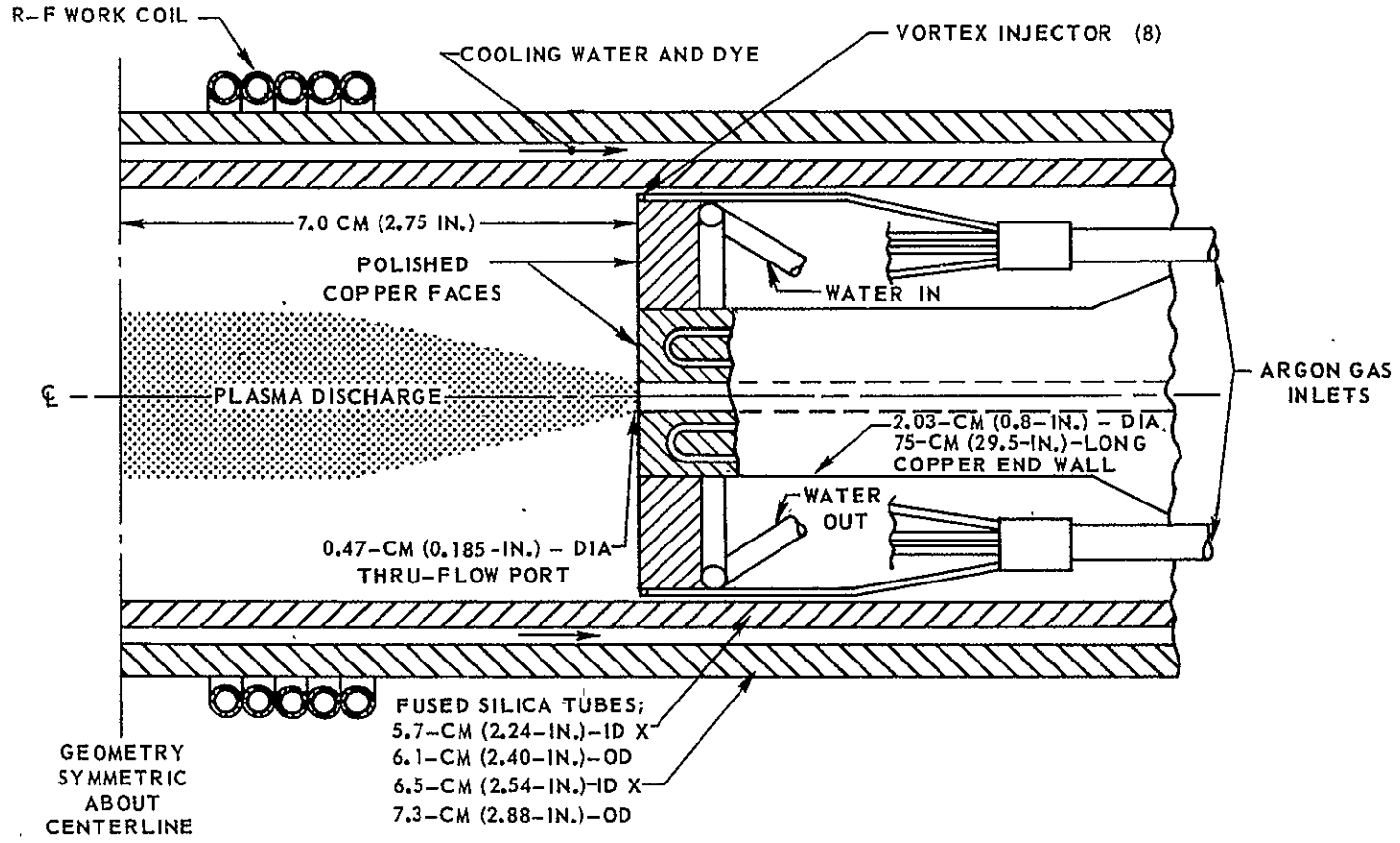

FIG. 9

SKETCH OF FILAMENT-WOUND PRESSURE VESSEL CONFIGURATION

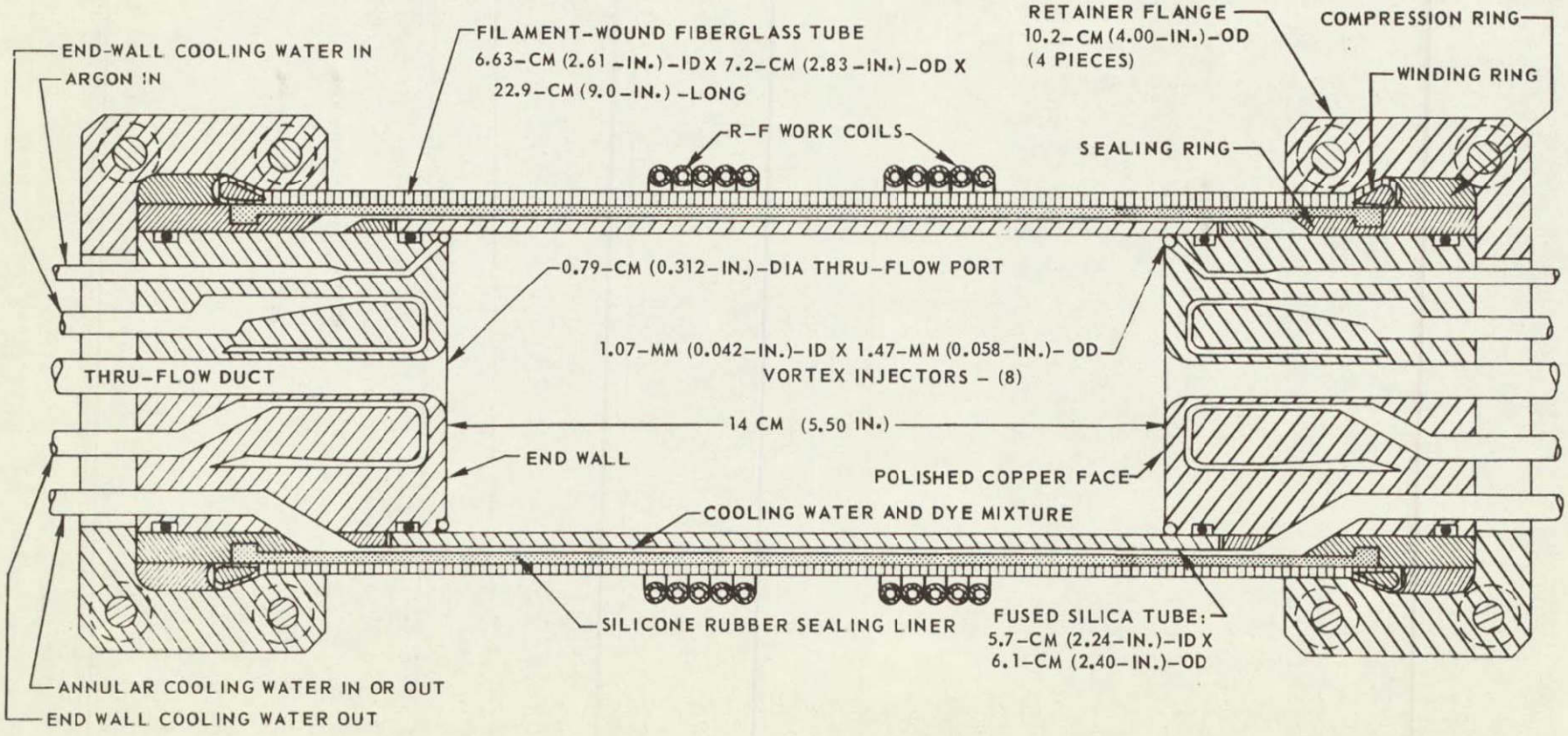

FIG. 10

PHOTOGRAPH OF COMPONENTS OF FILAMENT-WOUND PRESSURE VESSEL CONFIGURATION

SEE FIG. 10 FOR DETAILS OF CONFIGURATION

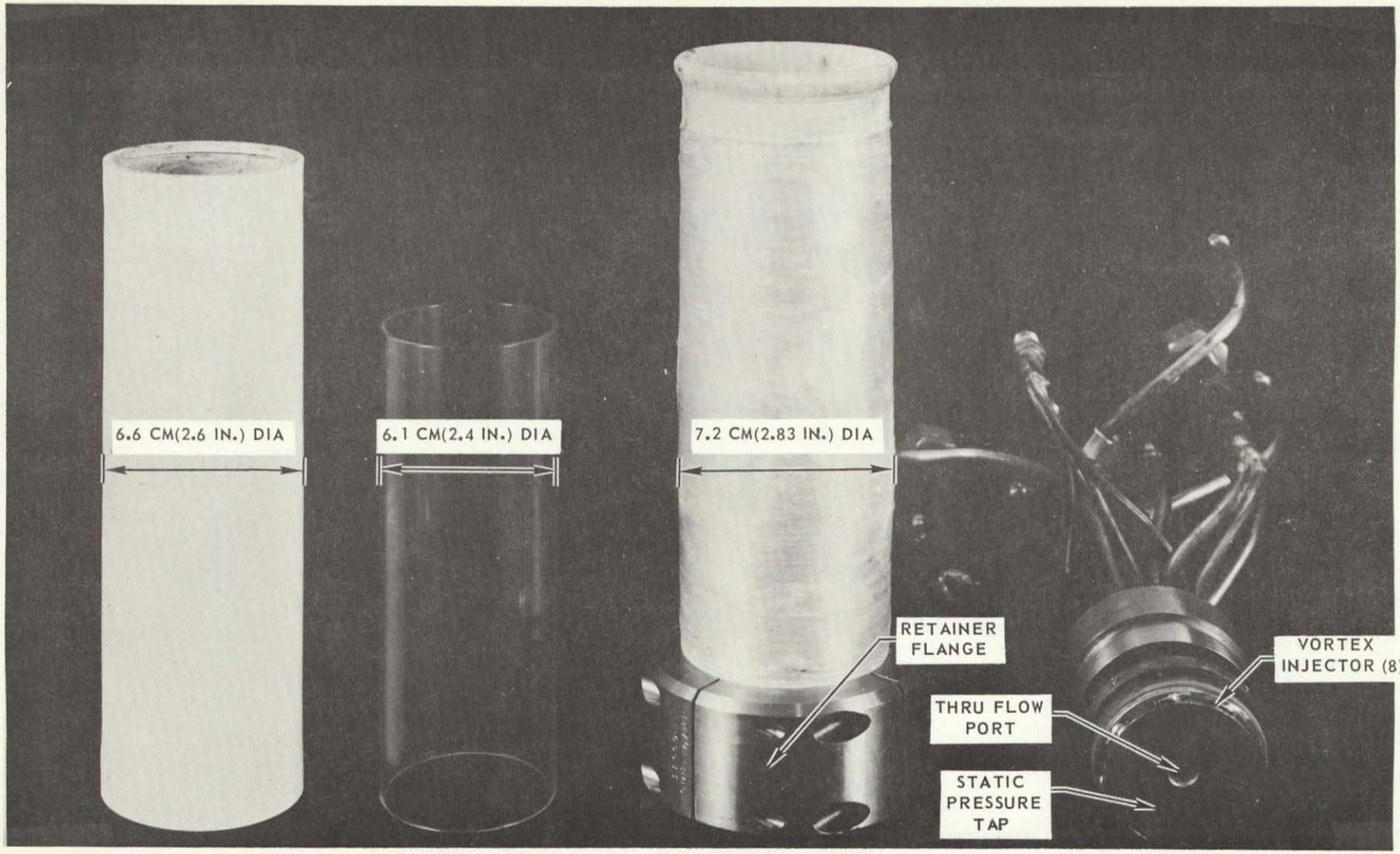

SILICONE RUBBER SEALING LINER

FUSED SILICA TUBE: 5.7-CM (2.24-IN.-ID X 6.1-CM (2.40-IN.)-OD

FIBERGLASS FILAMENT - WOUND PRESSURE VESSEL AND RETAINER FLANGE

END-WALL ASSEMBLY

K-910900-7

FIG. 11

PHOTOGRAPH OF FILAMENT-WOUND PRESSURE VESSEL CONFIGURATION INSTALLED IN 1.2-MEGW R-F INDUCTION HEATER

SEE FIG. 10 FOR DETAILS OF CONFIGURATION

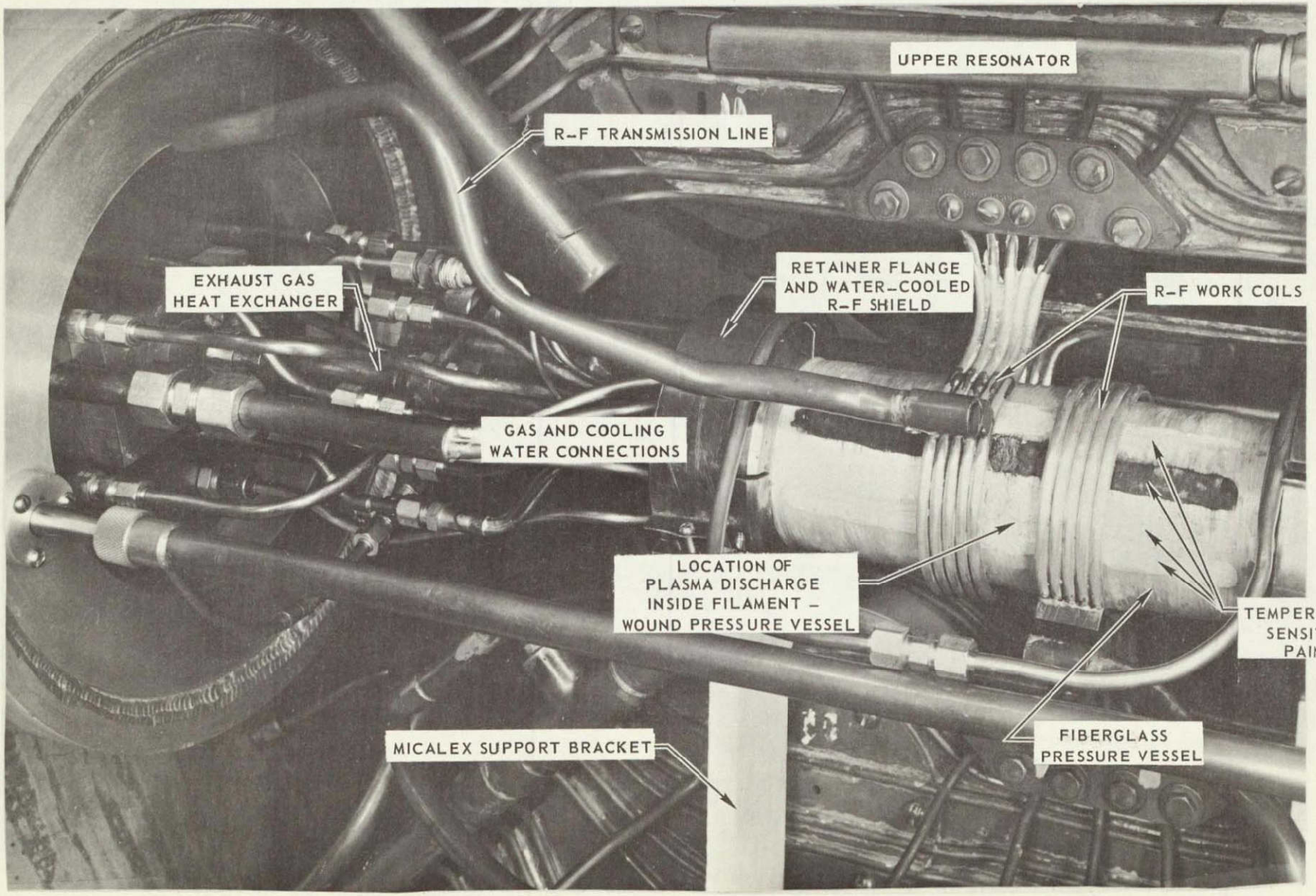

NOT REPRODUCIBLE

SKETCH OF RADIANT ENERGY SOURCE CONFIGURATION WITH FUSED-SILICA PRESSURE VESSEL SHOWING HIGHEST POWER OPERATING CONDITIONS

SEE FIG. 9 FOR DETAILS OF TEST CONFIGURATION

ARGON GAS, W_A = 9.1 GM/SEC , P_D = 15 ATM

DISCHARGE SURFACE AREA , A_S = 79.61 CM^2 (12.34 $IN.^2$)

DISCHARGE VOLUME, V = 39.66 CM^3 (2.42 $IN.^3$)

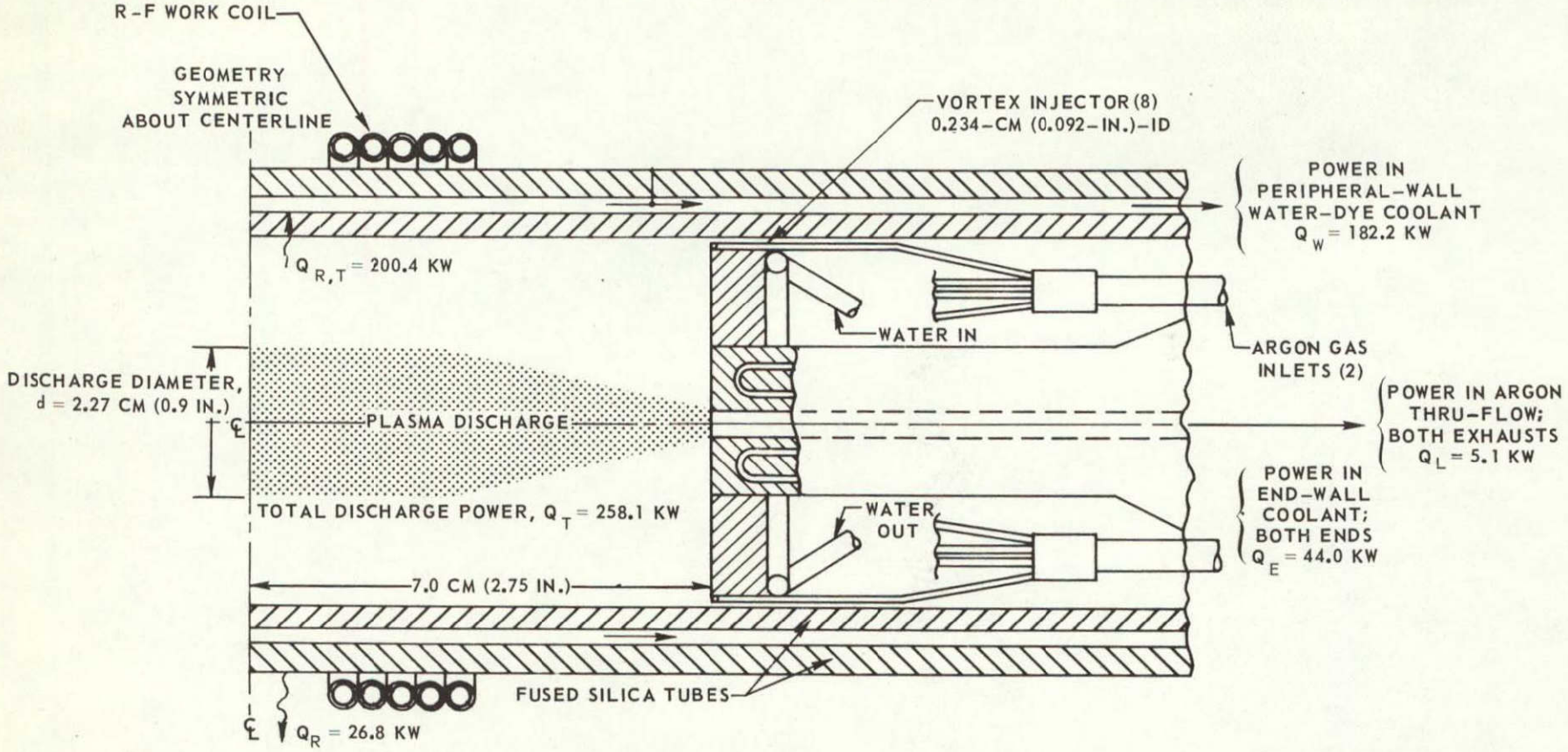

TOTAL D-C INPUT POWER, Q_I = 685 KW AT 5.5083 MHz

TOTAL DISCHARGE POWER, Q_T = 26.8 + 182.2 + 44.0 + 5.1 = 258.1 KW

R-F SYSTEM COUPLING EFFICIENCY, η = 258.1/685 = 37.8 PERCENT

PROBABLE MAXIMUM POWER CONDUCTED THROUGH PERIPHERAL WALL, Q_C = 9.1 KW

TOTAL POWER RADIATED THROUGH INNER PERIPHERAL WALL, $Q_{R,T}$ = 182.2-9.1 + 26.8 = 200.4 KW

$Q_{R,T}/A_S$ = 200.4/79.61 =2.52 KW/CM^2 (T^* = 4670 K)

FRACTION OF DISCHARGE POWER RADIATED THROUGH INNER PERIPHERAL WALL, $Q_{R,T}/Q_T$ = 204.1/258.1 = 0.79

FIG. 13

FIG. 14

VARIATION OF DISCHARGE DIAMETER WITH TOTAL DISCHARGE POWER

SEE FIG. 9 FOR DETAILS OF TEST CONFIGURATION

TOTAL INJECTION AREA, $A_j = 0.686$ CM^2 (0.107 IN.^{2})

RANGE OF CHAMBER PRESSURE, $P_D = 1$ TO 22.5 ATM

RANGE OF ARGON WEIGHT FLOW, $W_A = 2.27$ TO 13.62 GM/SEC (0.005 TO 0.030 LB/SEC)

RANGE OF R-F OPERATING FREQUENCY, $f = 5.4896$ TO 5.5147 MHz

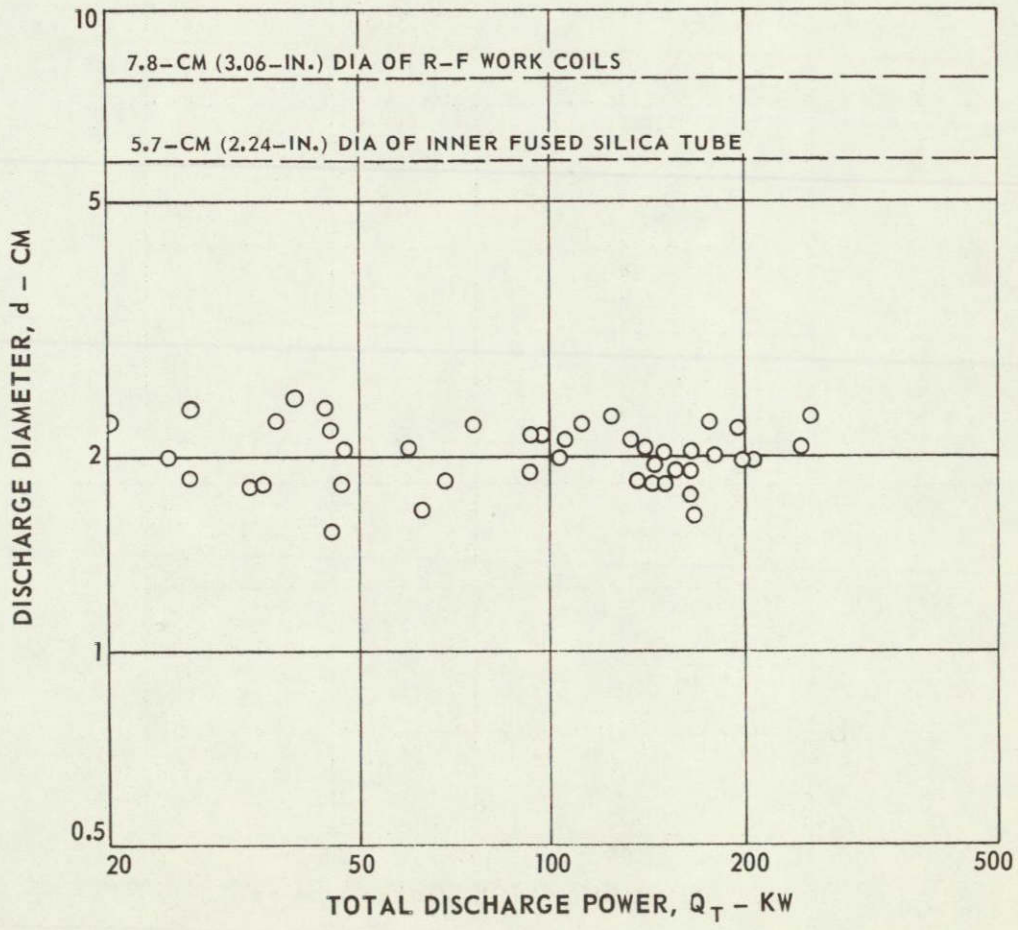

VARIATION OF RADIANT ENERGY FLUX WITH TOTAL DISCHARGE POWER

SEE FIG. 9 FOR DETAILS OF TEST CONFIGURATION

TOTAL INJECTION AREA, $A_j = 0.686\ CM^2$ ($0.107\ IN.^2$)

RANGE OF CHAMBER PRESSURE, P_D = 1 TO 22.5 ATM

RANGE OF ARGON WEIGHT FLOW, W_A = 2.27 TO 13.62 GM/SEC (0.005 TO 0.030 LB/SEC)

RANGE OF R-F OPERATING FREQUENCY, f = 5.4896 TO 5.5147 MHz

$1.0\ KW/CM^2 = 880\ BTU/SEC-FT^2$

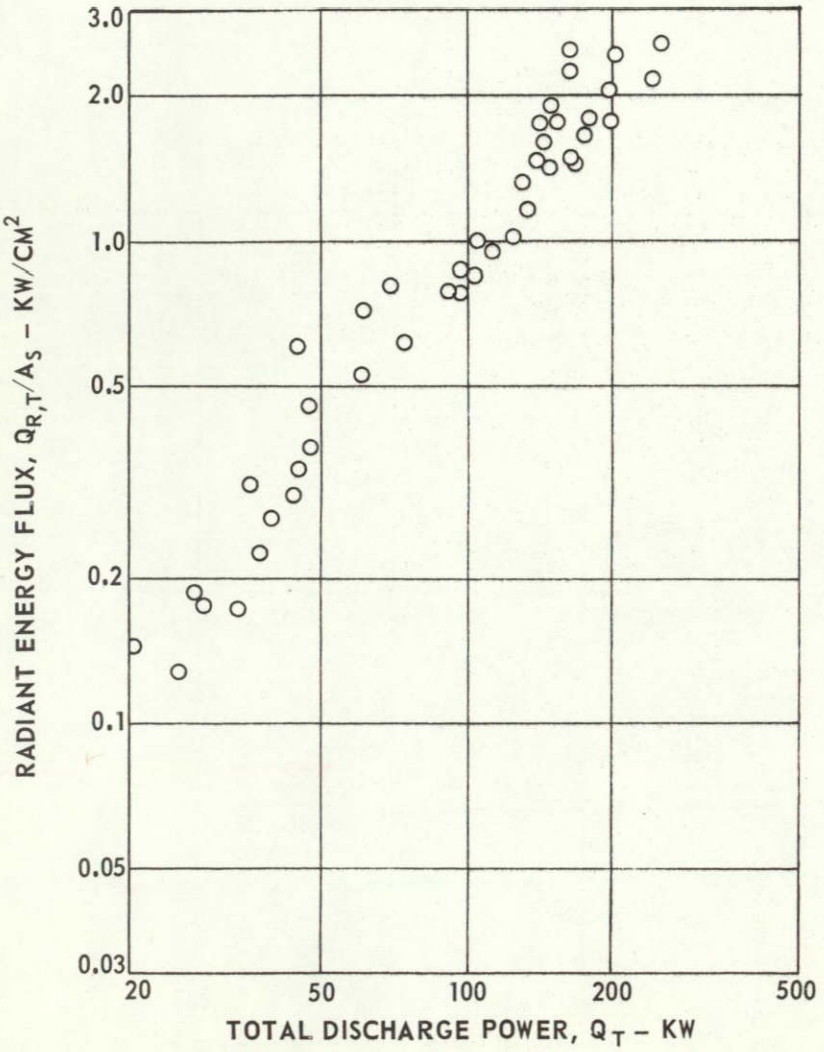

VARIATION OF RADIATED POWER EFFICIENCY, TOTAL DISCHARGE POWER AND ARGON WEIGHT FLOW WITH CHAMBER PRESSURE

SEE FIG. 9 FOR DETAILS OF TEST CONFIGURATION

TOTAL INJECTION AREA, $A_j = 0.686\ CM^2$ (0.107 IN.^{2})

RANGE OF R-F OPERATING FREQUENCY, f = 5.4896 TO 5.5147 MHz

(a) VARIATION OF RADIATED POWER EFFICIENCY

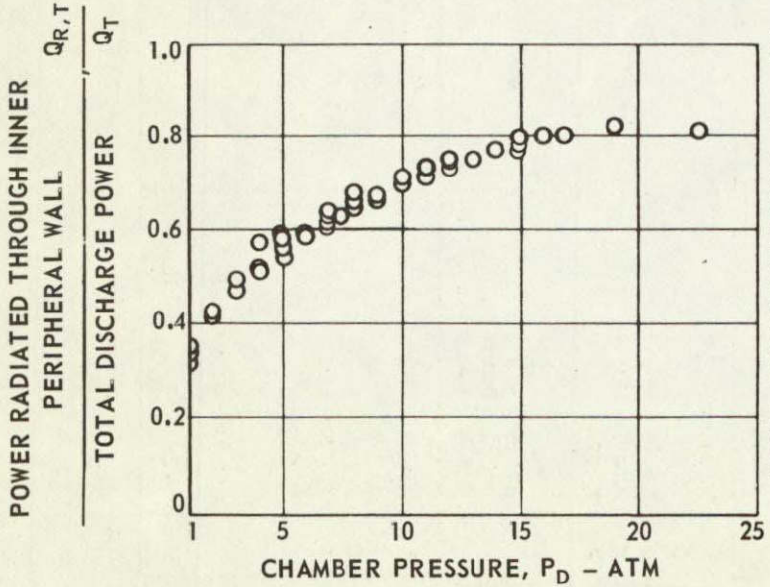

(b) VARIATION OF TOTAL DISCHARGE POWER

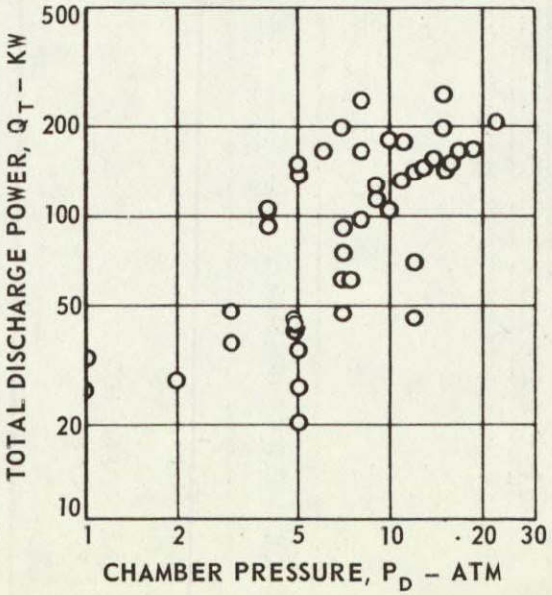

(c) VARIATION OF ARGON WEIGHT FLOW

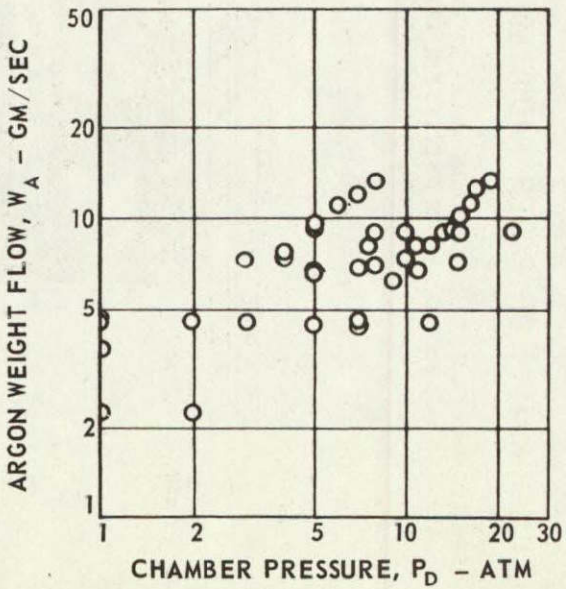

FIG. 16

FIG. 17

SPECTRAL DISTRIBUTION OF POWER RADIATED THROUGH PERIPHERAL-WALL COOLANT

SEE FIG. 7a FOR DETAILS OF RADIOMETER OPTICAL TRANSMISSION CHARACTERISTICS
SEE FIG. 7b FOR DYE ATTENUATION CHARACTERISTICS
SEE FIG. 9 FOR ADDITIONAL DETAILS OF TEST CONFIGURATION

NUMBER IN PARENTHESES IN TABLE INDICATE FRACTION OF NO DYE CASE

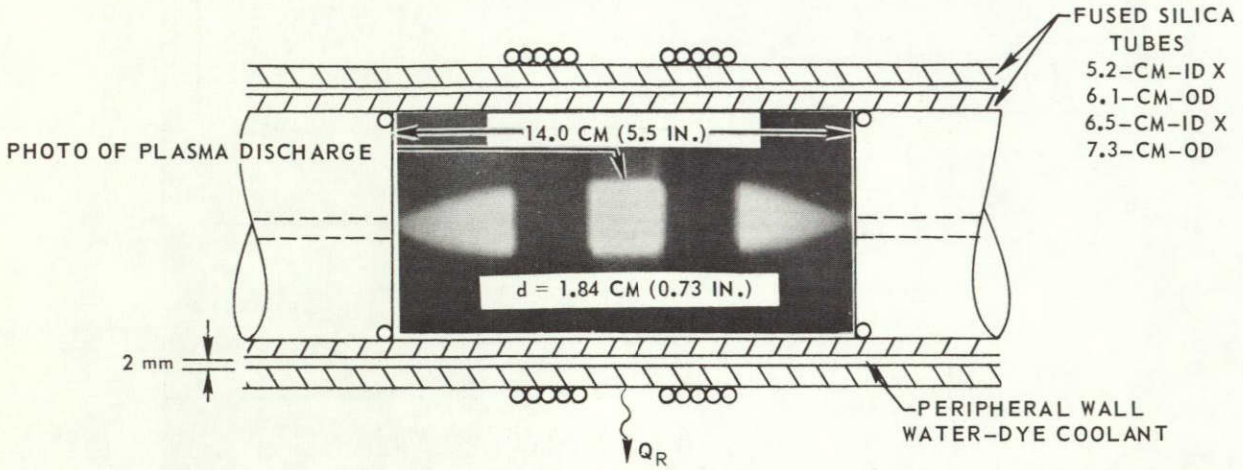

	TEST CONDITIONS	POWER RADIATED THROUGH PERIPHERAL-WALL COOLANT IN KW			
		WAVELENGTH BAND - MICRONS			
		0.25-0.30	0.30-0.72	0.72-1.00	1.00-1.30
	$P = 5.5083$ MHz $Q_T = 58.4$ KW $Q_R = 30.6$ KW $W_A = 7.04$ GM/SEC $P_D = 10$ ATM NO DYE IN ANNULAR COOLING WATER	1 KW (1.0)	6.4 KW (1.0)	13.3 KW (1.0)	9.9 KW (1.0)
SEE PHOTO ABOVE	$f = 5.5083$ MHz $Q_T = 58.8$ KW $Q_R = 7.5$ KW $W_A = 7.04$ GM/SEC $P_D = 10$ ATM 800 PPM NIGROSINE DYE ADDED TO PERIPHERAL WALL COOLANT	0.2 KW (0.2)	0.7 KW (0.11)	3.7 KW (0.28)	2.9 KW (0.29)
	$f = 5.5083$ MHz $Q_T = 59.1$ KW $Q_R = 3.4$ $W_A = 7.04$ GM/SEC $P_D = 10$ ATM 1600 PPM NIGROSINE DYE ADDED TO PERIPHERAL WALL COOLANT	0.1 KW (0.1)	0.3 KW (0.05)	1.7 KW (0.13)	1.3 KW (0.13)

TYPICAL RADIAL DISTRIBUTIONS OF TEMPERATURE OBTAINED IN R-F PLASMA RADIANT ENERGY SOURCE TESTS

SEE FIG. 6 FOR DETAILS OF OPTICAL SYSTEM USED IN SPECTRAL MEASUREMENTS
SEE FIG. 8 FOR DETAILS OF TEST CONFIGURATION
SEE FIG. 17 FOR DETAILS OF TEST CONDITIONS
TEMPERATURE DETERMINED FROM ARGON CONTINUUM AT 4320 Å

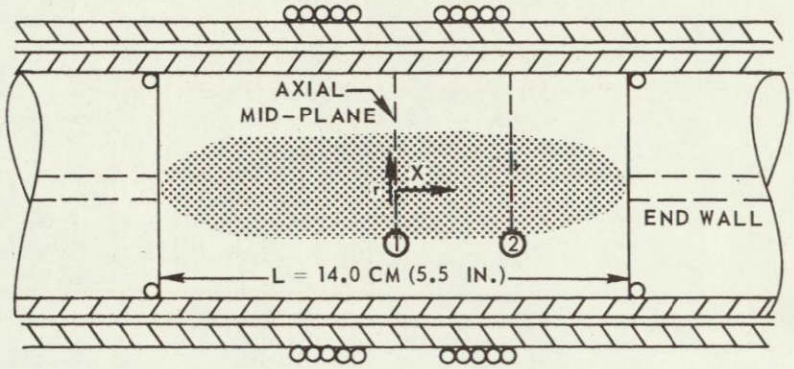

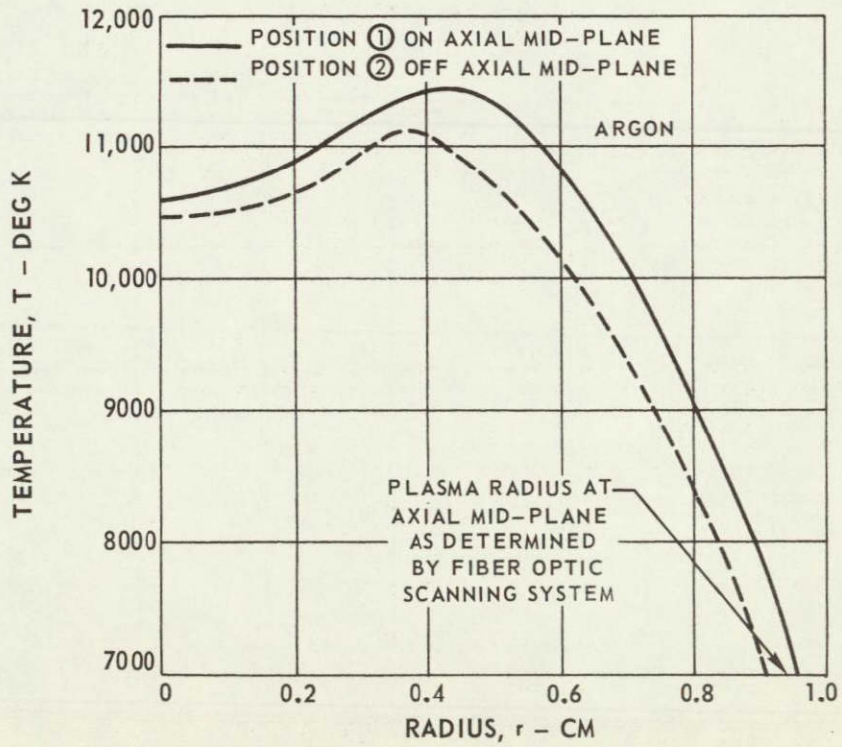

FIG. 19

SUMMARY OF RESULTS FOR 2/3-SCALE IN-REACTOR RADIANT ENERGY SOURCE TESTS WITHOUT SIMULATED FUEL INJECTION

FUSED SILICA PRESSURE VESSEL CONFIGURATION - SEE FIG. 9

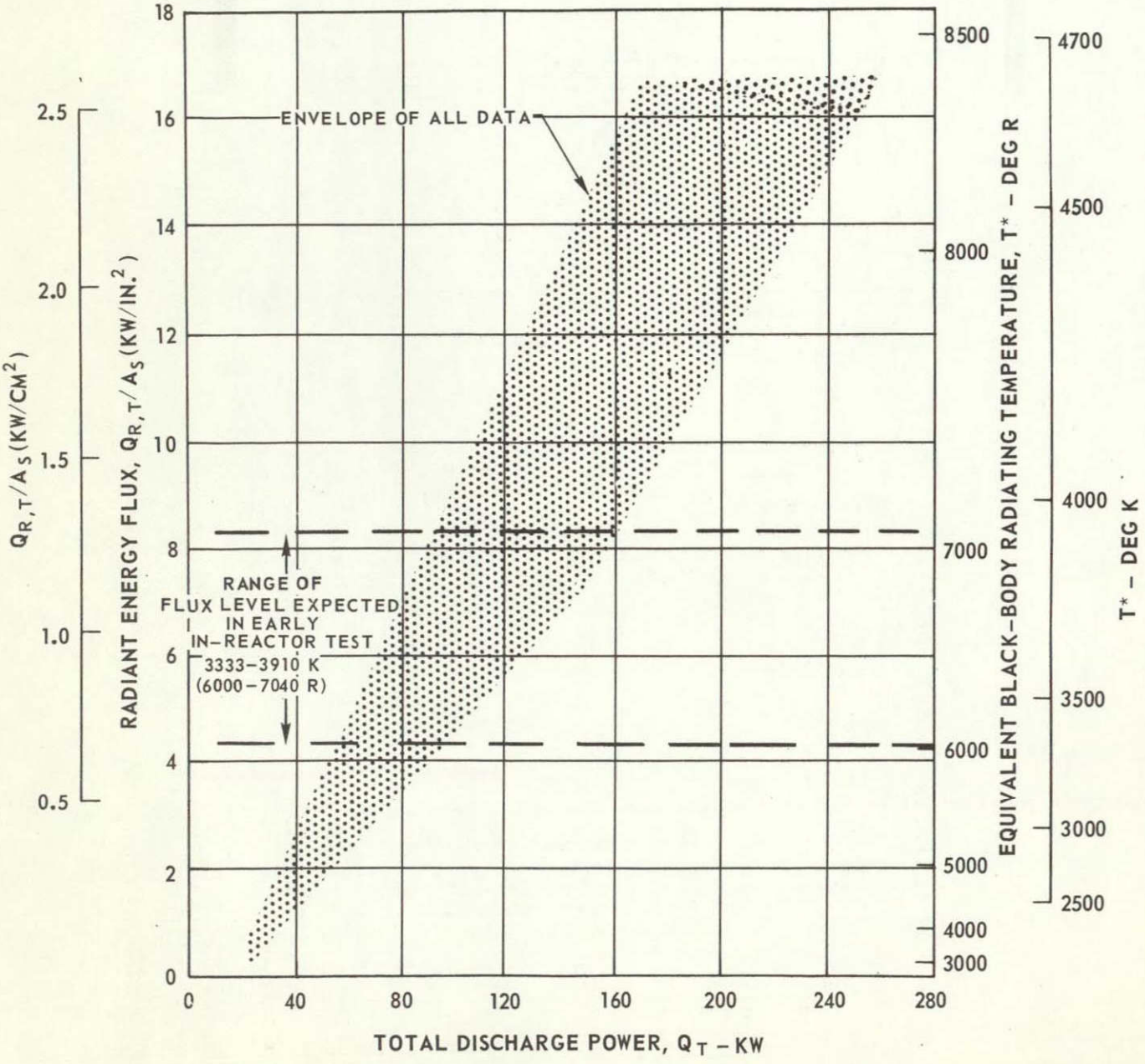

SKETCH OF POWER LOSSES FOR HIGHEST PRESSURE OPERATING POINT IN RADIANT ENERGY SOURCE TESTS EMPLOYING FILAMENT-WOUND PRESSURE VESSEL

SEE FIG. 10 FOR DETAILS OF TEST CONFIGURATION
OPERATING FREQUENCY, $f = 5.5945$ MHz
CHAMBER PRESSURE, $P_D = 40$ ATM
TOTAL DISCHARGE POWER, $Q_T = 35$ KW
PLASMA REFLECTED IMPEDANCE, $Z_P = 280$ OHMS
ARGON WEIGHT FLOW RATE, $W_A = 4.5$ GM/SEC
ARGON INJECTION VELOCITY, $V_J = 4.5$ M/SEC
INJECTION REYNOLDS NUMBER, $R_{e_{t_j}} \approx 4.5 \times 10^5$

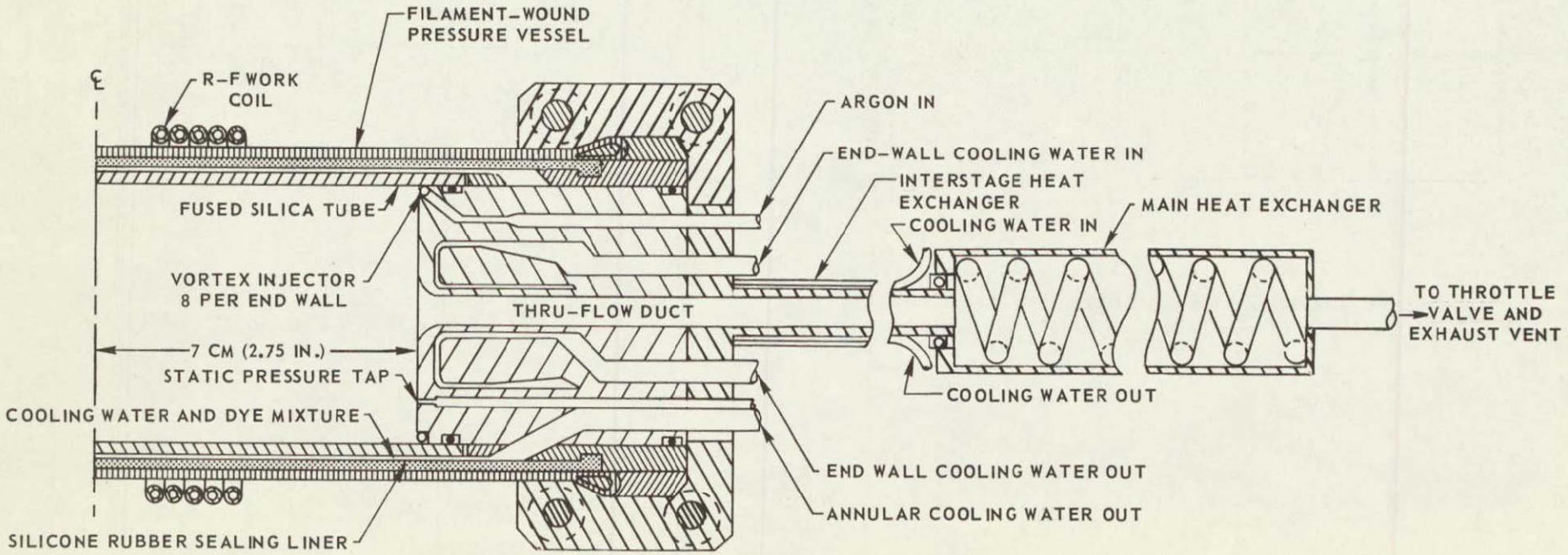

POWER IN ANNULAR WATER-DYE COOLANT; $Q_W = 23.1$ KW

POWER IN END-WALL COOLANT; BOTH ENDS $Q_E = 5.6$ KW

POWER IN HEAT EXCHANGER COOLANT; BOTH ENDS $Q_{EX} = 6.3$ KW

K-910900-7

FIG. 20

SUMMARY OF RESULTS OF RADIANT ENERGY SOURCE TESTS USING FILAMENT-WOUND PRESSURE VESSEL

NOTE: NO ATTEMPT MADE TO MAXIMIZE PLASMA DISCHARGE POWER WITH INCREASING PRESSURE
SEE FIG. 10 FOR DETAILS OF TEST CONFIGURATION
RANGE OF ARGON WEIGHT FLOW RATE, W_A = 2.3 TO 4.5 GM/SEC (W_A CONSTANT AT 4.5 GM/SEC FOR P_D>6 ATM)
RANGE OF R-F OPERATING FREQUENCY, f = 5.5721 TO 5.5945 MHz
□ SYMBOLS DENOTE DATA FROM PRIOR TESTS USING FUSED SILICA PRESSURE VESSEL W_A = 2.1 TO 2.5 GM/SEC

(a) VARIATION OF TOTAL DISCHARGE POWER WITH CHAMBER PRESSURE

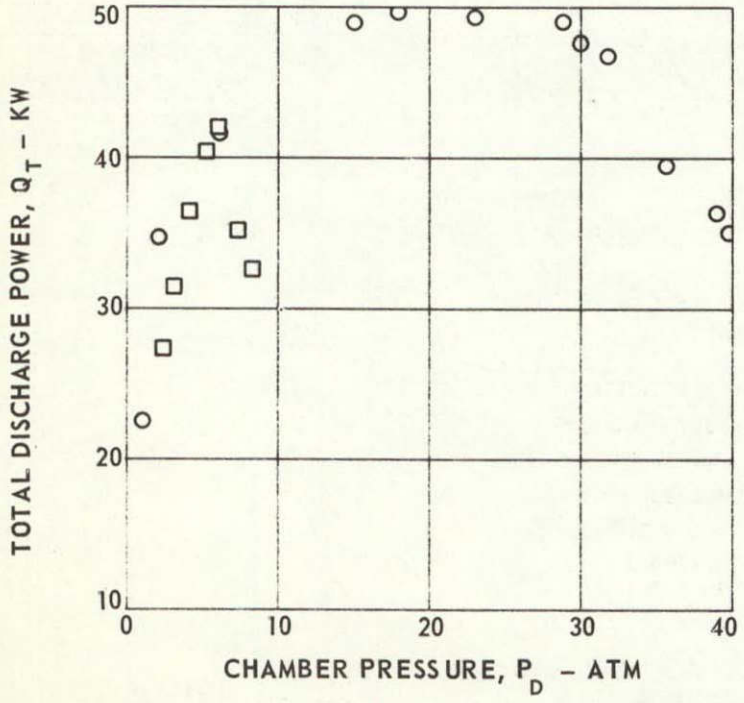

(b) EFFECT OF CHAMBER PRESSURE ON THE FRACTION OF TOTAL DISCHARGE POWER DEPOSITED INTO THE ANNULAR COOLANT

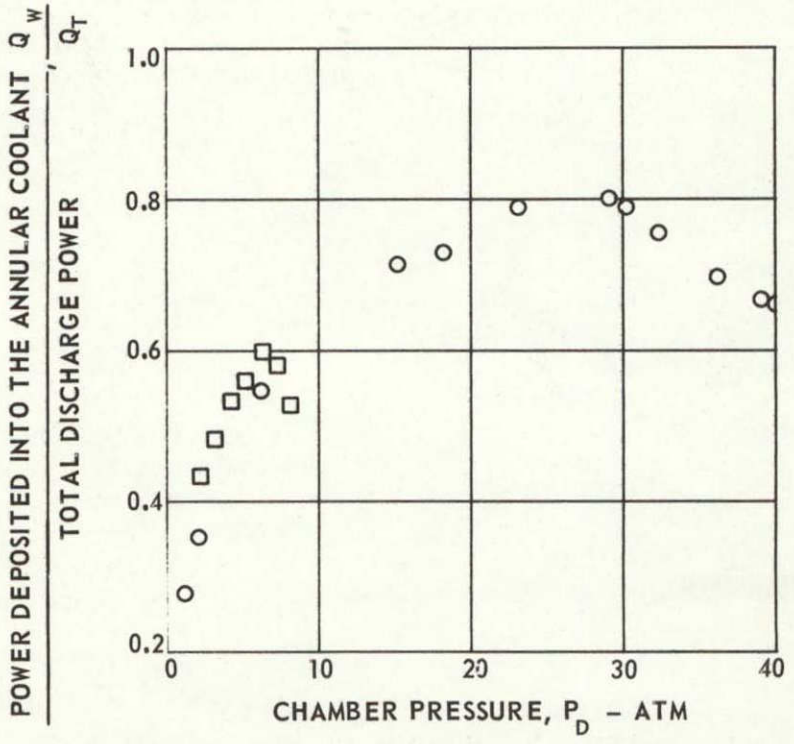

FIG. 21

SKETCH OF CONFIGURATION USED IN TESTS WITH SIMULATED FUEL INJECTION

CONFIGURATION SAME AS THAT SHOWN IN FIG. 10 EXCEPT FOR ADDITION OF SIMULATED-FUEL INJECTION PROBE AND REPLACEMENT OF FILAMENT-WOUND PRESSURE VESSEL WITH FUSED SILICA TUBE.

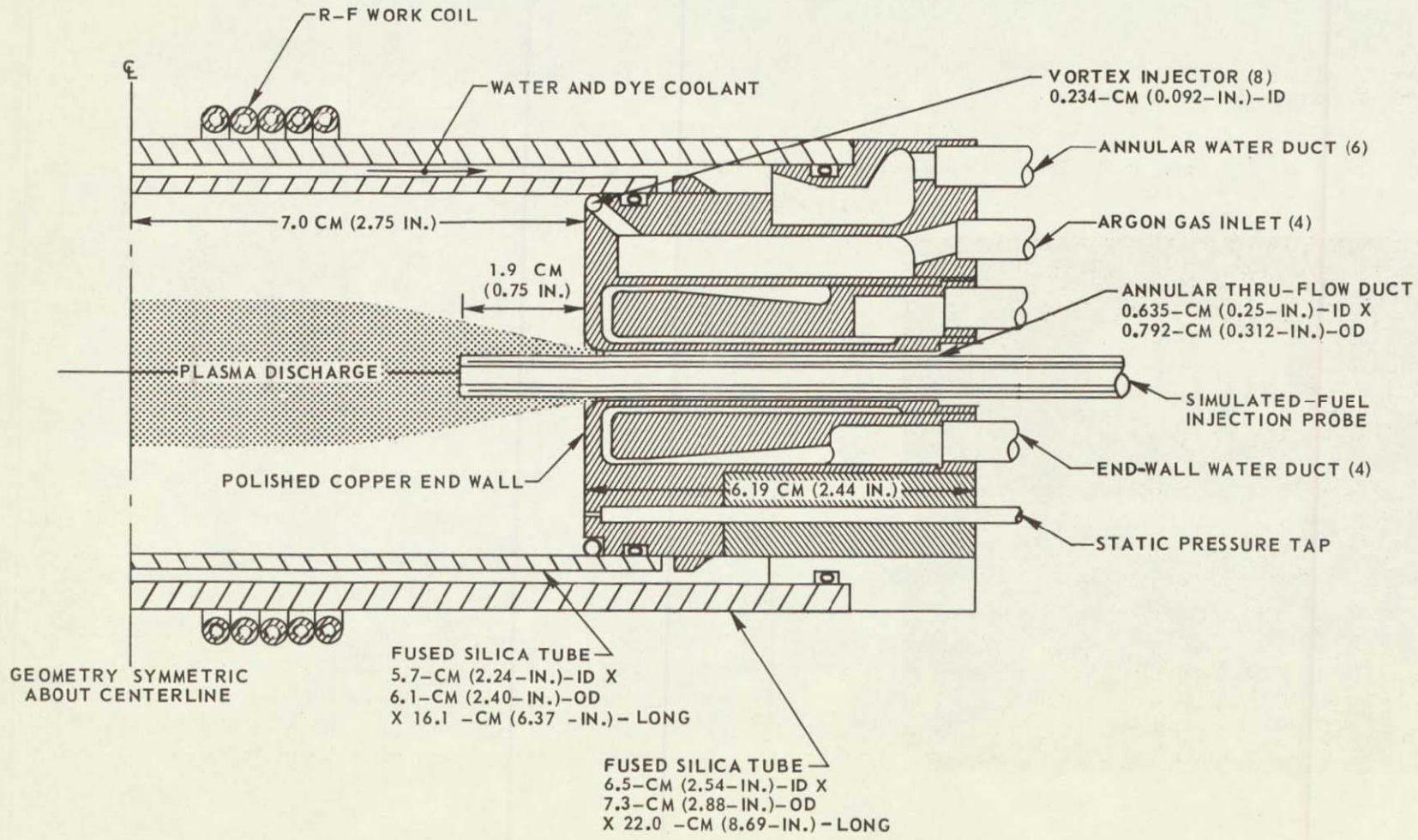

FIG. 22

SKETCH AND PHOTOGRAPHS OF SIMULATED-FUEL INJECTION PROBE

SEE FIG. 25 FOR SCHEMATIC OF SIMULATED-FUEL FLOW SYSTEM

SEE FIG. 22 FOR SKETCH OF SIMULATED FUEL INJECTION CONFIGURATION

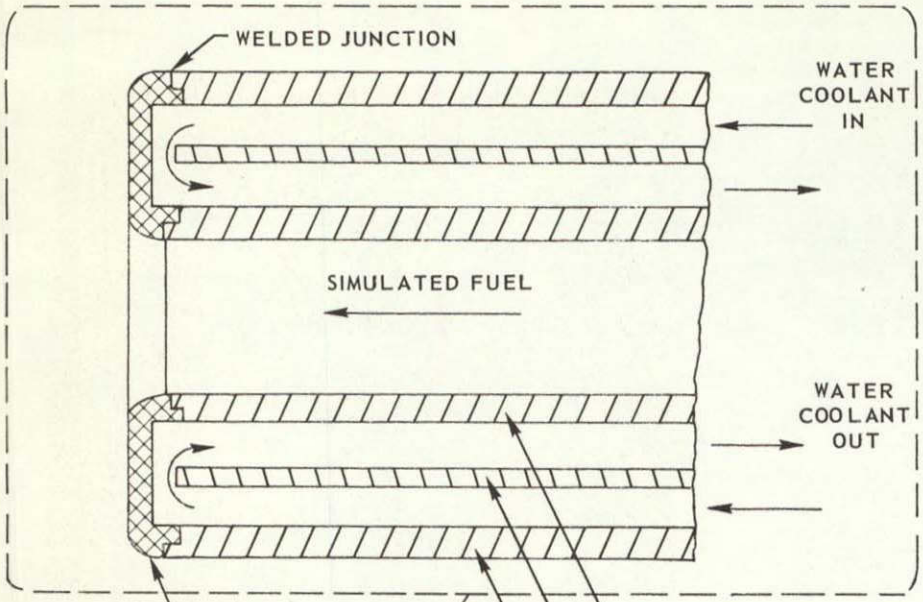

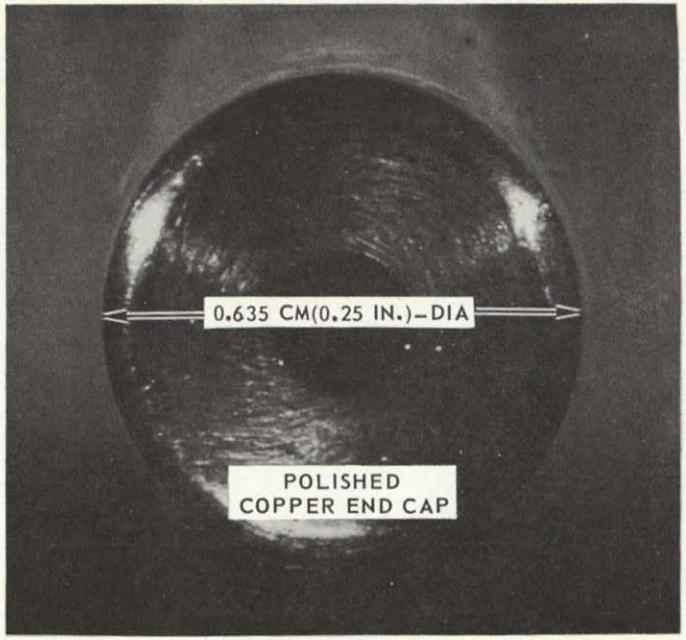

VIEW A-A

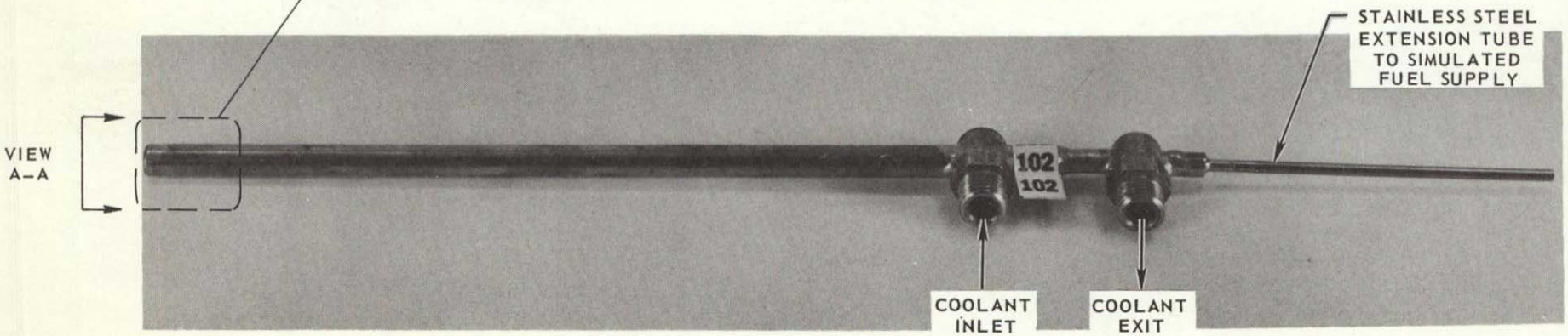

FIG. 23

PHOTOGRAPHS OF 2/3-SCALE IN-REACTOR CONFIGURATION

NO SIMULATED FUEL INJECTION

(a) VIEW THROUGH CENTRAL VIEWPORT WITH NO PLASMA PRESENT

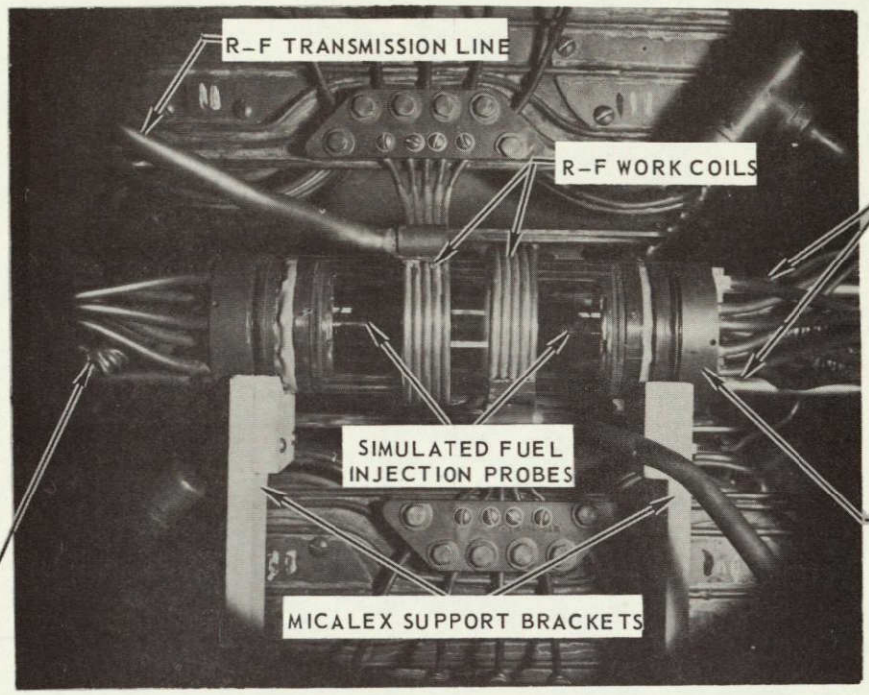

(b) VIEW THROUGH CENTRAL VIEWPORT WITH PLASMA PRESENT

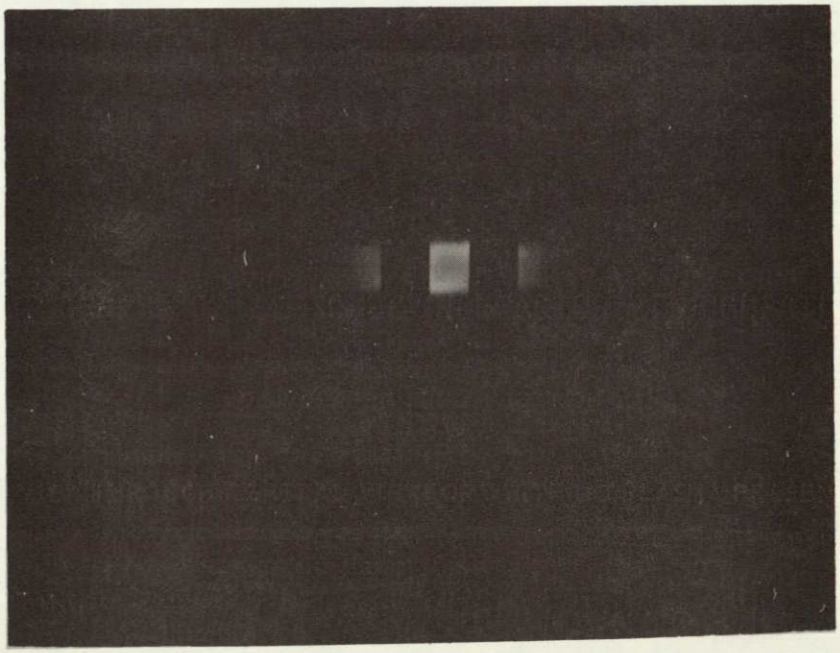

EXPOSURE DATA:
f/32 AT 1/250 SEC
FILTER-1.5 N.D
FILM-ASA 400

SCHEMATIC OF FLOW SYSTEM FOR TESTS WITH URANIUM HEXAFLUORIDE AND TUNGSTEN HEXAFLUORIDE SIMULATED-FUEL INJECTION

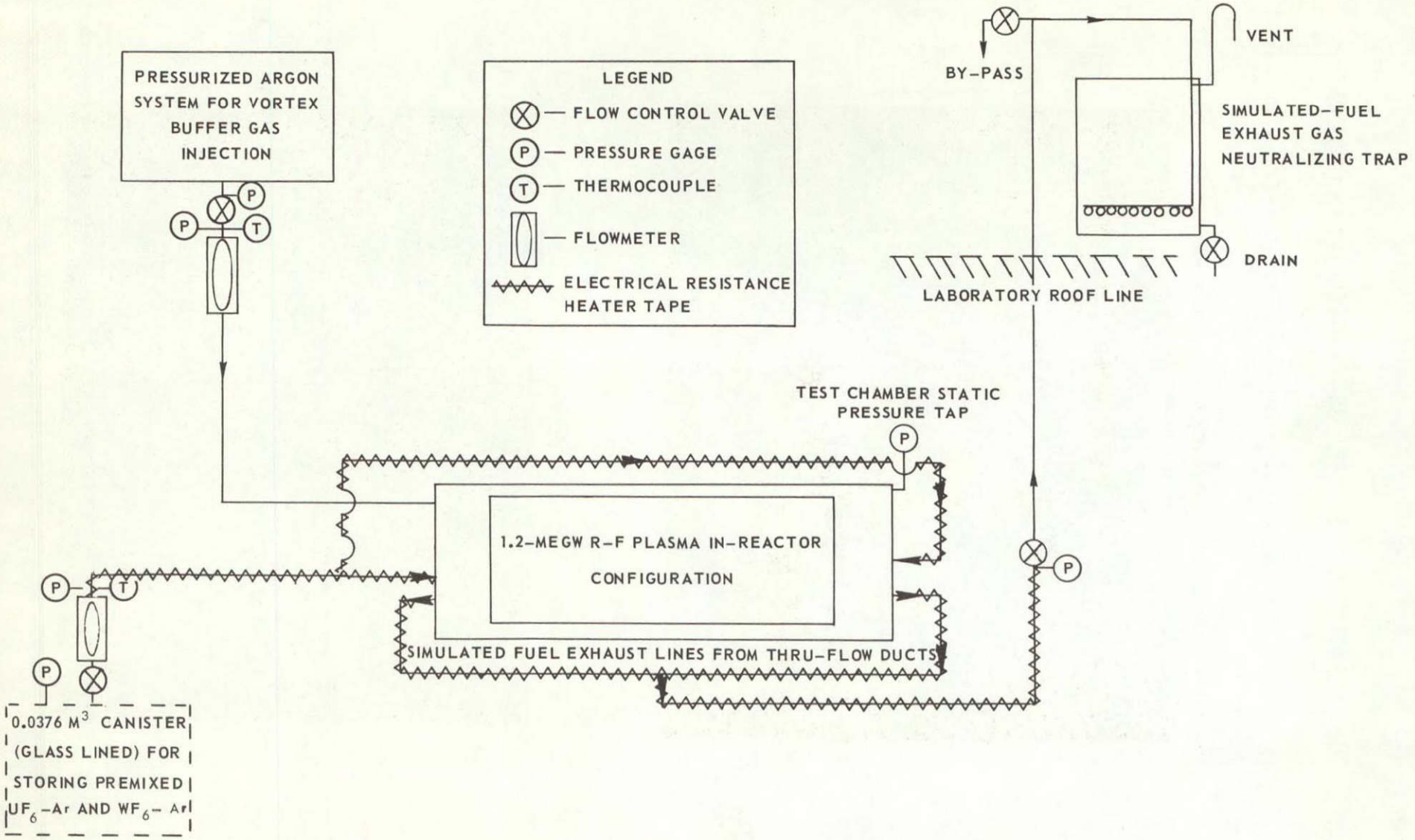

K-910900-7

FIG. 25

SCHEMATIC OF PARTICLE FEEDER SYSTEM USED IN TESTS WITH TUNGSTEN PARTICLE SIMULATED FUEL INJECTION

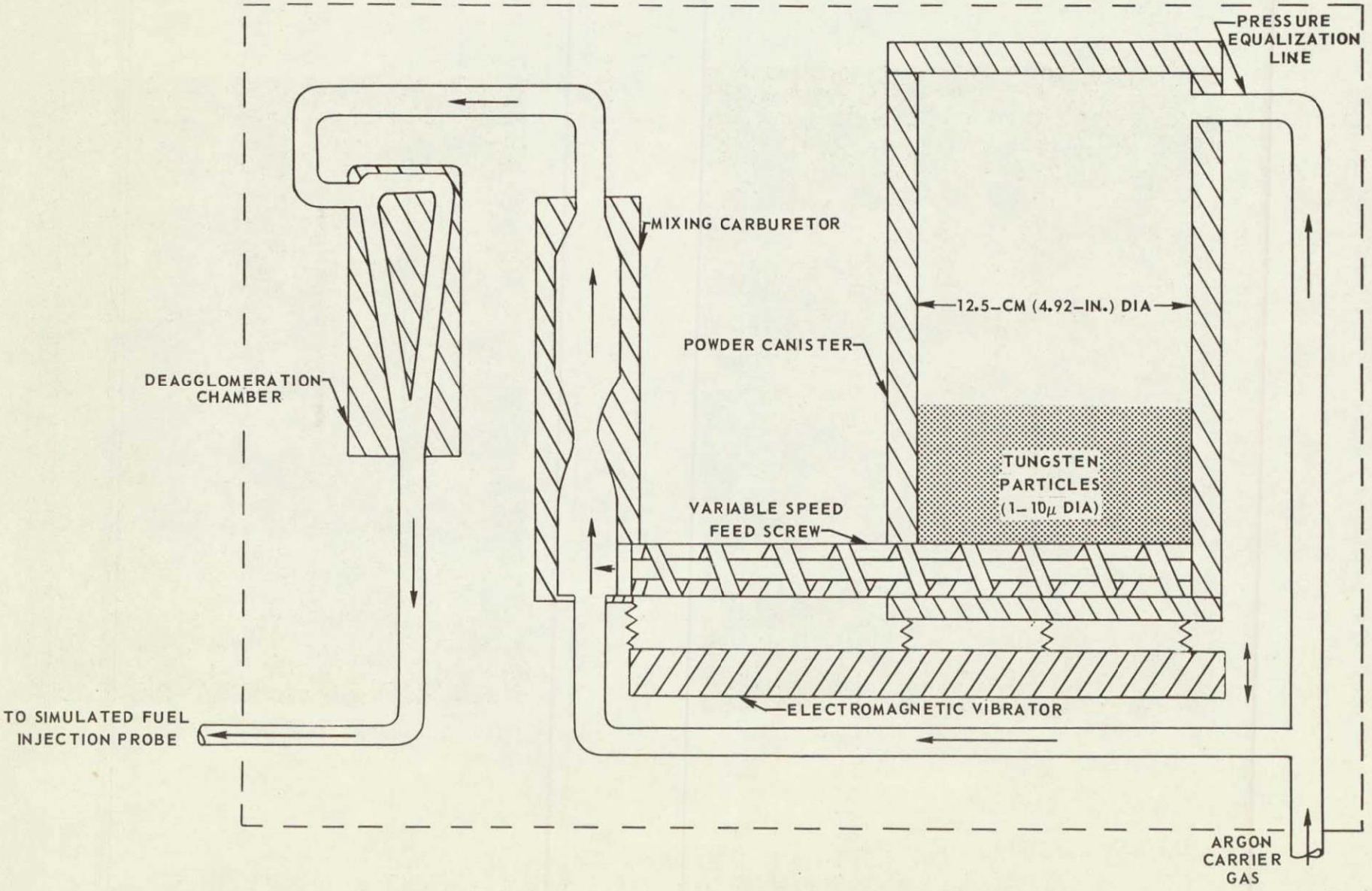

K-910900-7

FIG. 26

FIG. 27

PHOTOGRAPHS OF 2/3-SCALE IN-REACTOR CONFIGURATION WITH SIMULATED FUEL INJECTION

SEE TABLE II FOR DETAILS OF TEST CONDITIONS

(a) VIEW THROUGH LEFT VIEW PORT WITH NO PLASMA PRESENT

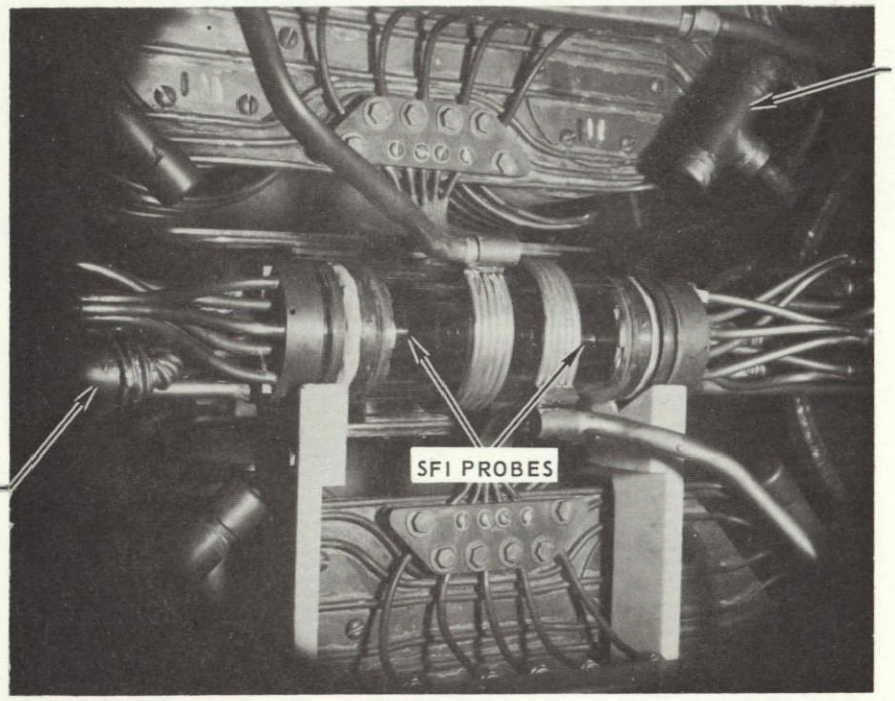

(b) VIEW THROUGH LEFT VIEW PORT WITH PLASMA PRESENT DURING SIMULATED-FUEL INJECTION TEST

SIMULATED FUEL-4% WF_6

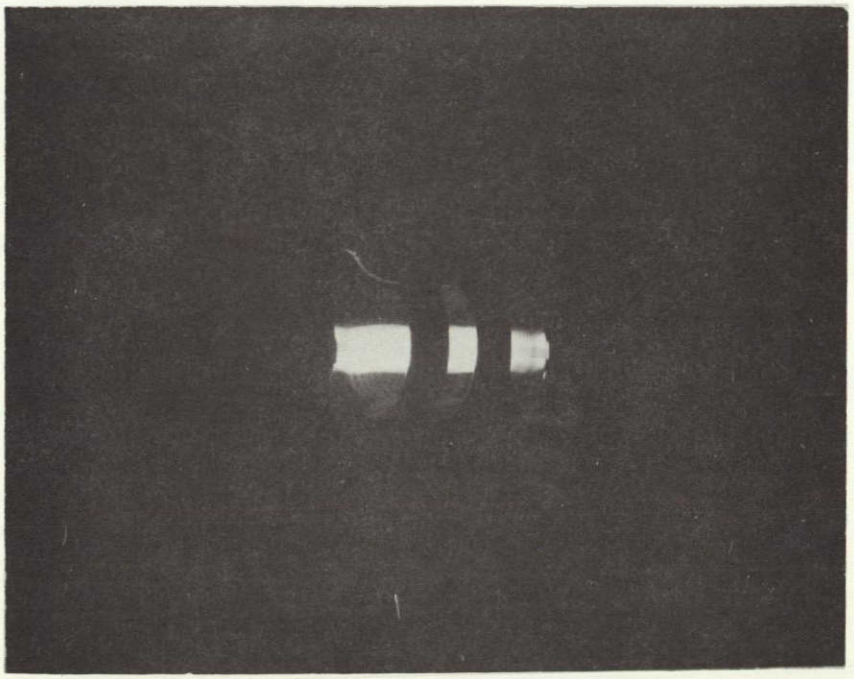

EXPOSURE DATA:
f/32 AT 1/250 SEC
FILTER-1.5 N.D.
FILM-ASA 400

FIG. 28

COMPARISON OF EMISSION SPECTRA BETWEEN 4044.42 Å AND 4333.56 Å TAKEN DURING INITIAL SIMULATED-FUEL INJECTION TESTS

DATA TAKEN ON CENTERLINE OF DISCHARGE – SEE FIG. 22 FOR TEST CONFIGURATION
SEE TABLE II FOR TEST CONDITIONS CORRESPONDING TO 4 PERCENT WF_6 CASE

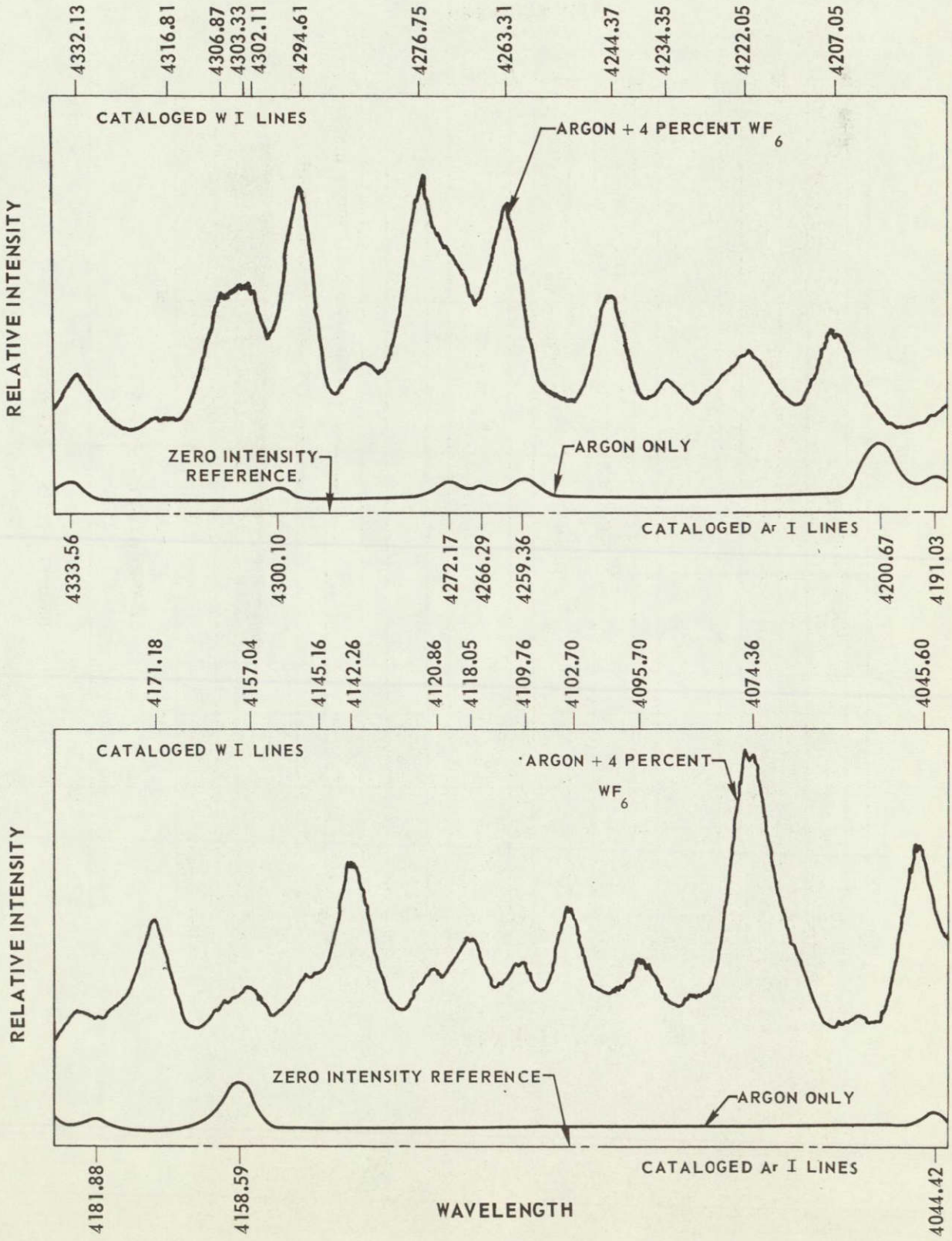

VAPOR PRESSURE CURVES FOR TUNGSTEN HEXAFLUORIDE AND URANIUM HEXAFLUORIDE

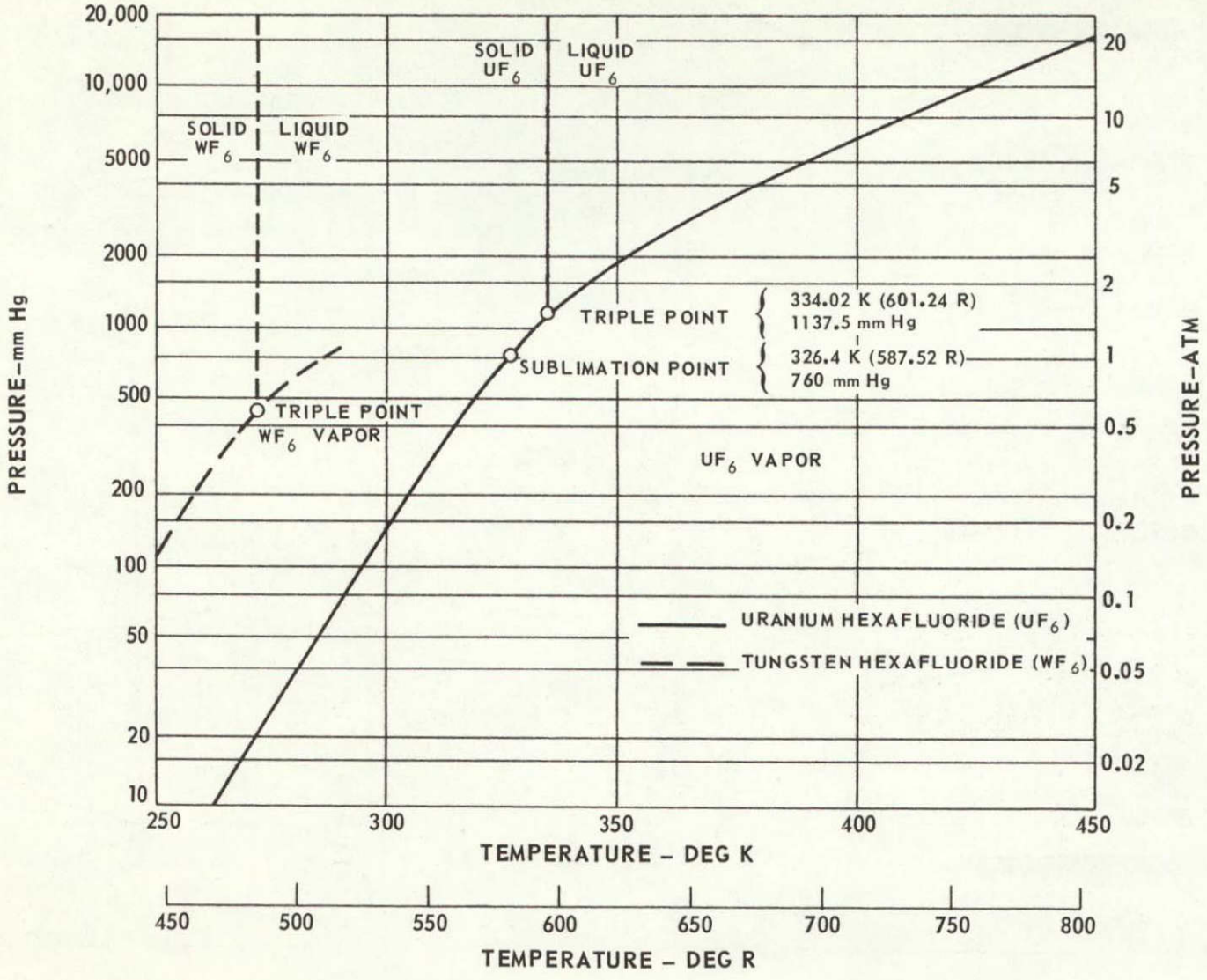

FIG. 29

SKETCH OF TRANSPARENT-WALL MODEL CONFIGURATION

SEE FIG. 31 FOR SKETCH OF INJECTOR AND COOLANT TUBES

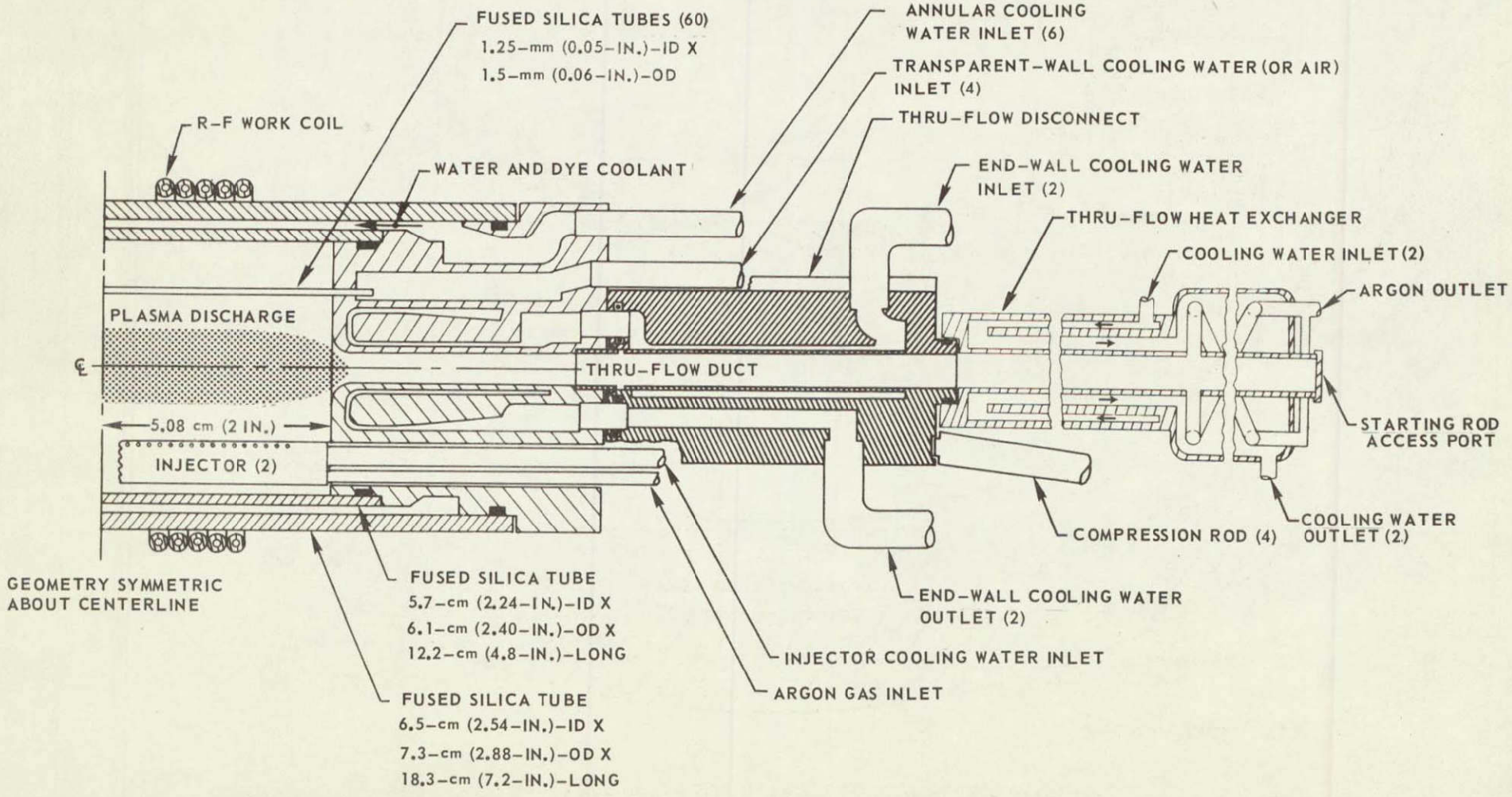

FIG. 30

SKETCH OF INJECTOR AND COOLANT TUBES

SEE FIG. 30 FOR DETAILS OF OVERALL MODEL CONFIGURATION

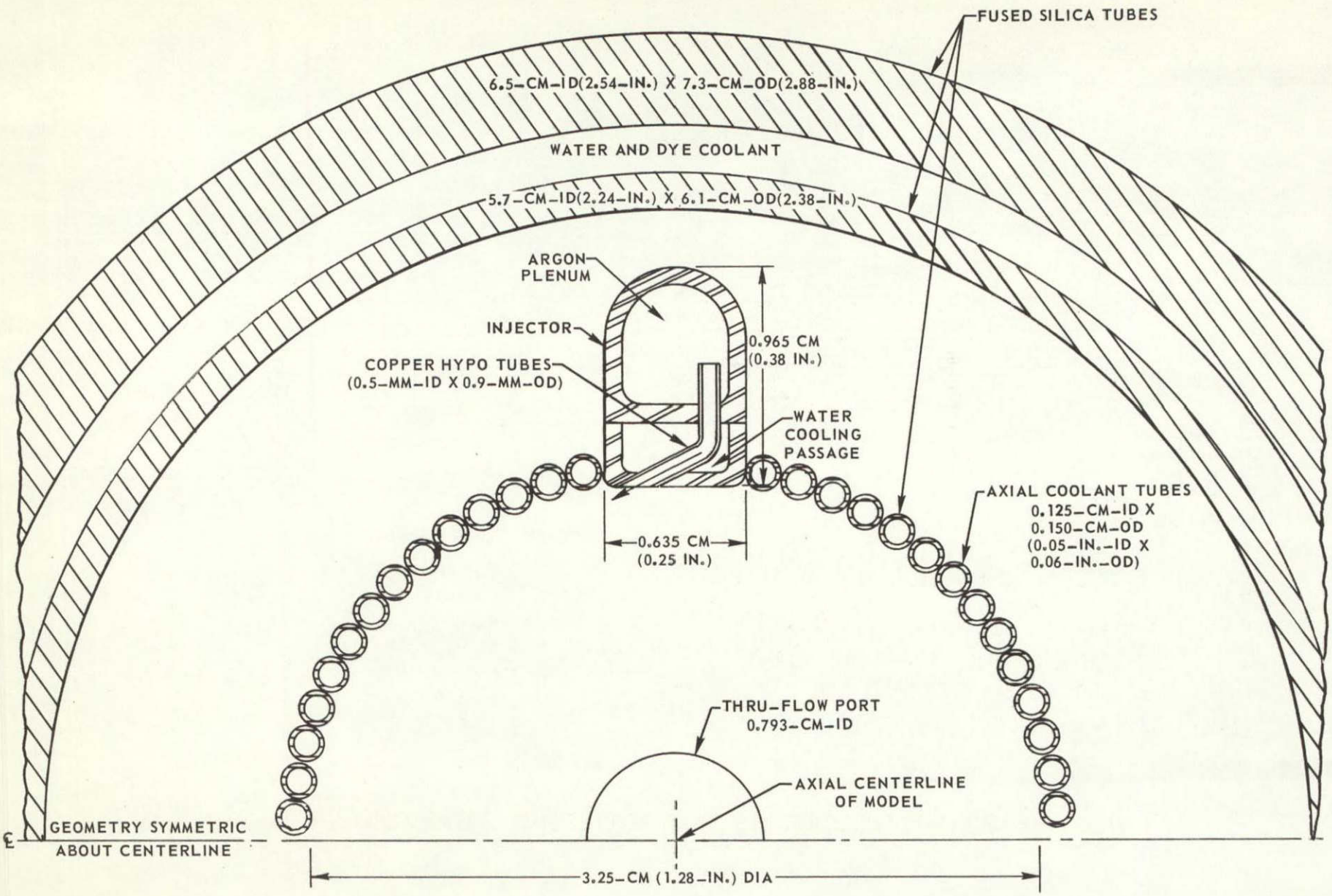

FIG. 31

SKETCH OF TRANSPARENT-WALL MODEL CONFIGURATION USED IN FLOW VISUALIZATION TESTS

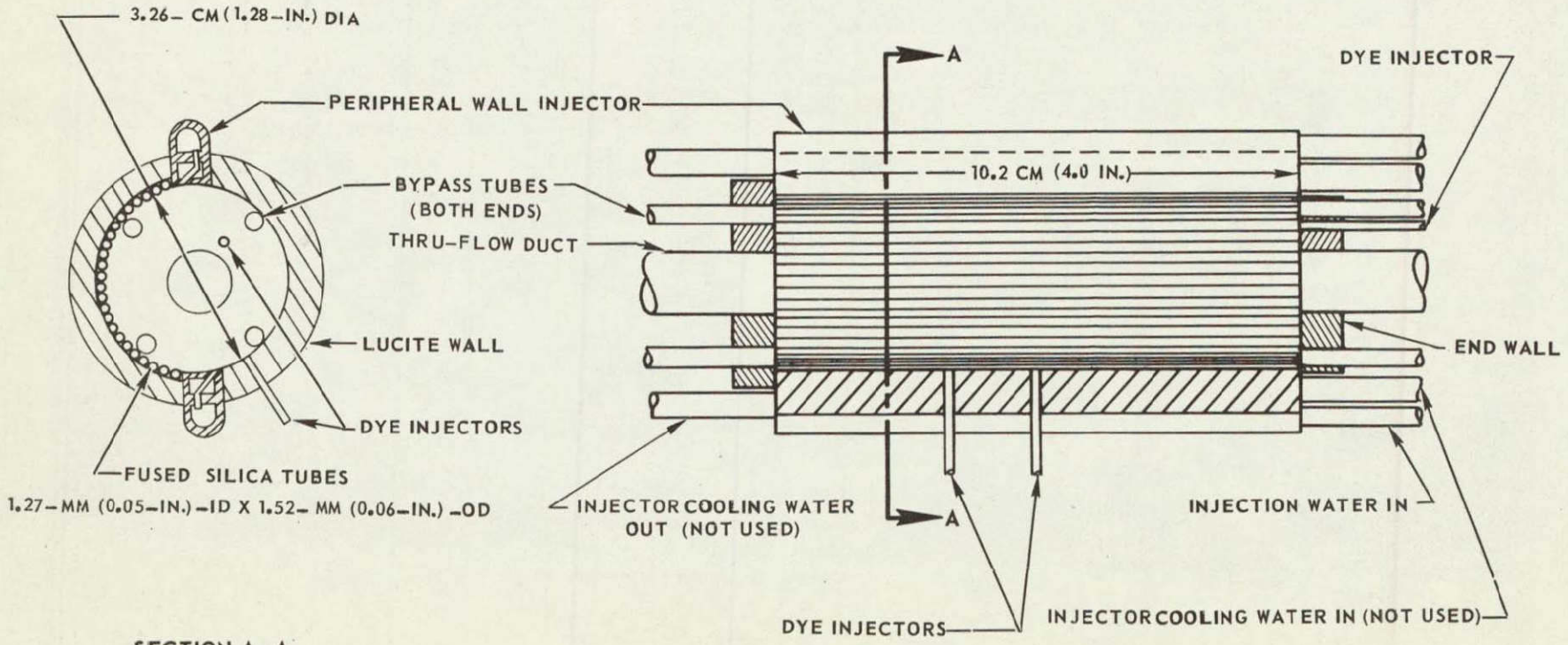

SECTION A-A

FIG. 32

PHOTOGRAPH SHOWING TRANSPARENT-WALL MODEL INSTALLATION IN 1.2 MEGW R-F INDUCTION HEATER

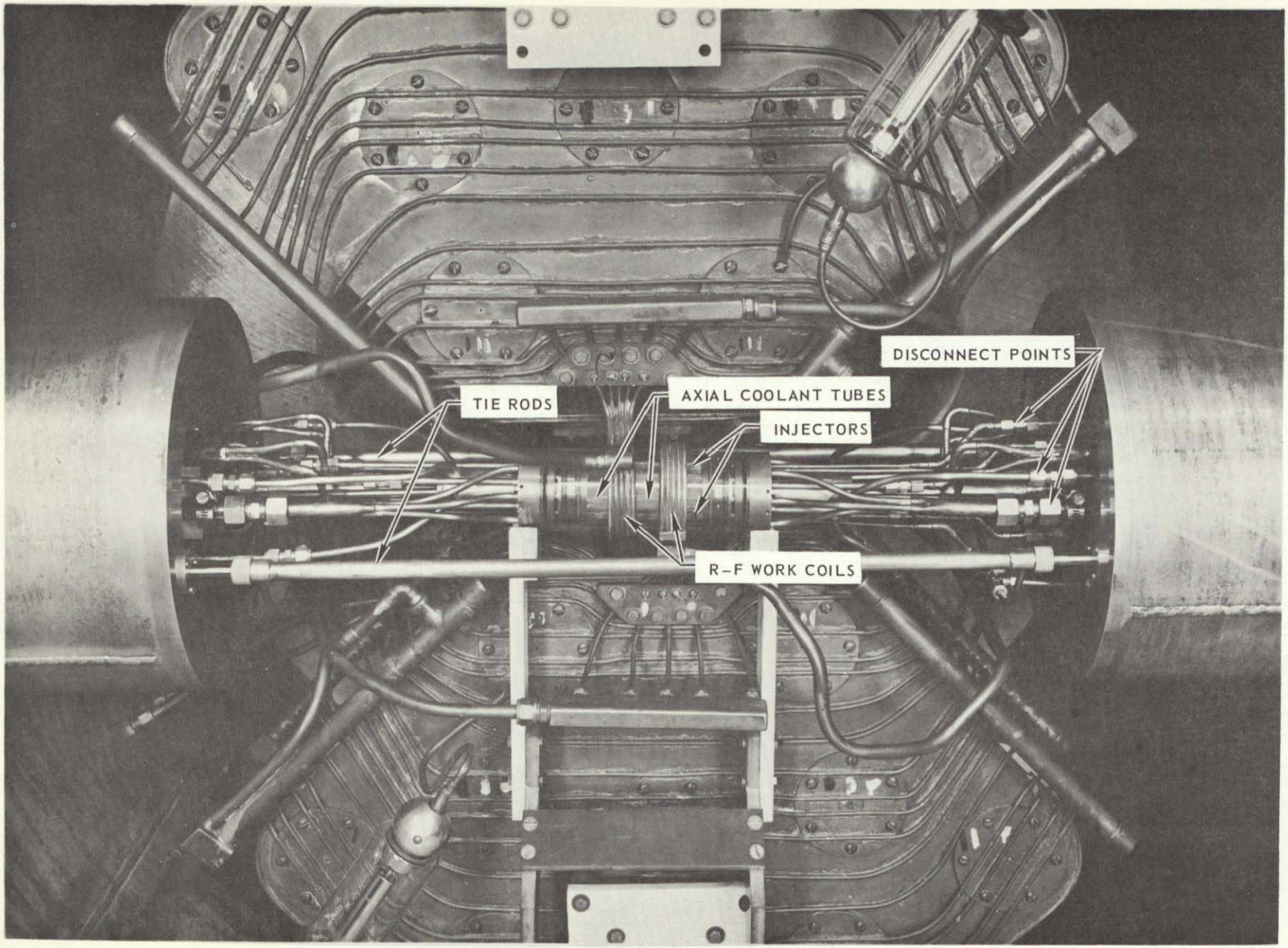

FIG. 33

SUMMARY OF TEST RESULTS FOR AXIAL-COOLANT-TUBE MODEL TESTS

SYMBOL	MODEL COOLANT	CHAMBER PRESS-ATM	ARGON FLOW RATE, W_A - GM/SEC	COOLANT TUBE WALL THICKNESS-MM
●	WATER	1-21	1.8-7.7	0.25
■	AIR	1-13.6	3.0-16.3	0.125

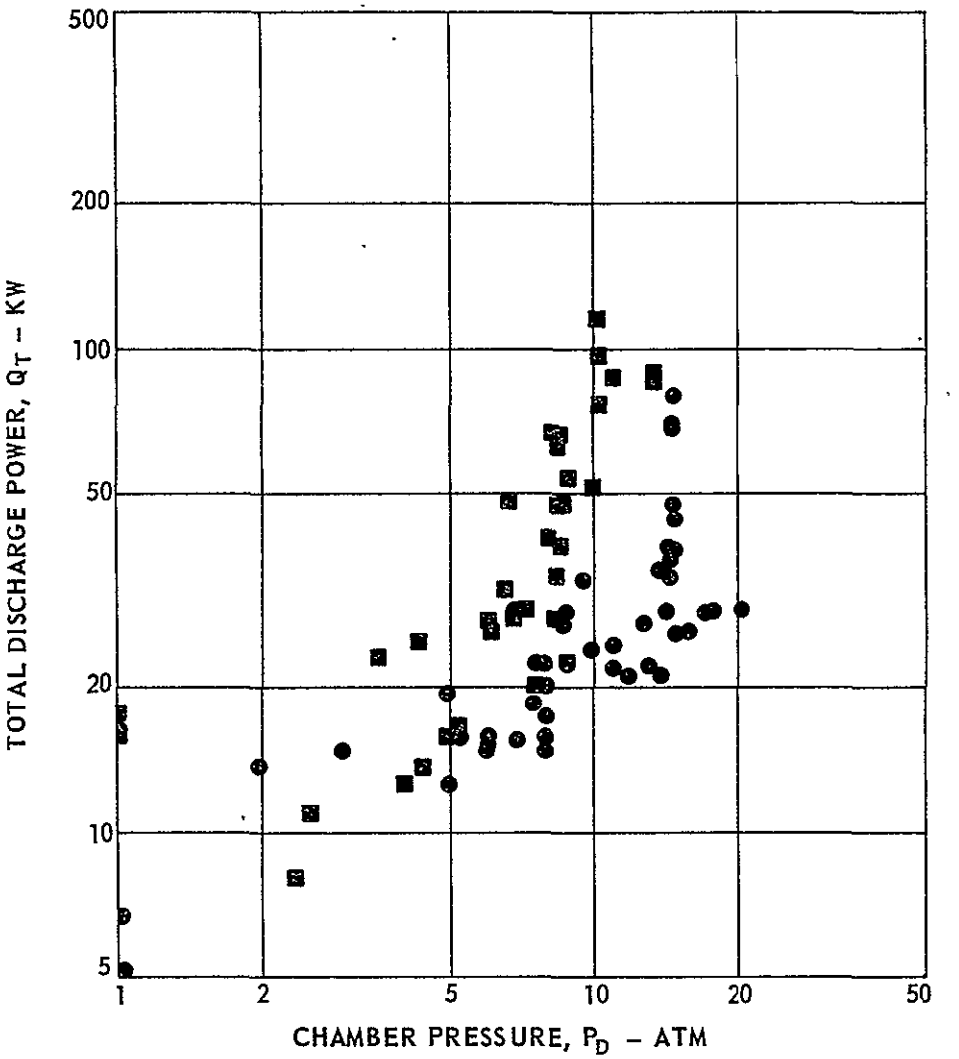

POWER BREAKDOWN FOR HIGHEST POWER OPERATING POINT WITH AXIAL-COOLANT-TUBE MODEL

SEE FIG. 30 FOR DETAILS OF MODEL CONFIGURATION

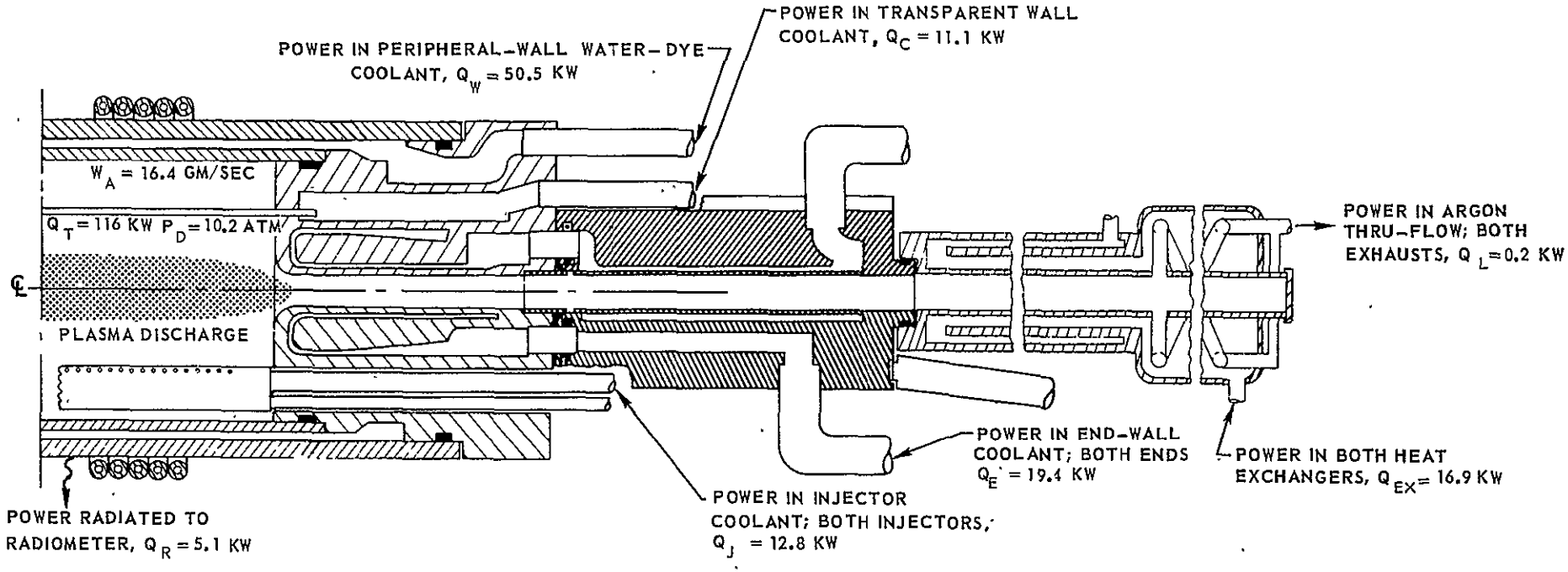

TOTAL D-C INPUT POWER, Q_I = 470 KW AT 5.6661 MHZ

TOTAL DISCHARGE POWER, Q_T = 116 KW

R-F SYSTEM COUPLING EFFICIENCY, η = 25 PERCENT

APPROXIMATE TOTAL POWER RADIATED THROUGH MODEL WALL = 56 KW

RADIANT ENERGY FLUX ON MODEL WALL, $Q_{R,T}/A_M$ = 0.77 KW/CM^2

FIG. 35

VARIATION OF POWER RADIATED THROUGH TRANSPARENT WALL WITH TOTAL DISCHARGE POWER IN AXIAL-COOLANT-TUBE MODEL TESTS

SEE FIG. 30 FOR DETAILS OF MODEL CONFIGURATION

SYMBOL	MODEL COOLANT	CHAMBER PRESSURE - ATM	ARGON FLOW RATE, W_A - GM/SEC	DATA FROM
●	WATER	1-21	1.8-7.7	PRESENT PROGRAM
■	AIR	1-13.6	3.0-16.3	PRESENT PROGRAM
▨	WATER	1-9.9	0.7-11.5	REFS 7 AND 20

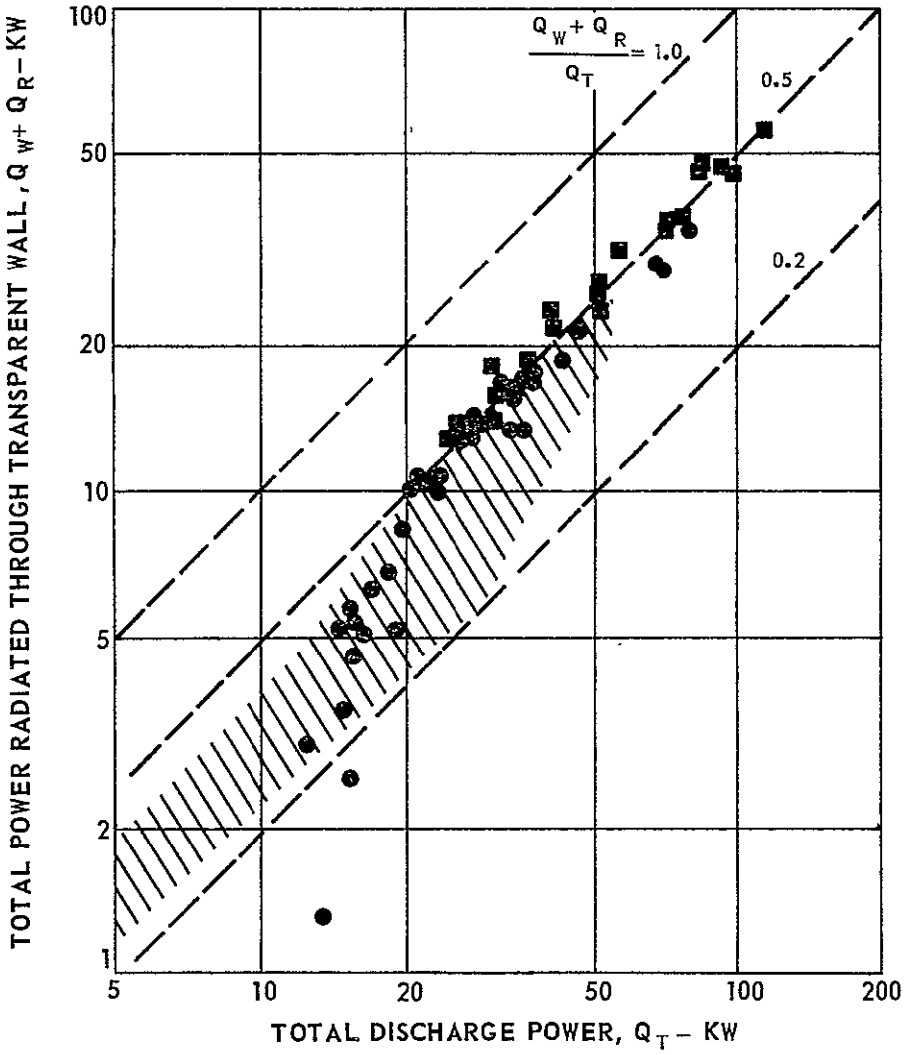

VARIATION OF POWER DEPOSITED INTO COOLANT TUBES WITH TOTAL DISCHARGE POWER IN AXIAL-COOLANT-TUBE MODEL TESTS

SEE FIG. 30 FOR DETAILS OF MODEL CONFIGURATION

SYMBOL	MODEL COOLANT	CHAMBER PRESS-ATM	ARGON FLOW RATE, W_A - GM/SEC	DATA FROM
●	WATER	1-21	1.8-7.7	PRESENT PROGRAM
■	AIR	1-13.6	3.0-16.3	PRESENT PROGRAM
▨	WATER	1-9.9	0.7-11.5	REFS 7 AND 20

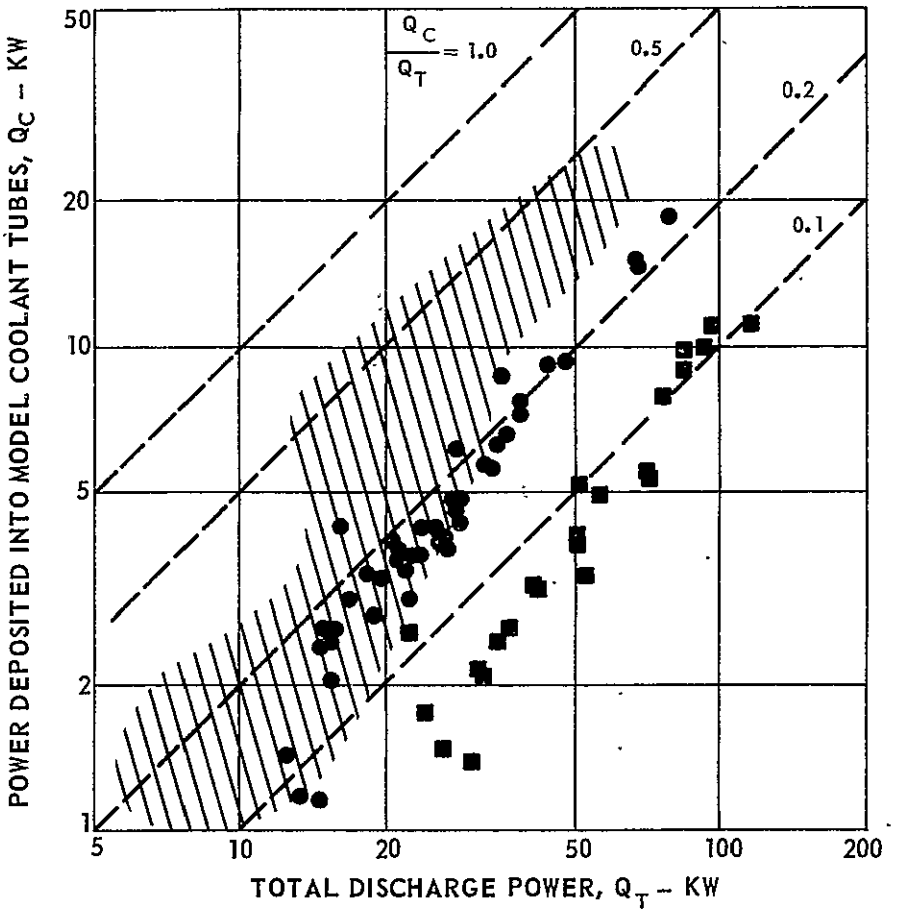

VARIATION OF POWER DEPOSITED INTO INJECTORS WITH TOTAL DISCHARGE POWER IN AXIAL-COOLANT-TUBE MODEL TESTS

SEE FIG. 30 AND 31 FOR DETAILS OF MODEL CONFIGURATION

NOTE: PRESENT INJECTORS AND INJECTORS OF REFS. 7 AND 20 HAD DIFFERENT COOLING CONFIGURATIONS AND DIFFERENT SURFACE AREAS EXPOSED TO PLASMA DISCHARGE

SYMBOL	MODEL COOLANT	CHAMBER PRESS-ATM	ARGON FLOW RATE, W_A-GM/SEC	DATA FROM
●	WATER	1-21	1.8-7.7	PRESENT PROGRAM
■	AIR	1-13.6	3.0-16.3	PRESENT PROGRAM
//////	WATER	1-9.9	0.7-11.5	REFS 7 AND 20

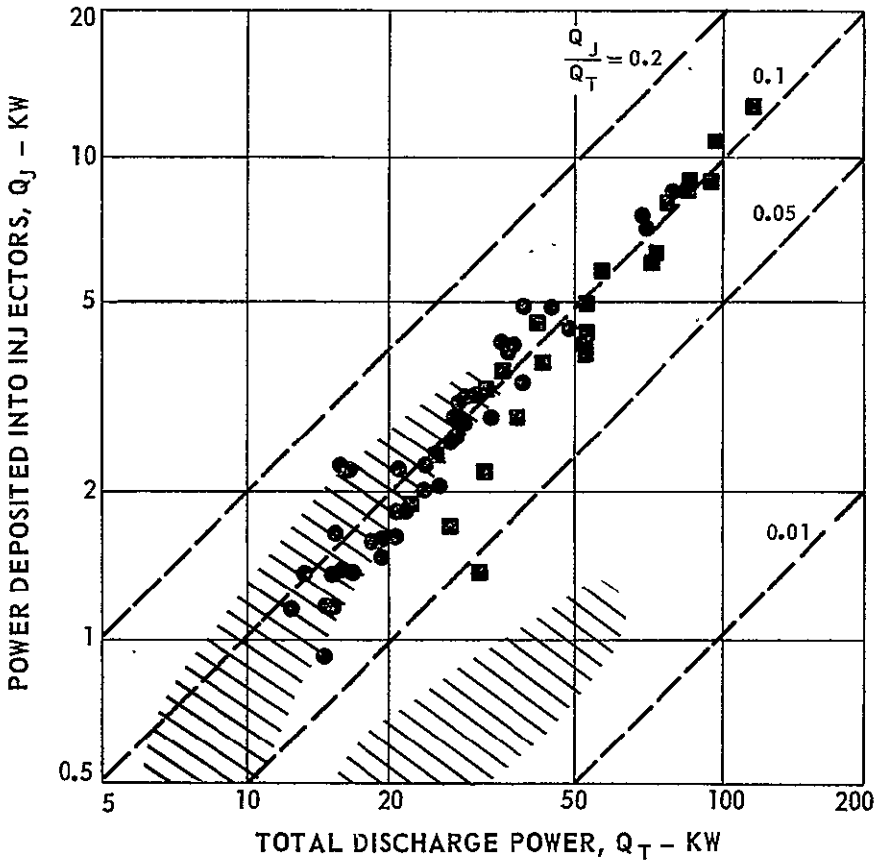

VARIATION OF POWER DEPOSITED IN END WALLS AND THRU-FLOW EXHAUSTS WITH TOTAL DISCHARGE POWER IN AXIAL-COOLANT-TUBE MODEL TESTS

SEE FIG. 30 FOR DETAILS OF MODEL CONFIGURATION

SYMBOL	MODEL COOLANT	CHAMBER PRESS-ATM	ARGON FLOW RATE, W_A - GM/SEC	DATA FROM
●	AIR	1-21	1.8-7.7	PRESENT PROGRAM
■	WATER	1-13.6	3.0-16.3	PRESENT PROGRAM
▨	WATER	1-9.9	0.7-11.5	REFS 7 AND 20

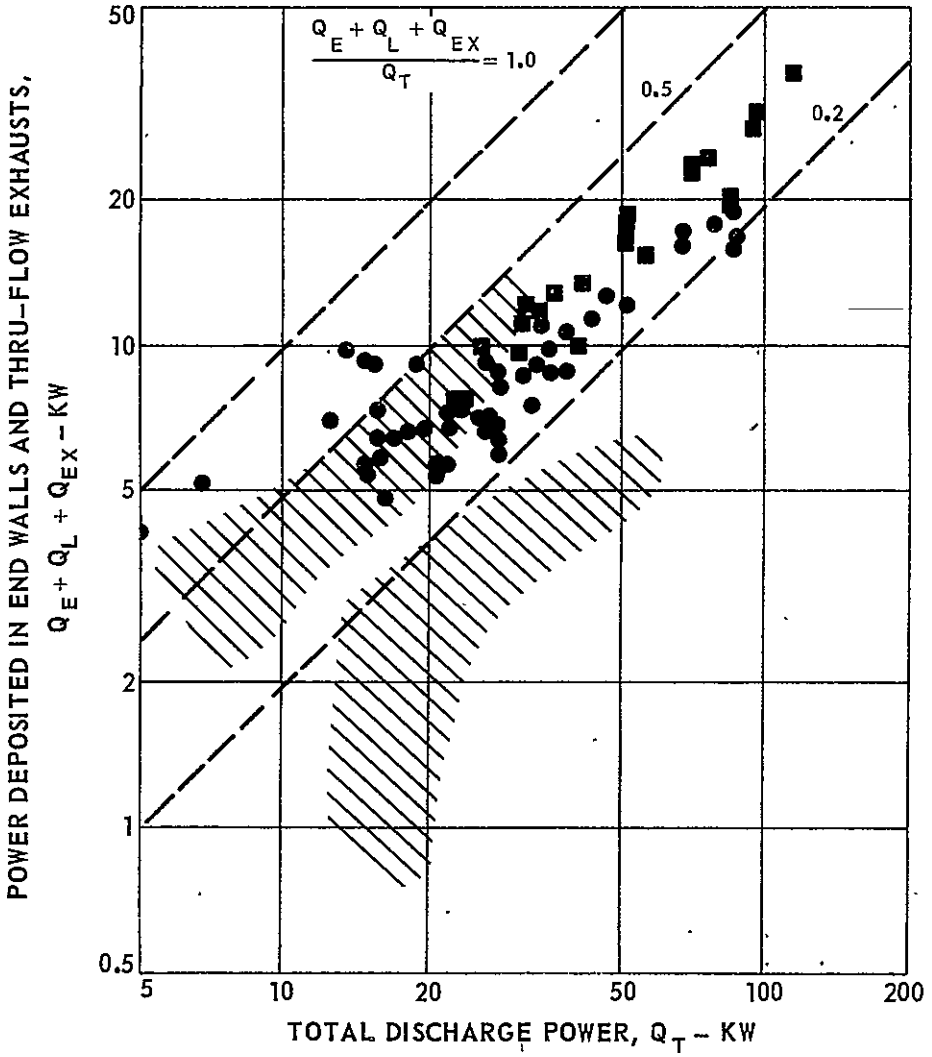

EFFECT OF CHAMBER PRESSURE ON THE FRACTION OF TOTAL DISCHARGE POWER RADIATED THROUGH TRANSPARENT WALL IN AXIAL-COOLANT-TUBE MODEL TESTS

SEE FIG. 30 FOR DETAILS OF MODEL CONFIGURATION

SYMBOL	MODEL COOLANT	ARGON FLOW RATE, W_A - GM/SEC	TOTAL DISCHARGE POWER, Q_T - KW
●	WATER	1.8-7.7	5.0-80.0
■	AIR	3.0-16.3	11.6-116.0

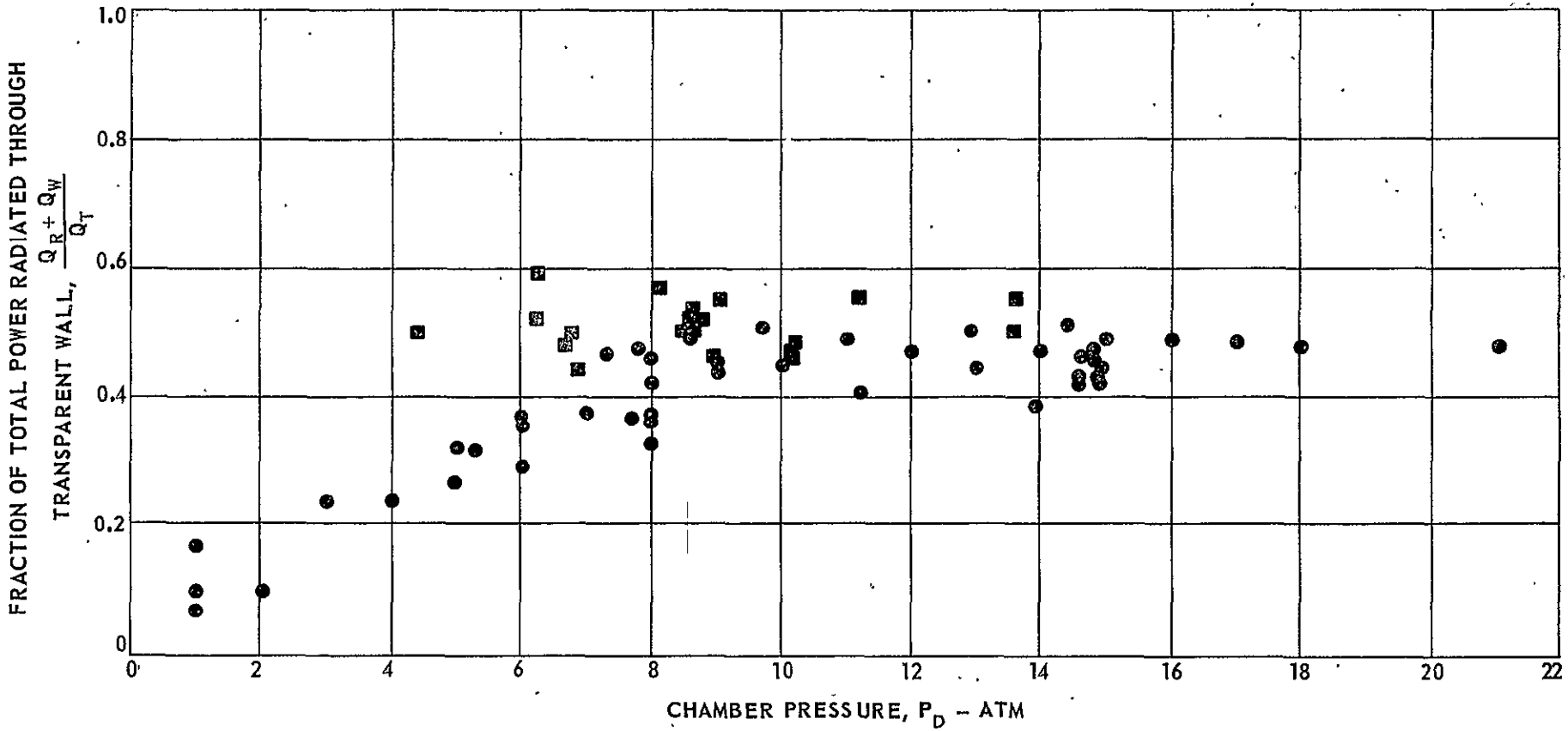

FIG. 40

SKETCH OF FILAMENT-WOUND PRESSURE VESSEL CONFIGURATION FOR 500 ATM HYDROSTATIC TESTS

SEE TABLE VI FOR TEST RESULTS

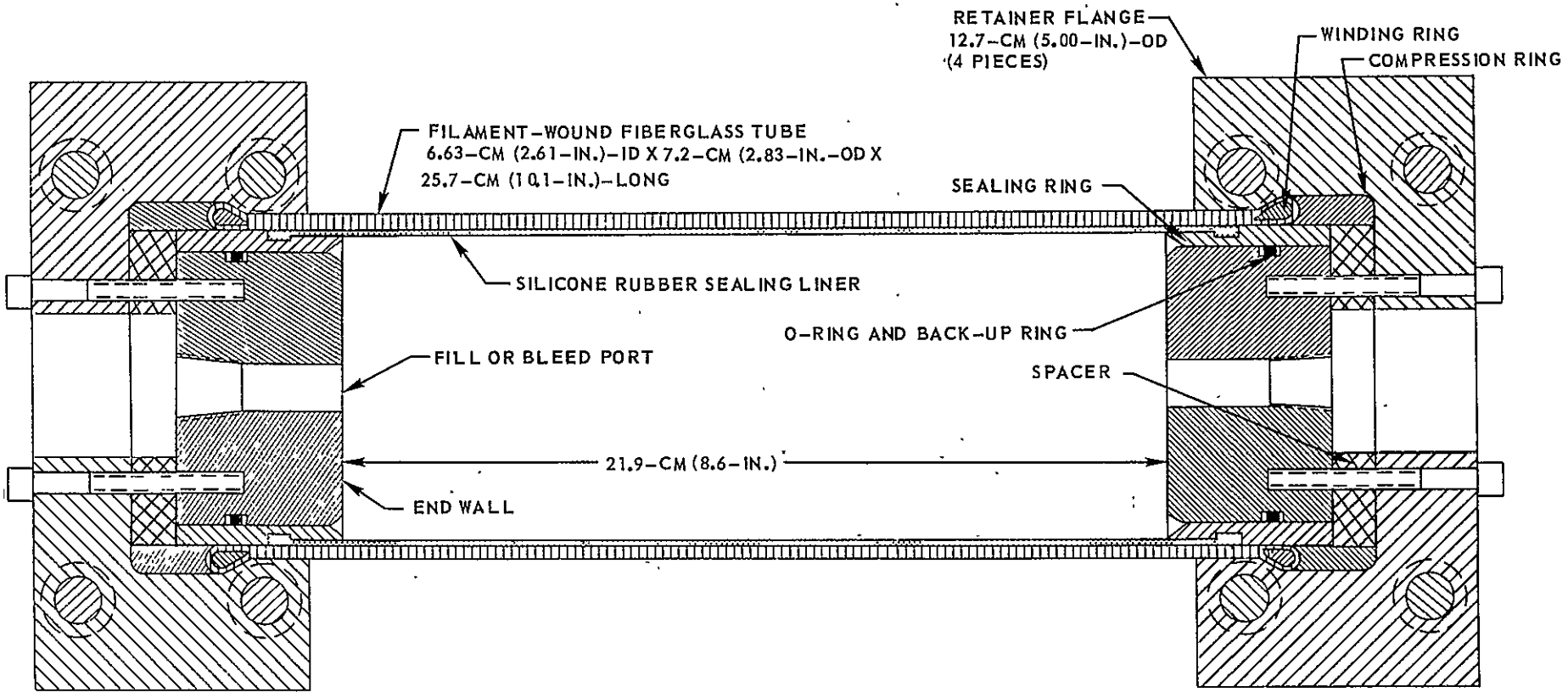

FIG. 41

DIAGRAM OF FORCES ON END OF FILAMENT-WOUND PRESSURE VESSEL

SEE FIG. 41 FOR PARTS NOMENCLATURE.

$U = F = F'$,
$G = G'$

(a) END FLANGE GEOMETRY WITHOUT SPACER

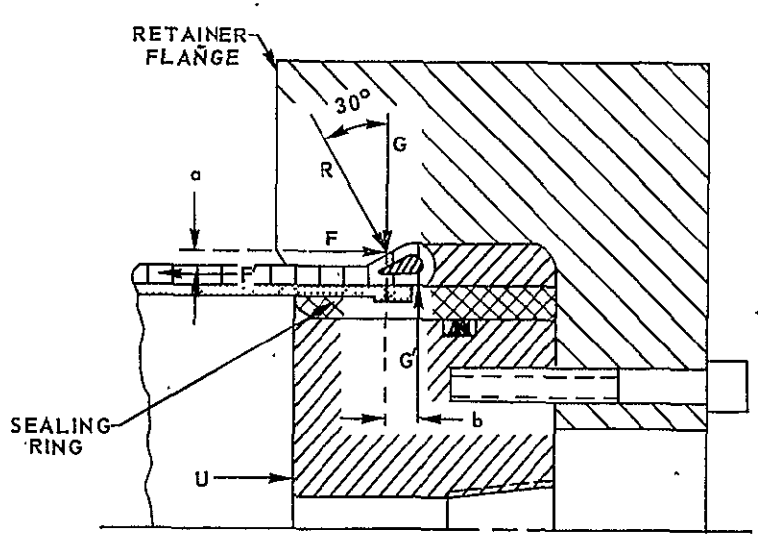

(b) END FLANGE GEOMETRY WITH SPACER

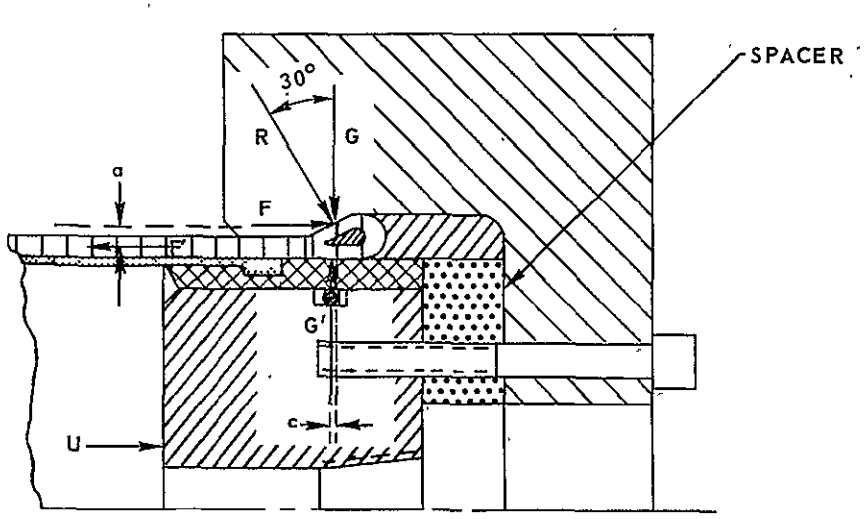

SKETCH OF FILAMENT WINDING FIXTURE AND ILLUSTRATION OF WINDING TECHNIQUE

(a) SKETCH OF WINDING CONFIGURATION – AXIAL LAYERS

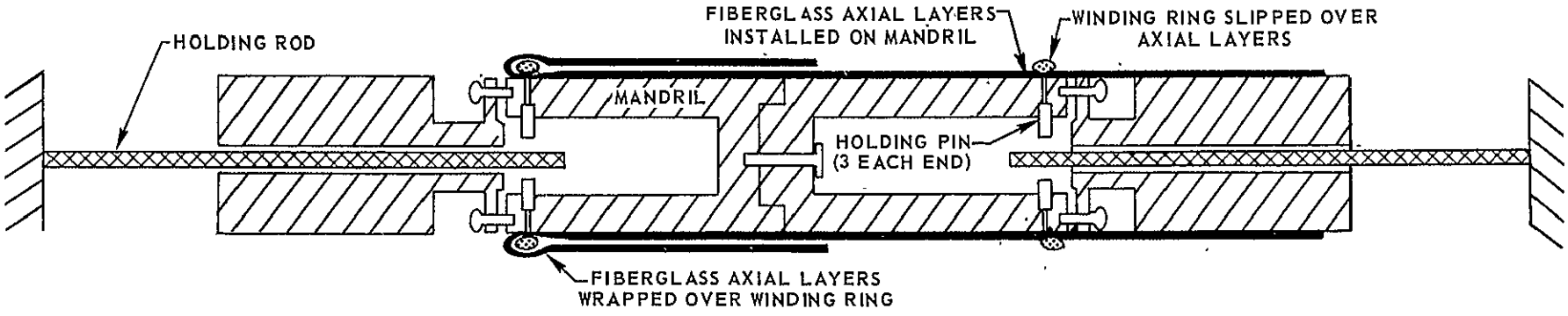

(b) SKETCH OF WINDING CONFIGURATION – HOOP LAYERS

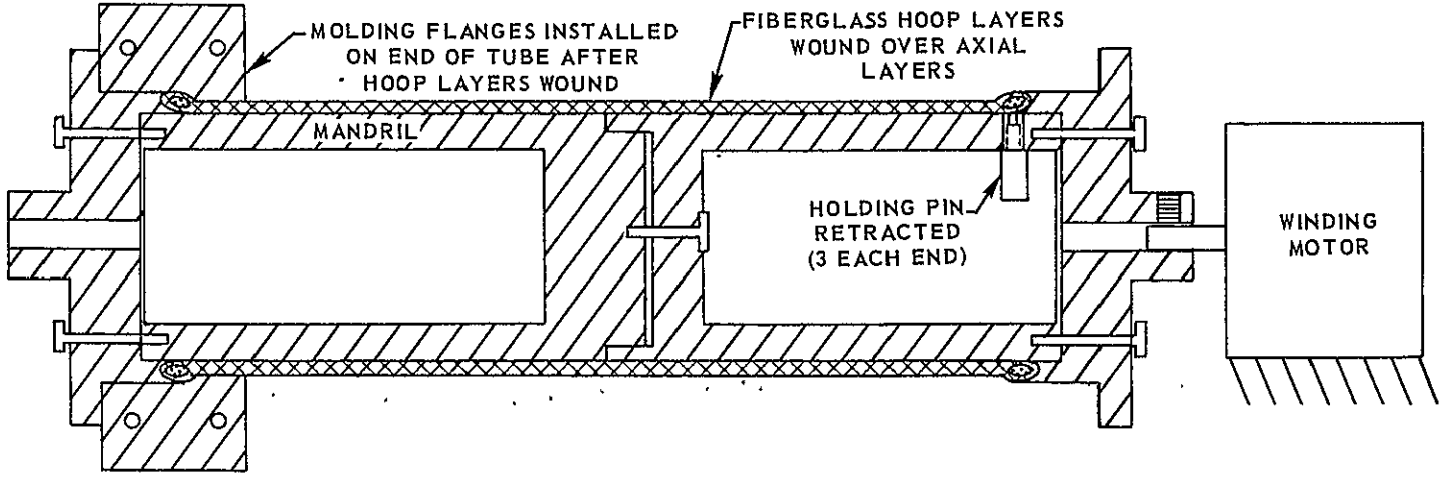

FIG. 43

PHOTOGRAPH OF FILAMENT WOUND TUBES AFTER HYDROSTATIC TESTS

SEE TABLE XI FOR SUMMARY OF 500-ATM FILAMENT-WOUND PRESSURE VESSEL TESTS
SEE FIG. 41 FOR DETAILS OF TEST CONFIGURATION

(a) TUBE 1

(b) TUBE 6